The Effects of Allelic Hinge Variation in IgG3 Antibodies on Protein Dynamics and Effector Functions

A thesis

submitted in partial fulfilment

of the requirements for the degree

of

Master of Science (Research) in Molecular and Cellular Biology

at

The University of Waikato

by

Marina Kuplich Barcellos

THE UNIVERSITY OF
WAIKATO
Te Whare Wānanga o Waikato

2024

Abstract

Antibodies play a crucial role in eliminating infections by recognising foreign antigens with high specificity and affinity. If a target is not directly neutralised, antibodies can mediate potent effector function responses by coordinating the recruitment of immune cells through their constant regions. These powerful immune functions are being widely explored in the form of IgG-based monoclonal antibody therapies for the treatment of infections, cancer, and autoimmune diseases. However, the antibody constant region exhibits significant genetic polymorphism, and new variants are rapidly being discovered by advances in genomic sequencing techniques. The documented effects of this diversity include differences in structural dynamics, thermal stability, and Fc-mediated effector functions among a number of antibody subclasses, including IgG1, IgG2, and IgG3. Some variants are reported to be a contributing factor to variability in the outcome of disease and responsiveness to vaccines in humans. The IgG3 subclass, in particular, displays striking differences in the antibody hinge region – responsible for connecting target binding with constant-region-mediated immune function. Here, exon duplications mean the hinge region can vary by as many as 45 amino acids in length. This work seeks to better understand some of the functional consequences of this unusual IgG3 variation.

To assess the effects of allelic hinge variation on protein dynamics and effector functions, we have expressed a panel of seven anti-CD20 antibodies with unique constant region allele sequences from subclasses IgG1, IgG2, and IgG3. Sequence-verified plasmids were used to express full-length antibodies in HEK293 cells at high purity. We first used small angle X-ray scattering (SAXS) to assess the variability in size and structural flexibility between the allelic variants and compared our data with previous research on the same variant panel with anti-HER2 variable domain sequences. Following this structural analysis, we next undertook ADCC (antibody-dependent cellular cytotoxicity) and ADCP (antibody-dependent cellular phagocytosis) assays to determine if differences in structural dynamics between the polymorphic variants could be linked to differences in effector function. These assays specifically used genome-engineered reporter cell lines to evaluate the ability of allelic variants to engage constant region binding FcγRIIIa and FcγRIIa Fc receptors, typically found on peripheral blood

mononuclear cells. Activation was measured by quantifying the levels of luciferase expressed as a reporter.

The findings provided in this study demonstrate that allelic variants with longer hinges have larger and more flexible structures and tend to present weaker ADCC and ADCP responses. The data presented here is the basis for future work on the influence of IgG constant region diversity on antibody structural dynamics and effector functions, which could contribute to improvements in the design of therapeutic antibodies.

Acknowledgements

Firstly, I would like to thank my Chief Supervisor, Dr William Kelton, for all the amazing support throughout my degree. I appreciate very much all the advice, feedback, and great effort to help me achieve as much as possible in my Masters. My co-supervisor, Dr Annmaree Warrender, also deserves a warm thank you for closely helping me during the initial learning curve in the first few months of the degree and with all the help while writing this thesis. I could not have asked for better supervisors.

There are many people from the C2 Lab that I would like to thank. The lab mums Dr Judith Burrows and Dr Geetanjali Rai did an amazing job supporting me in the lab, and I am very grateful for all the advice I have received. I am thankful to the LIT group for being such a fun (and smart) group to be around. Thank you very much to my lab mates who have listened to me ramble, cry, and overshare about my personal life, with a special mention to Jolyn, Jess, Kirsten, Ally, and Kyrin. This degree was an awesome experience thanks to all these people.

Thank you to my friends and family in Brazil, who have supported me from the far. I cannot wait to celebrate this achievement with you. I am also thankful to my friend group in New Zealand for supporting me and believing in me.

Last but not least, I would like to thank my parents and my partner, Mitchell, for the unmeasurable support and for being my support system through everything. I was able to be strong through the stressful times because of you three. Thank you for always believing in me and being there for me no matter what. My dad deserves a special mention for being much more than a dad through this journey. There were many intellectual conversations about the research I was doing and lots of wise advice, and they greatly helped me to accomplish this achievement.

Acknowledgement of Funds: This research was supported by an AINSE Ltd. Pathway Scholarship and by the Royal Society Te Apārangi (Marsden Fast Start Grant; 19-FRI-002).

Table of Contents

List of Figures

List of Tables

List of Equations

List of Algorithms

List of Abbreviations

AAV5	adeno-associated virus 5
ADCC	antibody-dependent cellular cytotoxicity
ADCP	antibody-dependent cellular phagocytosis
Arg	arginine, amino acid
BioSAXS	biological small angle x-ray scattering
CDC	complement-dependent cytotoxicity
CDR3	complementarity-determining region 3
CH1/2/3	heavy chain constant domain 1/2/3
CV	column volume
D_{max}	maximum particle dimension
DPBS	Dulbecco's phosphate-buffered saline
DSF	differential scanning fluorimetry
Fab	fragment antigen-binding
FcR	Fc receptor
FcRL	FcR-like receptor
FcRn	neonatal Fc receptor
FcαRI	Fc alpha receptor I
Fcα/μR	Fc alpha/mu receptor
FcεR	Fc epsilon receptor
FcγR	Fc gamma receptor
FcμR	Fc mu receptor
FDA	U.S. Food and Drug Administration
FPLC	fast protein liquid chromatography
Gln	glutamine, amino acid
HEK293F	human embryonic kidney cell line 293F
His	histidine, amino acid
Ig	immunoglobulin
IGHC	immunoglobulin heavy-chain constant
IGLC	immunoglobulin light-chain constant
IFN-γ	interferon-gamma
Ile	isoleucine, amino acid
IMGT	International Immunogenetics Information System®
ITAM	immunoreceptor tyrosine-based activation motif

ITIM	immunoreceptor tyrosine-based inhibitory motif
K_D	dissociation constant
kDa	kilodalton
LB	Luria Bertani
Leu	leucine, amino acid
mAb	monoclonal antibody
min	minutes
MW	molecular weight
NET	neutrophil extracellular trap
NFAT	nuclear factor of activated T cells
NGC	next-generation chromatography
NK cells	natural killer cells
PBMC	peripheral blood mononuclear cell
PCR	polymerase chain reaction
PDB	protein databank
Phe	phenylalanine, amino acid
R_g	radius of gyration
REES	red edge excitation shift
SAXS	small angle x-ray scattering
SDS-PAGE	sodium dodecyl sulphate polyacrylamide gel electrophoresis
SEC	size exclusion chromatography
Ser	serine, amino acid
SPR	surface plasmon resonance
TAE	tris-acetate-EDTA
TEMED	tetramethyl ethylenediamine
TNF	tumour necrosis factor
TRIM21	tripartite motif 21
Trp	tryptophan, amino acid
Tyr	tyrosine, amino acid
VH	variable heavy chain
VL	variable light chain
v/v	volume per volume
w/v	weight per volume
x *g*	times the force of gravity

1 Chapter One

Introduction

This project encompasses the influence of allelic hinge variation in human immunoglobulin G (IgG) on their structural dynamics and Fc-mediated effector functions. An overview of the immune biology of antibodies and Fc receptors, along with a short review of the documented effects of constant region polymorphisms in human IgG antibodies, is presented in this chapter to provide the background for this research.

1.1 Antibody structure and biology

Antibodies are large glycoproteins that play a major role in the clearance of infections as part of adaptive immunity by recognising foreign antigens with high specificity and affinity (Ackerman et al., 2011; Damelang et al., 2024). Their ability to neutralise pathogens and target specific cells for elimination is being explored in antibody therapies, such as in the treatment of infections and cancer. After binding, they can directly neutralise pathogens by occluding critical surface structures or by forming an immune complex to trigger powerful effector functions (Bruhns et al., 2009; Temming et al., 2019). There are five classes of immunoglobulin (Ig) isotypes in humans: IgA, IgD, IgE, IgG, and IgM, each with varied heavy chain structures and immune effector functions (Vidarsson et al., 2014). Of these classes, immunoglobulin gamma (IgG) is the most abundant in human serum (constitutes 10 – 20% of the proteins in the plasma) and is comprised of four subclasses: IgG1, IgG2, IgG3, and IgG4. This work focuses on IgG antibodies only and investigates the effects of IgG genetic hinge diversity on effector functions.

1.1.1 Antibody structure

All human antibodies form a tetrameric structure with two fragment antigen-binding arms (Fab), each comprised of a variable heavy chain (VH) paired with a variable light chain (VL) (Figure 1.1) (Jay et al., 2018). Depending on the individual antibody, the VL may be either a kappa (κ) or lambda (λ) light chain, with a large

bias towards kappa in humans (Warrender & Kelton, 2020). Antibody classes and subclasses are defined by the heavy chain sequence – formed by a VH joined to as many as four constant domains (CH1, CH2, CH3, and CH4). The VH and the VL together form the region where the antigen binds, whereas the constant region contains the Fc domain, which binds to Fc receptors (FcRs) on the surface of immune cells (Bruhns et al., 2009). In some antibody classes (IgA, IgD, and IgG), a hinge region joins the first two constant domains. This stretch of amino acids works as a flexible linker between the Fab arms and the Fc region (Preud'homme et al., 2000; Vidarsson et al., 2014; Woof & Russel, 2011). The hinge allows the Fab arms to move and change their orientations relative to the Fc region (Yogo et al., 2019).

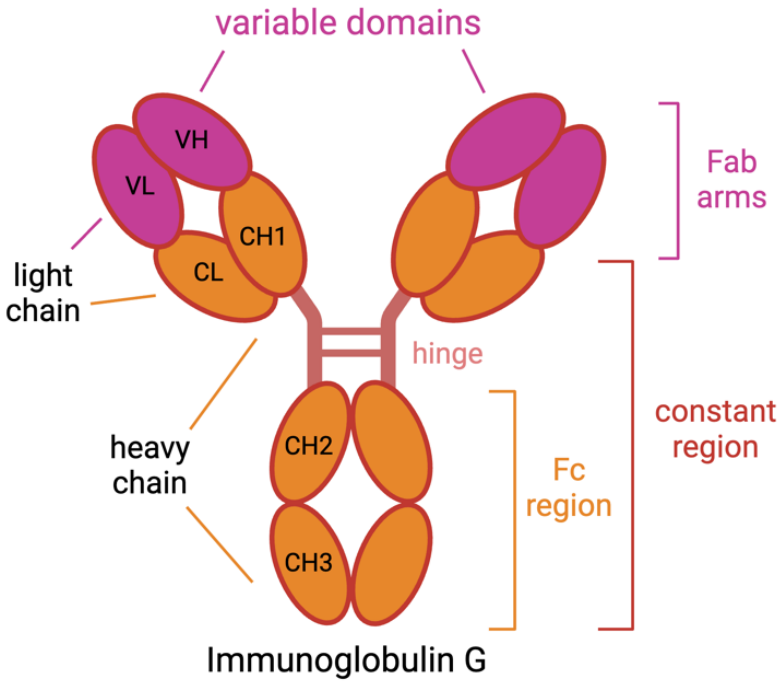

Figure 1.1. The fundamental structure of a human IgG antibody. Figure made using BioRender: https://www.biorender.com/.

1.1.2 Antibody variable domain sequence diversity

The targeting of antigens never seen by the immune system requires a large repertoire of antibody sequences to be generated and screened for activity. An individual's antibody repertoire may have as many as $1x10^{12}$ unique sequences (Schmitz et al., 2022). The generation of antibody diversity begins when the

variable domain exons undergo V(D)J recombination, in which the variable (V), diversity (D), and joining (J) gene segments are assembled via combinatorial recombination (Dudley et al., 2005; Roth, 2014). First, a pair of D and J segments are selected from the VH locus and combined by non-homologous end joining. Next, these segments are combined with a V segment to form the VH domain. The process of non-homologous end joining involves the introduction of DNA double-strand breaks between each segment and frequently created nucleotide losses or additions (Bassing et al., 2002). This process generates a highly diverse set of variable domains from a limited number of gene segments.

To further refine an antibody for high-affinity antigen binding, the variable region exons of B cells undergo somatic hypermutation in the germinal centres, which is the introduction of point mutations at a high rate (Dudley et al., 2005; Lau & Brink, 2020). During the affinity maturation process, B cells that express antibodies with high affinity for the foreign antigen are positively selected, and those with reactivity towards self-antigens are removed. The positively selected B cells will eventually undergo differentiation into plasma cells or memory B cells (Toyama et al., 2002)

The choice of antibody isotype generated in response to an infection is governed by complex cytokine programming and is biased towards the type of pathogen encountered (Manis et al., 2002; Stavnezer, 1996). In the process of class switch recombination, B cells can undergo sequential genomic rearrangements to change the isotype expressed and alter antibody effector functions (IgD>IgM>IgG>IgE>IgA). With each rearrangement, the DNA sequences of the existing heavy chain are irreversibly deleted, resulting in permanent changes to the secreted antibodies (Dudley et al., 2005; Stavnezer et al., 2008). In humans, viral infections typically trigger the secretion of IgG1 and IgG3 antibodies (Ferrante et al., 1990), whereas bacteria induce IgG2 responses (Vidarsson et al., 2014). Other isotypes, such as IgA, are required for specialised immune defence in mucosal tissues (Vidarsson et al., 2014). Antibodies that have undergone robust germinal selection and class switching are secreted by plasma cells (Ackerman et al., 2011). Finally, the antibodies can engage with a range of host cells and factors to activate cytotoxic activity against pathogens, infected cells, and tumour cells.

A final source of antibody diversity occurs at the population level because of naturally occurring allelic variation among antibodies. The most striking differences are found in IgG antibodies, where there are differences in the length and flexibility of the hinge region between and within subclasses. This variability determines the possible conformations of the Fab arms and Fc domains (Hamilton, 1987; Jay et al., 2018). Therefore, this variation can affect the binding of the Fc region to FcRs (Yogo et al., 2019). Additionally, multiple studies have shown that the hinge length of IgG influences neutralisation strength and the magnitude of Fc-mediated effector functions (Chu et al., 2020; de Taeye et al., 2020; Foss et al., 2022; Richardson et al., 2019).

1.2 Fc receptors

Fc receptors (FcRs) bind to antibody constant regions to modulate humoral and innate immunity, where they play a crucial role in the clearance of infections (Mkaddem et al., 2019). They are expressed on the surface of many haematopoietic lineages (e.g. macrophages, dendritic cells, and natural killer cells), and all antibody classes can bind to at least one type of FcR (Mkaddem et al., 2019; Takai et al., 2002). As a rule, the FcRs are named for the antibody class they recognise and bind to. Humans have several classes of FcRs, which are broadly classified into FcαRs (bind to IgA), FcμRs (bind to IgM), FcγRs (bind to IgG), and FcεRs (bind to IgE) (Kubagawa et al., 2009; Mancardi & Daëron, 2014). Each of these FcR classes has multiple members. The FcεR, for instance, is subdivided into FcεRI and FcεRII (Bruhns et al., 2005).

1.2.1 IgA, IgM, and IgE receptors

The high-affinity receptor for IgA, FcαRI/CD89, is capable of triggering multiple effector functions upon IgA binding, such as antibody-dependent cellular cytotoxicity (ADCC), endocytosis, phagocytosis, and release of inflammatory mediators (Li et al., 2017; Otten & van Egmond, 2004). FcαRI is only found on cells of the myeloid lineage, such as neutrophils and eosinophils, where it mediates endocytosis and recycling of IgA (Monteiro & van de Winkel, 2003). Another human receptor that binds to IgA but also to IgM is the Fcα/μR, which is found on follicular dendritic cells and is involved in the initial stages of the immune response

to microorganisms (Kikuno et al., 2007; Shibuya et al., 2000). The receptor that binds specifically to IgM is the FcμR, which is expressed mainly in adaptive immune cells such as B and T cells (Kubagawa et al., 2009).

For IgE antibodies, there are the high- and intermediate-affinity IgE receptors, known as FcεRI and FcεRII, respectively (Bruhns et al., 2005). The high-affinity receptor drives inflammation and allergic responses and triggers the adaptive immune response upon parasite infection (Arthur & Cruse, 2022). The intermediate-affinity receptor, FcεRII, transports IgE or IgE-immune complexes through enterocytes and can selectively transport IgE into colostrum (Hine et al., 2010; Yang et al., 2000).

1.2.2 IgG receptors

Regarding the FcRs that bind to IgG molecules, FcγRs are essential in the control of innate immune effector cell activation and the control of whether an immunogenic or tolerogenic response is triggered upon antigen recognition (Nimmerjahn & Ravetch, 2007). Humans express six different classical (or type I) FcγRs: FcγRI/CD64, FcγRIIa/CD32a, FcγRIIb/CD32b, FcγRIIc/CD32c, FcγRIIIa/CD16a, and FcγRIIIb/CD16b (Coënon & Villalba, 2022). These receptors belong to the immunoglobulin receptor superfamily because the IgG binding region contains two or three immunoglobulin domains (Sondermann et al., 2001). In addition, as part of the non-canonical (or type II) FcγRs, there are the tripartite motif-containing protein 21 (TRIM21), the FcR-like receptors (FcRL1-6), the lectin-like type II receptors (CD23 and CD209), and the neonatal Fc receptor (FcRn) (Foss et al., 2016; Wilson et al., 2012).

1.2.2.1 Classical Fcγ receptors

Within the classical FcγR class, there are both high- and low-affinity receptors with either activating or inhibitory functions (Ackerman et al., 2011). It is, therefore, unsurprising that each IgG subclass binds to a unique pattern of FcγRs with different binding affinities (Table 1.1), resulting in a precisely orchestrated set of effector functions (Bruhns et al., 2009). Studies have shown that the magnitude of the effector functions caused by the binding of IgG molecules to FcγRs is influenced

by the binding affinity of the antibody to the receptor, although it is not a direct correlation (Chu et al., 2020; Richards et al., 2008). The intensity of the immune response is also affected by the expression pattern of the FcRs on the cells, which, in turn, is influenced by the cytokine environment and the specific tissue niche where the cells are found (Delidakis et al., 2022). Together, these factors enable tight regulation of antibody-mediated adaptive immune responses (Nimmerjahn & Ravetch, 2008).

Table 1.1. Binding affinities of IgG subclasses to human FcγRs measured by surface plasmon resonance (SPR). The table shows the dissociation constant (K_D) in mol/L of each IgG subclass for the type I FcγRs. Results from Patel et al. (2013). "ND" stands for "not determined".

IgG subclass	FcγRI K_D (M)	FcγRIIa K_D (M)	FcγRIIb K_D (M)	FcγRIIIa K_D (M)	FcγRIIIb K_D (M)
IgG1	1.23E-10	8.00E-07	3.10E-06	8.50E-07	1.90E-06
IgG2	1.40E-06	3.78E-07	6.80E-06	2.20E-06	ND
IgG3	7.90E-11	8.97E-08	1.30E-06	3.90E-07	1.44E-06
IgG4	6.90E-10	6.00E-07	1.70E-06	3.46E-06	4.60E-06

The high-affinity IgG receptor, FcγRI/CD64, is an FcRγ-associated activating receptor that mediates endocytosis and phagocytosis functions (Anderson et al., 1990; Daëron, 1997; Duchemin et al., 1994). FcγRI interacts with the Fc region of IgG3 antibodies with a dissociation rate constant of 7.90×10^{-11} mol/L (Table 1.1), and it is the only FcγR that displays sub-nanomolar affinity for IgG (Bournazos & Ravetch, 2017).

In contrast, the lower affinity FcγRs have dissociation constants mostly in the micromolar range, with the exception of FcγRIIa, which displays affinities for IgG in the nanomolar range (Patel et al., 2013). The low-affinity and single-chained receptors FcγRIIa/CD32a and FcγRIIc/CD32c are found mainly on myeloid lineage cells, such as macrophages, neutrophils, megakaryocytic cells, and platelets (Daëron, 1997). FcγRIIa is the only FcγR that can significantly bind to IgG2 (Bruhns et al., 2009). Interestingly, there are two polymorphic variants of FcγRIIa with different binding properties. The one with arginine at position 131 (R131) has

a decreased affinity for IgG2, which lowers the phagocytic potential of IgG2 against a bacterial infection (Beppler et al., 2016). On the other hand, the variant with a histidine residue (H131) displays a high affinity for C-reactive protein, which is highly expressed during infection.

The only inhibitory FcγR, FcγRIIb/CD32b, is a single-chain receptor found on myeloid cells and B lymphocytes and shares 96% sequence identity with FcγRIIa/CD32a (Bruhns et al., 2009; Daëron, 1997). This receptor is essential for the regulation of IgG-mediated inflammation, B cell activation and selection, and the development of self-tolerance of the immune system (Bournazos & Ravetch, 2017; Nimmerjahn & Ravetch, 2008). Decreased expression of this receptor has been associated with the development or exacerbation of autoimmune diseases (Nimmerjahn & Ravetch, 2008).

Similarly to FcγRI, FcγRIIIa/CD16a is an activating receptor that modulates endocytosis of immune complexes and phagocytosis but binds to IgG less tightly than FcγRI (Bournazos & Ravetch, 2017; Daëron, 1997). FcγRIIIa is expressed mainly by human natural killer (NK) cells but also by T cells, macrophages, monocytes, and neutrophils (Björkström et al., 2008; Bruhns et al., 2009; Daëron, 1997). Furthermore, FcγRIIIa mediates antibody-dependent cellular cytotoxicity (ADCC) and is, therefore, a key target of antibody therapeutics for cancer treatments (Jefferis et al., 1998; Wang et al., 2015). FcγRIIIa can interact with all the IgG subclasses, although it binds to IgG1 and IgG3 with the highest affinity.

Finally, the FcγRIIIb/CD16b is a single-chain IgG receptor only found on neutrophils (Daëron, 1997). This unusual receptor has no signalling domains but is, instead, anchored by a glycosyl phosphatidyl inositol (GPI) domain (Yang et al., 2018). The signalling activity of FcγRIIIb for cell activation, particularly of neutrophils, remains unclear but likely involves associations with other FcRs (Bournazos et al., 2016; Bruhns et al., 2009).

Beyond the differences in binding affinity of the IgG subclasses to the Fcγ receptors, previous studies have shown that there is variability in binding affinity between population-level allelic variants of the same antibody subclass (de Taeye et al., 2020; Richardson et al., 2019). These variants have amino-acid mutations in the constant

heavy and/or light chains. For instance, the mutations E419 and K392 in IgG3 have been shown to enhance binding to FcγRIIIa and FcγRIIb and lead to stronger ADCC responses (Richardson et al., 2019; Warrender & Kelton, 2020). This finding shows that even point mutations can affect the binding affinity of antibodies to FcRs and potentially affect the Fc-mediated effector functions as well.

1.2.2.2 Non-canonical Fcγ receptors

With respect to some of the non-canonical FcγRs, TRIM21 is an intracellular receptor that binds to IgG and E3-ligase to clear viruses by antibody-dependent intracellular neutralisation (ADIN) (Foss et al., 2016). TRIM21 is, therefore, part of the last line of defence against pathogens that have reached the intracellular environment (Foss et al., 2022). In contrast to the classical FcγRs, TRIM21 is expressed in all tissues, not just haematopoietic cells, and is the highest affinity antibody receptor in humans (Bottermann et al., 2016).

Most FcR-like receptors contain both activating and inhibitory motifs and, hence, are speculated to be involved in the dual modulation of B cell activation (Capone & Matthew, 2016). For instance, FcRL4 and FcRL5 are involved in the modulation of innate and adaptive immunity by costimulating or inhibiting B cell signalling. FcRL4 and FcRL5 are expressed mainly by B cells and can bind to IgA and IgG, respectively (Wilson et al., 2012).

FcRn is an essential mediator of the plasma half-life of IgG antibodies (Ghetie et al., 1996). The half-life regulation is dependent on the uptake of IgG and its binding to FcRn in acidified endosomes. Thereupon, the FcRn-IgG complex escapes lysosomal degradation and is recycled to the cell surface (Goebl et al. 2008). Subsequently, contact with near-neutral pH in the blood leads to the extracellular release of IgG antibodies. Polymorphisms created by allelic variation can also have a significant influence on binding to this receptor. Most notably, the polymorphism H435R (arginine in the place of histidine at position 435) in the heavy chain of IgG3 antibodies reduces binding affinity to FcRn at pH 6 but enhances the binding at physiological pH (Shah et al., 2017).

1.2.2.3 Fcγ receptor signalling

The activating FcγRs require immunoreceptor tyrosine-based activation motifs (ITAMs) to induce cell signalling (Nimmerjahn & Ravetch, 2007). Aside from FcγRIIa and FcγRIIc, which are single-chain FcγRs with cytoplasmic tails, ITAM signalling is achieved by FcγR association with a common FcR γ-chain (Masuda & Roos, 1993; Ra et al., 1989; Takai, 2002). This chain interacts with the ligand-binding subunit (α-chain) of the majority of activating FcγRs (Ernst et al., 1993). As part of the late signalling pathways following FcγR ITAM crosslinking, activation of the transcription factor NFAT (nuclear factor of activated T cells) occurs in T cells, NK cells, and myeloid cells (Figure 1.2) (Bournazos et al., 2016; Fric et al., 2012). Initially discovered in T cells, NFAT proteins are expressed in most immune cells and are essential in the transcription of cytokine genes and other essential immune response genes (Rao et al., 1997). For instance, in T cells, NFAT proteins are involved in cell activation, control of thymocyte development, T cell differentiation, and self-tolerance (Macian, 2005). In NK cells, FcγRIIIa stimulation induces the transcription of NFAT-dependent cytokines, such as interferon-gamma (IFN-γ) and tumour necrosis factor (TNF), which are important in the innate immune response (Fric et al., 2012). Overall, signalling via the ITAM of FcγRs can induce a wide range of effector responses, including oxidative burst, phagocytosis, cytokine release by macrophages, ADCC by NK cells, and mast cell degranulation (Takai, 2002).

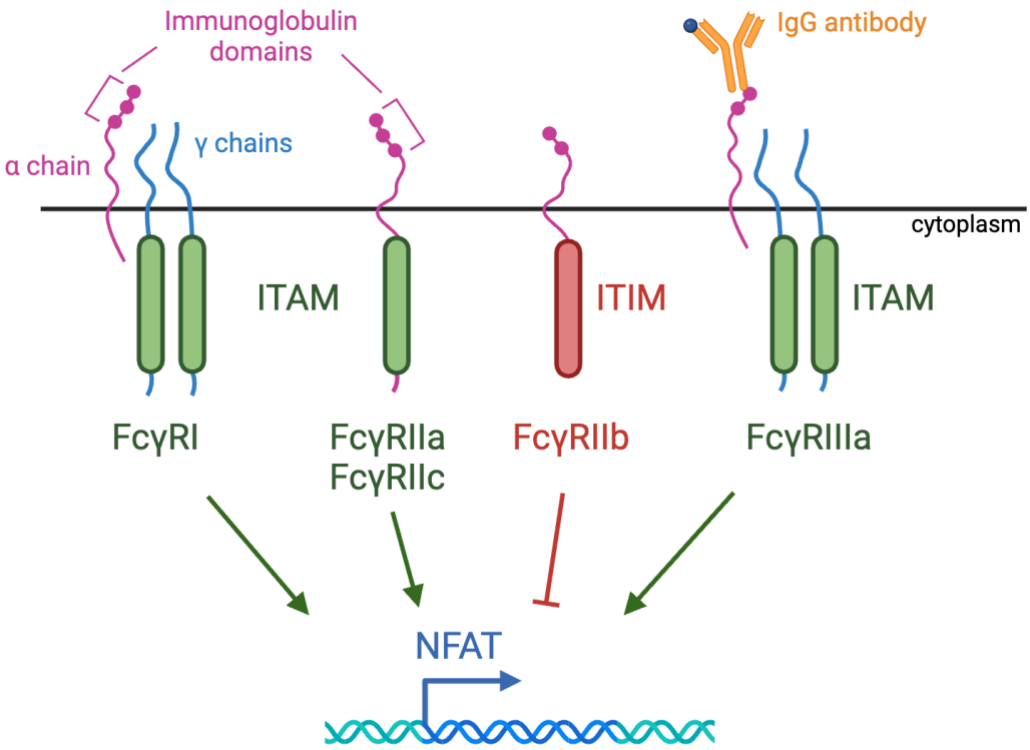

Figure 1.2. Signalling of immunoreceptor tyrosine-based activation motif (ITAM) and immunoreceptor tyrosine-based inhibition motif (ITIM) from FcγRs. All activating FcγRs contain an ITAM and have a similar signalling cascade following receptor cross-linking, which leads to NFAT expression (Bournazos et al., 2016). As an inhibitory receptor with an ITIM, FcγRII directly antagonises the stimulatory signals of the activating FcγRs. Figure made using BioRender: https://www.biorender.com/.

As for the inhibitory FcγRIIb, this receptor contains an immunoreceptor tyrosine-based inhibition motif (ITIM), which is most widely known for preventing B cell activation (Bournazos et al., 2016; Daëron, 1997). In addition to modulating B cell activity, ITIM signalling is a tolerance checkpoint for humoral immunity and serves as a key negative regulator in reactions triggered by immune complexes (Mkaddem et al., 2019; Nimmerjahn & Ravetch, 2008).

1.3 Fc-mediated effector functions

Antibodies trigger potent effector mechanisms upon FcR and antigen binding to clear disease. These responses are dependent on the antibody subclass involved and can be broadly classified into those that involve cellular responses and those that do not (Vidarsson et al., 2014). Antibody-induced cellular responses are highly

varied and can include antibody-dependent cell cytotoxicity (ADCC), antibody-dependent cellular phagocytosis (ADCP), complement-dependent cytotoxicity (CDC), trogocytosis, cytokine release, neutrophil extracellular trap (NET)osis, and antigen presentation (Bournazos & Ravetch, 2017; Lu et al., 2018; Miyake & Karasuyama, 2021; Vorobjeva & Chernyak, 2020). It is likely the full spectrum of responses mediated by the binding of the Fc region to FcRs remains incompletely described, although the best understood are ADCC and ADCP.

FcγRIIIa/CD16a is the main receptor involved in driving ADCC cytotoxic responses against target cells (Figure 1.3) (Richards et al., 2018). The response is initiated by the interaction of the Fc region of IgG antibodies with FcγRIIIa on NK or myeloid cells, leading to multiple signalling events, including the translocation of NFAT to the nucleus (Coënon & Villalba, 2022; Parekh et al., 2012). This transcription factor induces the expression of genes involved in the ADCC response, stimulating the release of cytokines, such as IFNγ and cytotoxic granules with perforin and granzymes (Parekh et al., 2012).

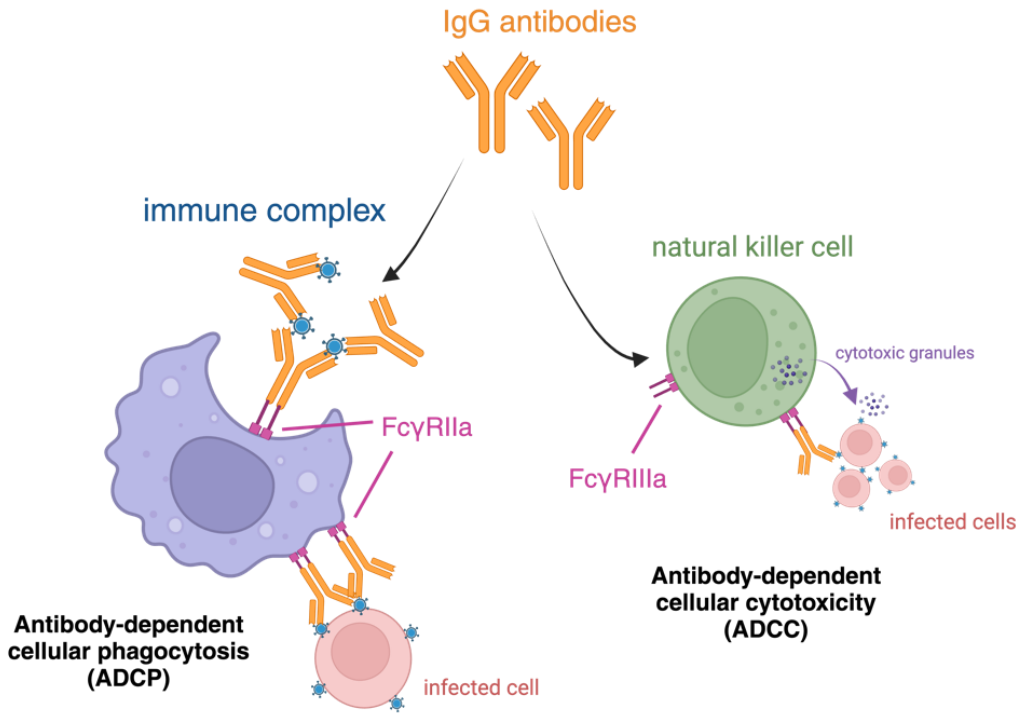

Figure 1.3. Mechanisms of antibody-dependent cellular phagocytosis (on the left) and antibody-dependent cellular cytotoxicity (on the right). Figure made using BioRender: https://www.biorender.com/.

On the other hand, ADCP is mediated by FcγRI/CD64, FcγRIIa/CD32a, and FcγRIIIa/CD16a (Brady et al., 2023). The ADCP response has an important role in the clearance of infections, innate immune activation, and the triggering of antigen presentation (Ackerman et al., 2011). In this process, multiple immune cells can act as phagocytes, such as macrophages, dendritic cells, monocytes, and mast cells. FcγR activation leads to cytoskeletal rearrangements and, eventually, the formation of a phagosome with the immune complex or target cell that was coated with antibodies (Cleary et al., 2017; Unkeless et al., 1995). Subsequently, the contents of the phagosome are degraded by lysosomal enzymes within the cell (Berón et al., 1995).

The activation of CDC, which is part of the first line of defence against pathogens, can be initiated by the binding of C1q to antigen-complexed IgG or IgM (classical pathway), by the recruitment of mannose-binding lectin (MBL) or ficolins to antibody-opsonised targets (lectin pathway), or by spontaneous hydrolysis of C3 (alternative pathway) (Lu et al., 2018; Merle et al., 2015). The three pathways lead to C3 cleavage and the formation of C3b bound to pathogens or infected cells and, subsequently, the engulfment of the opsonised target by phagocytes that express receptors for C3b. The last few stages of the complement activation pathway involve the assembly of C5b and C6-9 into a membrane attack complex that will directly destroy the target (Merle et al., 2015; van Erp et al., 2019).

1.4 Antibodies as therapeutics

Because of the ability of antibodies to target cells for destruction, they are widely used clinically for the treatment of cancer, autoimmune diseases, and cardiovascular diseases (Jay et al., 2018). Among the antibody classes, IgG antibodies are the most popular as therapeutics due to their long half-life and their ability to induce both complement activation and FcγR-mediated effector functions (Temming et al., 2019). Since antibodies have distinct functional domains, separate parts of the molecule can be independently engineered. For example, the VH can be engineered to improve affinity for an antigen, or the Fc domain can be modified to alter the FcR engagement profile depending on the treatment they are being developed for (Chowdhury & Wu, 2005; Lyu et al., 2022; Richards et al., 2008).

Antibody technology has rapidly developed since the first mouse monoclonal antibody (mAb) was developed in 1975 using hybridoma technology (Köhler & Milstein, 1975). This approach revolutionised antibody production by fusing immortal tumour cells with B cells (hybridomas) to produce large amounts of mAbs. However, one of the initial limitations of first-generation murine mAbs was a limited ability to trigger ADCC-coupled high immunogenicity in patients (van der Horst et al., 2020). To solve this challenge, chimeric versions were engineered with murine variable domains paired to human constant regions (Morrison et al., 1984). Further improvements resulted in humanised antibodies in which the complementarity-determining regions (CDR) from murine antibodies are grafted into a human VH framework sequence (Jones et al., 1996). The current state of the art is now to discover completely human mAbs using phage display libraries or transgenic mice containing fully human antibody gene loci (Jefferis & Lefranc, 2009).

In 1986, the first mAb was approved to be used as a therapeutic: the anti-CD3 OKT3, known as muromonab-CD3 (Lyu et al., 2022). It took a further 8 years for another antibody therapy to be approved. The pace of antibody development has since grown exponentially, and over 150 mAbs have now been approved for therapy (Lyu et al., 2022). This work uses one of these FDA (U.S. Food and Drug Administration) approved monoclonals, Rituximab, a humanised anti-CD20 IgG1 antibody for the treatment of B cell lymphomas (Lyu et al., 2022; Maloney et al., 1997). Rituximab binds directly to target tumour cells and aids tumour clearance via Fc-mediated effector functions (ADCC, ADCP, and CDC) or direct cell killing, in which the binding of the mAb to two CD20 molecules in separate tetramers causes the induction of lipid raft rearrangement and CD20 clustering in the tumour cells, leading to caspase-dependent apoptosis (Cleary et al., 2017; Constantinides et al., 2023).

Antibody properties such as half-life, antigen affinity, FcR binding, stability, and effector functions are commonly manipulated during the development of mAbs for immunotherapy (Chowdhury & Wu, 2005). A thorough understanding of the interaction of antibody isotypes with human ligands is essential when developing these therapeutics (Jefferis et al., 1998). There remains significant scope to improve

the clinical efficacy of current mAbs by better understanding and tuning the Fc-mediated effector functions that they trigger (Coënon & Villalba, 2022).

Most of the clinically approved mAbs are from the IgG backbone since this class displays superior pharmacokinetics and effector functions than the other antibody classes (Carter, 2006). However, only three of the four IgG subclasses (IgG1, IgG2, and IgG4) have favourable developability properties, even though IgG3 triggers the strongest Fc-mediated effector functions and has stronger neutralisation potential (Izadi et al., 2023; Richardson et al., 2019). Some of the biological limitations of the mAbs with IgG3 backbone, such as their shorter half-life compared to the other subclasses, could potentially be improved by engineering the Fc region to display higher affinity to FcRn (Izadi et al., 2023; Ko et al., 2022).

Already, some therapeutic antibodies have been engineered with modified Fc regions to increase their binding affinity to select FcRs and trigger stronger Fc-mediated effector functions, such as ADCC and ADCP (van der Horst et al., 2020). For instance, HuM195 is a mAb that contains an engineered Fc domain with the triple mutation Ser293Asp/Ala330Leu/Ile332Glu, known as DLE (Romain et al., 2014). The DLE mutant displays increased binding affinity to FcγRIIIa/CD16a and enhanced NK cell-mediated ADCC, but it has not been approved for therapeutic use by the FDA. Another example of an Fc-engineered mAb is Motavizumab, which contains the amino acid substitutions M252Y/S254T/T256E, known as YTE (Robbie et al., 2013). This variant displays a stronger binding affinity to human FcRn by approximately 4-fold at acidic pH, which confers an extended serum half-life (Brady et al., 2023; Robbie et al., 2013). In contrast, some mAbs engineered with YTE have shown reduced *in vitro* ADCC activity compared to mAbs without this mutation, possibly because they displayed lower binding affinity to FcγRIIIa (Brady et al., 2023). Considering that the introduction of mutations can have a range of effects, thoroughly understanding the possible outcomes of these manipulations is important when engineering mAbs.

In spite of the overall success of antibody therapies, immunogenicity has been an issue even for some of the human mAbs, such as adalimumab (Humira) (Jefferis & Lefranc, 2009). During treatment, mAbs can provoke undesired anti-drug antibody responses in certain subsets of patients. One potential driver of this issue is the

widespread presence of genetic polymorphisms among IgG antibodies (Jefferis & Lefranc, 2009; Rodriguez et al., 2023). This genetic variability is associated with possible differences in antibody-mediated responses between patients, which can affect the outcome of disease and responsiveness to therapeutics and vaccines (Kratochvil et al., 2017; Richardson et al., 2019; Rodriguez et al., 2023).

1.5 Genetic polymorphisms among human IgG antibodies

Despite the name, the constant region of IgG antibodies, including the hinge and the Fc region (Figure 1.1.), is genetically diverse across human populations (Calonga-Solís et al., 2019). There are polymorphisms in both the immunoglobulin heavy-chain constant (IGHC) (Figure 1.4.) and light-chain constant (IGLC) loci (Warrender & Kelton, 2020). Studies have shown that this diversity affects the stability (Warrender et al., 2023), structure (Jay et al., 2018; Vidarsson et al., 2014), and effector functions of the IgG antibodies (Chu et al., 2020; de Taeye et al., 2020; Richardson et al., 2019). This genetic variability may be the cause behind the varied antibody responses observed for infection and diseases such as cancer and autoimmunity across human populations (Rodriguez et al., 2023).

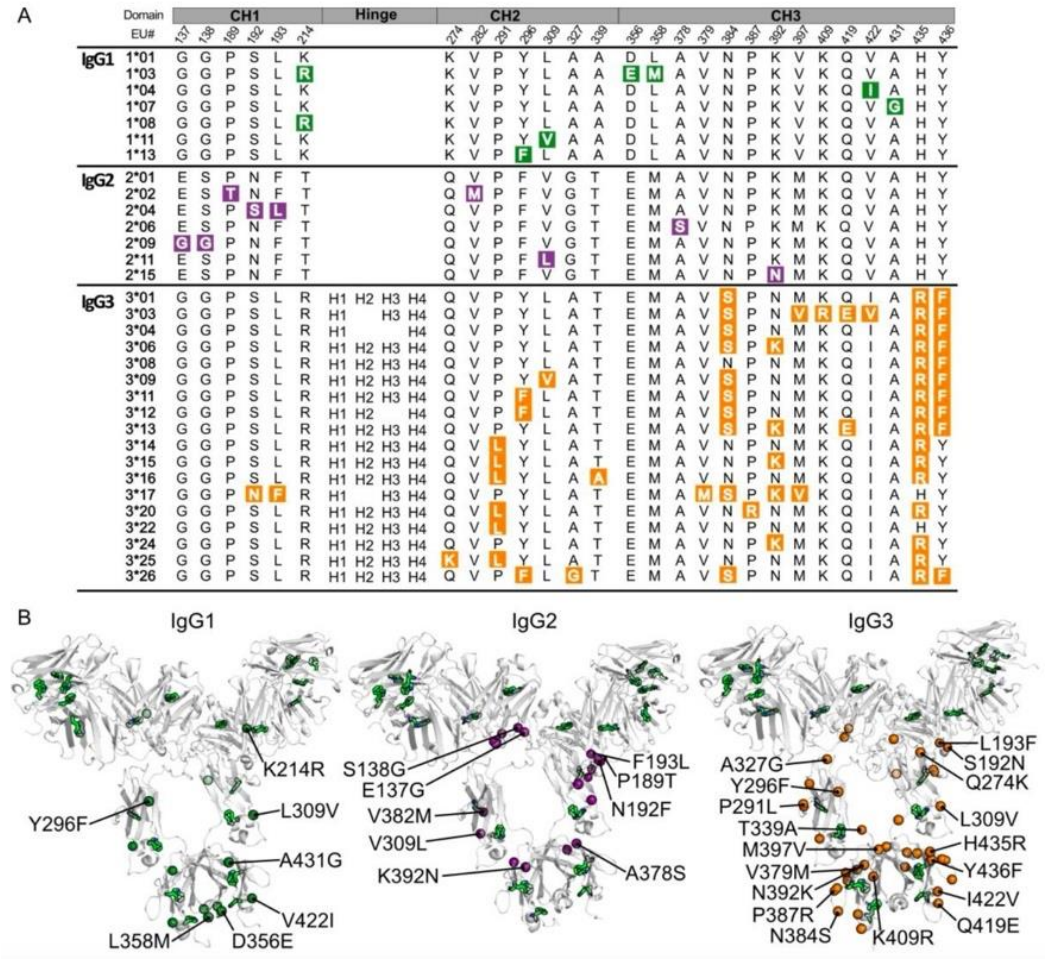

Figure 1.4. (A) Table of some of the known amino acid polymorphisms among IgG1, IgG2, and IgG3 subclasses. The amino acid position is based on the EU numbering. Most of the known allelic variants are from the IgG3 subclass. IgG1 and IgG2 have the same hinge sequence. IgG3 polymorphic variants have variability in the number of hinge exons. H1-4 refers to what exons are found in each allele. (B) Location of these allele polymorphisms on IgG1, IgG2, and IgG3 antibodies. Figure from Warrender et al. (2023).

Antibody genetic polymorphism was initially discovered in *ex vivo* serological studies, in which agglutination of erythrocytes was observed in a host serum following contact with antibodies in a donor serum (Grubb, 1956). Termed allotypes, they were identified predominantly in the heavy chain of IgG antibodies, but there are also allotypes among IgA and IgE antibodies and the kappa light chain (Jefferis & Lefranc, 2009; van Loghem et al., 1984). A unique nomenclature for allotypes was developed using the natural genetic marker (Gm) along with their subclass (e.g., G1m for IgG1 antibodies) and the allotype number, such as G1m3, in the case of IgG1*03 (Kratochvil et al., 2017). Likewise, IgA and IgE allotypes

are designated as Am and Em, respectively, and the kappa light chain variants are Km allotypes (Lefranc & Lefranc, 2020). The advent of modern genetic sequencing techniques has revealed many more polymorphisms that are not allotypes, i.e., they contain mutations to the constant region amino-acid sequence but do not have an immunogenic phenotype reported. It is also now known that amino-acid mutations in the constant heavy or light chain may be inherited in a codominant Mendelian fashion (Calonga-Solís et al., 2019; Jefferis & Lefranc, 2009; Kratochvil et al., 2017).

Both allotypic and polymorphic diversity among IgG antibodies have been useful markers in paternity testing and forensic medicine, mainly before the human leukocyte antigen (HLA) typing method was developed (Jefferis & Lefranc, 2009). Moreover, allotyping can be used to track genetic linkage between human populations, which is useful in the study of population genetics (Johnson et al., 1977).

1.5.1 Documented effects of constant region diversity

1.5.1.1 Infection and disease susceptibility

From a health perspective, some IgG allelic variants have been associated with susceptibility to cancer, autoimmunity, and infectious diseases (Calonga-Solís et al., 2019; Granoff & Holmes, 1992; Pandey et al., 2012; Pandey & Namboodiri, 2014). For example, Kratochvil et al. (2017) demonstrated that IgG1 allotypes influence the quality of HIV-vaccine-induced humoral responses by affecting the distribution of IgG subclasses following vaccination and, consequently, the antibody effector functions triggered. They found that HIV-vaccine recipients who were carriers of a certain IgG1 allele (G1m1) had higher vaccine-induced IgG1:IgG2 ratios than other recipients. This allele was associated with enhanced FcγR engagement due to the higher affinity of IgG1 over IgG2 and, potentially, stronger ADCC and ADCP responses. There is, likewise, evidence that the allelic variation in the hinge region and CH3 domain of IgG3 influences the response to vaccination and the efficacy of passive immunisation by affecting neutralisation potency and the magnitude of Fc-mediated effector functions (Richardson et al., 2019).

For cancer indications, Pandey et al. (2012) determined that allelic variation affects the antibody response of cancer patients to specific tumour antigens, and certain variants are associated with increased ADCC activity against breast cancer cells. Additionally, an investigation by Pandey & Namboodiri (2014) showed that different combinations of three IgG1 allotypes and two FcγRIIIa variants lead to significantly distinct intensities of the ADCC response against prostate cancer cells. Given the potential influence on natural antibody function by constant region polymorphisms, it is important to understand the functional differences between these variants and the different ways people respond to cancer treatments and vaccines in order to produce more effective therapeutic mAbs and vaccines.

1.5.1.2 Antibody stability

When developing therapeutic antibodies, it is essential to consider the thermal stability of the mAbs. For robust clinical efficacy and reliability, mAbs should be engineered for both high activity and stability (Knight et al., 2020). Thermal stability is associated with the dynamic flexibility of the protein structure, as protein scaffolds that are more rigid (less flexible) have shown enhanced thermal stability (Karshikoff et al., 2015). Nonetheless, the stability of a protein is not dependent on the absence of internal fluctuations and mobility. In the case of antibodies, those that exhibit more intradomain flexibility tend to be less stable than the more rigid antibodies (Warrender et al., 2023).

With the development of red edge excitation shift (REES), it became easier to assess the structural dynamics of antibodies and their thermal stabilities using common laboratory equipment (Warrender et al., 2023). This technique uses the fluorescent properties of tryptophan (Trp) residues to determine the conformational state of the protein molecules (Catici et al., 2016). In addition, REES can be used to qualitatively measure changes in the free energy of the proteins and assess the equilibrium of the conformational states. REES measurements of IgG3 antibodies showed this subclass displays the lowest overall stability of all IgG subclasses as characterised by enhanced exposure of hydrophobic residues to the surrounding aqueous environment and a loss of structural flexibility after undergoing thermal stress. These measurements were further confirmed by differential scanning fluorimetry (DSF) measurements, where the temperatures at which IgG3 molecules

underwent the unfolding transitions were significantly lower (up to 3°C) than those of IgG1 and IgG2 (Warrender et al., 2023). This data is further evidence that IgG3 antibodies are the most prone to aggregation, whereas IgG1 is the most stable subclass, followed by IgG2 and IgG4 (Ito & Tsumoto, 2013; Warrender et al., 2023).

Deeper analysis of polymorphic IgG3 allelic variants by Warrender et al. (2023) has shown that those with longer hinge regions (i.e., more hinge exons) displayed improved thermal stability. In this study, there were considerable differences in stability between variants with three and four hinge exons, in which there were significantly smaller changes in REES parameters for the four-exon variants compared to the three-exon variants. Furthermore, variants with Arg-435/Tyr-436 mutations showed greater stability than those with His-435/Tyr-436 or Arg-435/Phe-436. This is likely due to the limited motion of CH2 relative to CH3 caused by the interactions of Arg-435 with Leu-251 and Ile-253, making the structure more rigid than that of variants that contain His-435. Additionally, the hydroxyl group of Tyr-436 has the potential to improve the stability of the molecule by forming hydrogen bonds with Ser-426 and Gln-438, which does not occur in variants with Phe-436. This demonstrates that point mutations have the potential to significantly affect the stability of the constant region of IgG antibodies. Overall, IgG1*01 proved to be the most stable of the allelic variants tested in the study (Warrender et al., 2023).

The lower thermal stability of IgG3 compared to the other subclasses makes it prone to aggregation even when exposed to minor temperature variations (Ito & Tsumoto, 2013; Knight et al., 2020). Because therapeutic antibodies need to be stable in order to be effective, the weaker stability of IgG3, along with its shorter half-life, renders it a less attractive option as the backbone for therapeutics than the other antibody subclasses (Ito & Tsumoto, 2013).

1.5.1.3 Antibody structure and flexibility

While IgG1 is composed of a hinge of 15 amino acids and both IgG2 and IgG4 have short hinges of 12 amino acids, IgG3 antibodies can have longer hinges of up to 77 amino acids (five exons) (Bashirova et al., 2021; Vidarsson et al. 2014). The extended hinges of the IgG3 allelic variants are composed of differing numbers of

exons - between two and five. The upper-hinge exon is 17 amino acids long, and the middle-hinge exon is 15 amino acids long and can be in a combination of one to four exons (Bashirova et al., 2021; Roux et al., 1998). Consequently, the shortest hinge among the IgG3 variants is composed of 32 amino acids, which is more than twice as long as the hinge of the other subclasses.

The hinge length of antibodies determines the degree to which the Fab domains can move in relation to the Fc region (Chu et al., 2020). The fact that IgG3 antibodies have a longer hinge facilitates conformational changes around the antibody binding sites and can prevent steric hindrance when binding to FcγRs, thus allowing easier binding (Canfield & Morrison, 1991; Lu et al., 2007). In contrast, shorter hinges facilitate the contact between target and effector cells, which might lead to more efficient cell signalling and transfer of cytotoxic granules (de Taeye et al., 2020). Not only does hinge length considerably affect Fc-mediated effector functions, but it also affects the binding of antibodies to antigens (Spiteri et al., 2021).

To better understand how differences in hinge length can affect antibody function in detail, it is useful to define the structural configurations and dynamics of the various allelic variants. Since IgG molecules have high flexibility and are, therefore, difficult to crystallise, structural studies using X-ray crystallography have proved to be quite challenging for full-length antibodies (Belviso et al., 2022; Spiteri et al., 2021). Instead, solution-based small angle X-ray scattering (SAXS) has been used to study full-length antibody dynamics and their flexibility and compare the ensembles of structural configurations between subclasses (Ashish et al., 2010; Belviso et al., 2022; Eryilmaz et al., 2013; Hui et al., 2019; Spiteri et al., 2021). For instance, by using SAXS, Eryilmaz et al. (2013) found that there are major differences in the angles between the Fab arms and Fc region among IgG1 and IgG3 antibodies. Because it is a low-resolution technique, SAXS is often used in combination with other complementary methods, such as cryo-negative-staining (cryo-NS) and analytical ultracentrifugation along with computational modelling (Belviso et al., 2022; Jay et al., 2018; Spiteri et al., 2021).

Prior to this project, SAXS was used to compare the flexibility of IgG3 hinge polymorphisms for a series of trastuzumab (anti-HER2) variants with the Herceptin variable domain sequence (Warrender, 2023). This data showed that longer hinges

conferred more flexibility than shorter hinge regions. Moreover, low-resolution bead models of IgG3 variants showed distinct structural conformations for variants of different hinge lengths. This data provides a preliminary snapshot into the power of SAXS analysis for comparing the structural dynamics and flexibility of polymorphic variants, which will lead to a deeper understanding of the reasons behind differences in Fc-mediated effector functions.

1.5.1.4 Fc-mediated effector functions

It has recently been observed in a series of systematic studies that polymorphisms among IgG antibodies influence the strength of the ADCC and ADCP responses that are triggered (de Taeye et al., 2020; Richardson et al., 2019). However, the variants triggering stronger ADCC responses among their subclass are not necessarily the same variants that can trigger stronger ADCP.

Prior work has shown that the length of the IgG hinge region affects the magnitude of FcγR-mediated effector functions (Chu et al., 2020; de Taeye et al., 2020). Differences in hinge length and mutations in the Fc domain, predominantly within the CH2 domain of IgG3 allelic variants, considerably affected binding to FcγRIIIa/CD16a and the strength of the ADCC response triggered (de Taeye et al., 2020). In this context, IgG3 allotypes with shorter hinges are known to trigger stronger ADCC than allotypes with longer hinges.

In contrast to the responses observed in ADCC assays, a study using HIV-specific antibodies found IgG3 variants with longer hinges instead triggered greater ADCP responses (Chu et al., 2020). This result was also observed when hinge regions of 62 amino acids were inserted into IgG1 antibodies, whereas IgG3 variants that were engineered with hinges of 15 amino acids showed significantly reduced ADCP (Richardson et al., 2019). The extended hinge led to enhanced ADCP possibly because it can reduce the steric hindrance when the antibody is binding to the FcγRs and allow for more productive conformational changes (Canfield & Morrison, 1991; Lu et al., 2007).

Both ADCC and ADCP are important mechanisms driving the clinical efficacy of many mAbs for cancer treatment (Gül et al., 2014; Pandey & Namboodiri, 2014). However, Jefferis and Lefranc (2009) showed that most of the mAbs being used

clinically at the time, including Rituximab, were based on a select few allelic variants of the constant domain, mainly the IgG1 allotypes G1m3 and G1m17,1. Given that there is genetic variability among natural IgG antibodies, determining which hinge length and constant domain sequence confer mAbs with enhanced ADCC and ADCP responses is relevant for designing future antibody drugs.

To determine the differences in the magnitude of ADCC response between constant region alleles, previous studies have performed reporter gene assays using a Jurkat cell line engineered to express human FcγRIIa or FcγRIIIa and target cells expressing anti-CD20 (Cheng et al., 2014; Parekh et al., 2012). The Jurkat cell line contains the NFAT signalling pathway, which drives the expression of the reporter gene luciferase in these effector cells. In the case of ADCP responses, reporter gene assays using the Jurkat cell line and luciferase expression system had not been used previously to test the differences in this immune function between IgG allotypes.

To assess differences in ADCP response between some of the IgG1, IgG2, IgG3, and IgG4 allotypes, Crowley et al. (2023) used a phagocytosis assay of THP-1 cells and fluorescent beads coated with biotinylated antigen. The aim was to assess the impact of combinations of single-point amino-acid polymorphisms in the CH1, CH2, and CH3 domains on the ADCP response. All the IgG3 tested were modified to have the same hinge length to avoid its influence on the effector function. For the allotypes tested, this study showed that the genetic variability in these domains does not appreciably alter FcγR-mediated effector functions or antigen recognition.

Previous studies have used assays with monocytes, neutrophils, or macrophages to assess differences in ADCP response (Chu et al., 2020; Crowley et al., 2022; Richards et al., 2008; Richardson et al., 2019). There are different types of FcγRs on these cells, and possibly polymorphic variants as well, for the IgG antibodies to bind to. The presence of different receptors can influence the strength of the ADCP triggered due to the distinctions in binding affinity (Bruhns et al., 2009; Talathi et al., 2019). To reduce the number of variables affecting the ADCP response, genome-engineered effector cells with only FcγRIIa on their surface can be used to assess the effects of the genetic polymorphisms of IgG on ADCP. Furthermore, the effects on the ADCP response of the natural allelic diversity in the full antibody

structure had not been assessed. This work aimed to explore these effects using effector cells with only FcγRIIa on their surface.

1.6 Research objectives

This project sought to systematically analyse a panel of human IgG allelic variants to build towards a deeper mechanistic understanding of how variant sequence influences function. The main objective was to determine if differences in structural dynamics between polymorphic variants align with observed variability in Fc-mediated effector functions such as ADCP. There were three main aims for the project:

1. Use small angle X-ray scattering (SAXS) to explore how the differences in IgG hinge lengths affect the variant flexibility. Here, we compared the dynamics of IgG antibodies with different variable domains (anti-CD20 and anti-HER2).
2. Perform ADCC assays using a genome-engineered reporter cell line and anti-CD20 IgG polymorphic variants. These ADCC results were compared to those described in the literature and provided validation of the assay method that we developed.
3. Perform ADCP assays with a genome-engineered reporter cell line and anti-CD20 IgG polymorphic variants using the methods developed in Aim 2. These assays provided new information on how the genetic polymorphisms in the hinge region of IgG molecules affect the intensity of the ADCP response triggered – this data has not been reported in the current literature.

2 Chapter Two

Materials and Methods

2.1 Antibody variant selection

Seven IgG allelic variants (IgG1*01, IgG2*02, IgG3*01, IgG3*03, IgG3*04, IgG3*08, and IgG3*12) were selected for the structural studies using small angle X-ray scattering (SAXS) and the functional assays (ADCC and ADCP assays). These variants were selected to cover the natural diversity in allelic hinge variation (12, 15, 32, 47, and 62 amino-acid long hinges). The exon sequences for the seven human IGHG1, IGHG2, and IGHG3 genes (Appendix A1) were obtained from the International Immunogenetics Information System® (IMGT) database (Giudicelli et al., 2006).

For hinge lengths with multiple variants the hinge exons are identical, however, each allele contains polymorphisms outside this region. By selecting variants with the fewest amino acid polymorphisms, we have reduced confounding effects from the point mutations. This approach makes deconvolution of the influence of the hinge length on the antibody structure and Fc-mediated effector functions easier. We have only used variants defined in the internationally recognised IMGT database, although it should be noted that there are recent reports of IgG3 variants outside this select population (Bashirova et al., 2021; Ford et al., 2023).

2.2 Cloning plasmid for transformation into *Escherichia coli* cells

All seven alleles were ordered from Twist Bioscience™ as gene fragments cloned into pTwist CMV BetaGlobulin WPRE Neo vectors (Twist Bioscience™). The plasmid vectors were originally ordered containing anti-HER2 variable heavy chain sequences from Herceptin, which were then replaced by either anti-CD20 or anti-human adenovirus 5 (AAV5) hexon variable heavy sequences. To express full-length heavy chains, the constant region allelic sequences were attached to plasmid vectors with anti-CD20 or anti-AAV5 sequences and to a rabbit IGHG endoplasmic reticulum signal sequence (Appendix A1). The anti-CD20 variable domain sequence (Appendix A1) is from Rituximab chimeric anti-CD20 obtained from the

IMGT monoclonal antibodies database (IMGT/mAb-DB) (Lefranc et al., 2009). The anti-AAV hexon variable domain sequence (Appendix A1) was obtained from antibody 9c12 from Bottermann et al. (2016). For all variants, a universal light chain was made by joining either the anti-CD20 or anti-AAV5 variable light chain sequence to the human IGKC*01 kappa constant allele with a rabbit IGKC signal peptide (Appendix A1). Dr Annmaree Warrender provided valuable assistance in cloning the plasmids with anti-CD20 alleles.

2.2.1 Restriction digest of plasmids

Restriction digests were performed to excise constant region sequences by adding 1 µL of either XhoI or NheI along with 1 µL of ClaI (New England BioLabs) to 1000 ng of plasmid in rCutSmart™ Buffer (New England BioLabs) and ultrapure water. Restriction digests were performed on both the plasmid vector backbone (pTwist CMV BetaGlobulin WPRE Neo vectors) and individual allelic inserts (Twist Bioscience™). Reactions were incubated for 1 hour at 37 °C in a T100 Thermal Cycler (Bio-Rad).

Electrophoresis was used to isolate digested samples using a 1.5% agarose gel. Briefly, 0.6 g of agarose in 40 mL of Tris-acetate-EDTA (TAE) buffer (Appendix B) was heated until boiling, and 4 µL of 10,000x thiazole orange dye (13 mg/mL stock in DMSO) was added to the gel prior to casting. 10 µL of DNA Loading Dye (New England BioLabs) was added to each digested sample. 5 µL of SiZer™ 1000 plus was added to one of the wells in each gel. The gel was run at 100 V for 40 min. Afterwards, the desired band was extracted from the gel and then purified using the QIAquick Gel Extraction Kit (Qiagen) according to the manufacturer's instructions.

2.2.2 Ligation of plasmid vectors and inserts

The ligations to form the plasmids containing heavy chain alleles were performed by using 0.5 µL of T4 DNA Ligase and 1 µL of 10x T4 DNA ligase reaction buffer (New England BioLabs) in 10 µL reactions. The ratio of the plasmid vector to insert was 1:3, with a final vector concentration of 2 nM. Each ligation reaction contained approximately 62 ng of ligated plasmid (mass of plasmid vector added to the mass of insert). Reactions were incubated at room temperature for 15 min, followed by 65°C for 10 min in a T100 Thermal Cycler (Bio-Rad).

2.2.3 Transformation into *Escherichia coli* DH5α cells

Heat shock (1 min at 42°C, followed by 2 min on ice) was used to transform 50 µL of *E. coli* DH5α cells with the ligated plasmids. After heat shock, 200 µL of warm Luria Bertani (LB) broth made with Luria Broth Base powder (Invitrogen™) was added to the cells. Then, 200 µL of each sample was added onto LB agar plates made from LB Agar powder (Invitrogen™) and 100 µg/mL Carbenicillin, and cultures were spread on the plate using a sterile spreader. Agar plates were incubated at 37°C overnight. On the following day, one colony from each plate was inoculated into 2 mL of LB broth containing 100 µg/mL Carbenicillin and incubated at 37°C with shaking at 200 rpm overnight. Glycerol stocks were prepared by adding 0.5 mL of the overnight culture to 0.5 mL sterile 50% glycerol (w/v) and stored at -80 ℃.

2.2.4 Extracting and purifying the plasmids

Overnight *E. coli* bacterial cultures containing transformed plasmids were centrifuged at 5,000 x *g* for 10 min to pellet the cells. A QIAprep Spin Miniprep Kit (Qiagen) was used to extract and purify the plasmids according to the manufacturer's instructions. After purification, plasmid concentration was determined using Nanodrop™ 2000 (Thermo Fisher), measuring absorbance at 280 nm. Plasmids were stored at -20°C. Approximately 350 ng of each plasmid was sent for sequencing by the Massey Genome Service (Massey University, New Zealand) to confirm whether the cloning was successful and that no mutations were introduced. Sequencing results were pairwise aligned to the respective allele sequence on Geneious Prime® version 2024.0.7.

For large-scale transfection grade plasmid preparation, successfully sequenced colonies from glycerol stocks were streaked onto LB agar plates containing 100 µg/mL Carbenicillin and incubated at 37°C overnight. On the following day, one colony from each plate was inoculated in 15 mL of LB broth containing 100 µg/mL Carbenicillin and incubated at 37°C with shaking at 200 rpm overnight. Plasmids were purified using the E.Z.N.A.® Endo-free Plasmid DNA Mini Kit II (Omega Bio-Tek) to remove bacterial endotoxins. Purified plasmids were stored at -20°C until the day of transfection into mammalian cells.

2.3 Antibody expression in Expi293 cells

An Expi293™ Expression System (Gibco) was used to produce all IgG antibodies by transient transfection of human embryonic kidney 293 cells (HEK293). The cells were passaged with Expi293 Expression Medium (Gibco) every 2-3 days to maintain growing densities of between 0.4 x 10^6 and 3 x 10^6 cells/mL. Cells were maintained in a humidified incubator at 37°C, 8% CO_2, with shaking at 125 rpm for the duration of the experiment, and the passage number did not exceed 20 for transfection experiments. Prior to transfection, cells were grown overnight to high density and diluted to 3 x 10^6 cells/mL in prewarmed Expi293 Expression Medium. To assemble full-length antibodies, plasmids containing heavy and light chain sequences were co-transfected at a 2:1 ratio of light chain to heavy chain (1 μg total plasmid for every 1 mL of culture). Anti-CD20 antibodies were transfected at a 25 mL scale and anti-AAV5 antibodies at a 50 mL scale according to the manufacturer's instructions.

Six days after transfection, antibodies that were secreted into the supernatant were harvested by centrifuging at 6000 x *g* for 30 mins at 4°C. Supernatants were filtered through 0.45 μm and 0.22 μm filters and stored at 4°C. Finally, the filtered supernatants were purified via one of the two methods: gravity feed purification with Protein G Sepharose resin (see section 2.4.1) or affinity chromatography using HiTrap™ MabSelect™ VL Protein L resin column (see section 2.4.2).

2.4 Antibody purification

2.4.1 Gravity feed purification with Protein G Sepharose resin

Initially, the method used to purify the filtered supernatants containing anti-CD20 antibodies was gravity feed purification with Protein G resin columns. Each column was packed with 1.5 mL of Protein G Sepharose (Thermo Fisher) and equilibrated with 1X phosphate-buffered saline (PBS) (Appendix C1), pH 7.4, prior to each purification. Antibody supernatants were passed through the Protein G column three times, and the columns were then washed with 30 mL of PBS, pH 7.4. Antibodies were eluted with 4 x 1 mL volumes of formic acid, pH 2.5, directly into 10 kDa Amicon® Ultra Centrifugal Filter (Merck Millipore) tubes containing 500 μL of 1 M ammonium carbonate. A 5-minute pause step was included after

each formic acid addition to enable antibody dissociation from the resin. The filter units were centrifuged four times at 5000 x *g* for 15 min at 4°C for buffer exchanging into PBS, pH 7.4. Buffer-exchanged samples were stored at 4°C, and antibody concentrations were determined by Nanodrop™ 2000 (Thermo Fisher), measuring absorbance at 280 nm. Absorbance readings were corrected by dividing the Nanodrop™ reading (1 Abs = 1 mg/mL) by the mass absorption coefficient of that antibody variant with the respective variable domain (Appendix C2). Theoretical mass absorption coefficients were calculated from the amino acid sequences using the ProtParam tool of the Expasy website (https://web.expasy.org/protparam/) (Gasteiger et al., 2005).

2.4.2 Affinity chromatography using HiTrap™ MabSelect™ VL Protein L

Alternatively, HiTrap™ MabSelect™ VL Protein L resin column (Cytiva) was used for both anti-CD20 and anti-AAV5 antibody purifications. Each 1 mL column was connected to a Next-generation Chromatography (NGC) Fast Protein Liquid Chromatography (FPLC) system (Bio-Rad). Prior to beginning purification, at least 15 mL of 1 M NaOH was run through the NGC system for over 1 hour to remove endotoxin contaminants, followed by 30 mL of milli-Q water to rinse it. Before using a Protein L resin column for the first time, it was cleaned with 3 column volumes (CV) of 0.1 M NaOH, followed by 5 CV of milli-Q water. A flow rate of 0.5 mL/min was used throughout the purifications. First, the column was equilibrated with 5 CV of binding buffer (20 mM sodium phosphate and 0.15 M NaCl, pH 7.4). Next, supernatants were loaded and followed with 5 CV of binding buffer. Finally, samples were eluted using 50 mM sodium citrate, pH 2.5, by applying a 0-100% gradient over 2 CV with a further 4 CV of sodium citrate. After the elution, the column was washed with 5 CV of elution buffer before being re-equilibrated with binding buffer. The eluted antibodies were neutralised with 120 µL of 1 M Tris-HCl, pH 9.

To buffer exchange the purified antibodies, each of the samples was loaded into 10 kDa Amicon® Ultra Centrifugal Filter (Merck Millipore) tubes and PBS, pH 7.4, was added to a volume of 4 mL. The filter units were centrifuged four times at 5000 x *g* for 15 min at 4°C with additional PBS added up to 4 mL between each

spin. Buffer-exchanged samples were stored at 4°C, and antibody concentrations were determined by Nanodrop™ 2000 (Thermo Fisher), as explained in section 2.4.1.

2.4.3 SDS polyacrylamide gel electrophoresis (SDS-PAGE)

SDS polyacrylamide gel electrophoresis (SDS-PAGE) was used to evaluate antibody purity. The SDS-PAGE gels were composed of a 12% resolving and 5% stacking layer made in a multi-gel caster (Hoefer). The composition of the resolving and stacking gels is listed in Table 2.1. Firstly, the gel caster was filled with around 28 mL of resolving gel, leaving a 3 cm gap at the top of the gel plate. Each gel was overlayed with 2 mL of isopropanol and left for approximately 30 min to polymerise. Once polymerised, isopropanol was removed so that the stacking layer could be added to the gel caster. Each gel contained approximately 2 mL of stacking gel. Immediately after adding the stacking layer to the caster, 10-well combs were inserted into the top of each gel. After approximately 30 min, the gels were polymerised and stored at 4 °C for up to four weeks.

Table 2.1. Components to make five SDS-PAGE gels. 10% ammonium persulphate (APS) stock solution was prepared fresh every week that gels were being made.

Component	12% Resolving gel (mL)	5% Stacking gel (mL)
Resolving buffer (1.5 M Tris, pH 8.8)	7.5	-
Stacking buffer (1 M Tris, pH 6.8)	-	1.6
30% acrylamide/bis, 19:1 (Bio-Rad)	12	2.125
10% SDS (w/v)	0.3	0.125
10% APS	0.15	0.063
TEMED	0.015	0.0063
Milli-Q water	10.05	8.5

Samples were prepared by mixing 2 – 9 μg of each antibody with PBS, pH 7.4, to a final volume of 15 μL. After the addition of 5 μl of 4x SDS loading dye (Appendix C3), samples were then incubated at 95°C for 5 min in a T100 Thermal Cycler (Bio-Rad). Subsequently, 18 μL of sample was loaded into each well of the SDS-PAGE gel alongside one well containing 8 μL of Precision Plus Protein™ Standards (Bio-Rad). The gels were run in 1x Tris-Glycine SDS-PAGE running buffer (Appendix C3) at 80 V for approximately 135 min.

Protein bands were visualised by adding Coomassie Fairbanks stain (Appendix C3) to the gels and microwaving for 20 seconds. After incubating for 15 min at room temperature with agitation (120 rpm), the stained gels were rinsed with distilled water, and 10% acetic acid was added to the gels to destain them for at least 2 hours. Antibody gel images were captured using an Invitrogen iBRIGHT™ Imaging System (Thermo Fisher).

2.5 Size exclusion chromatography (SEC)

SEC was performed on the anti-CD20 antibodies to remove aggregated antibodies and IgG light chains that did not assemble into full antibodies. Only the anti-CD20 antibodies used in the functional assays (see section 2.8) were size-excluded.

Before every round of SEC, at least 15 mL of 1 M NaOH was run through the NGC FPLC system (Bio-Rad) for over 1 hour to remove endotoxin contaminants, followed by 30 mL of milli-Q water to rinse it. The SEC column was cleaned with 2 mL of 1 M NaOH followed by 2 CV of milli-Q water.

Antibody SEC used an ENrich™ SEC 650 10x300 (Bio-Rad) column connected to an NGC FPLC system (Bio-Rad). Alternatively, the Superdex 200 Increase 10/300 GL (Cytiva) column was used to perform SEC with some of the antibodies. The SEC method was the same for both columns. The running buffer was 1x PBS, pH 7.4, which was filter-sterilised and degassed prior to use. The column was equilibrated with 2 CV of PBS before approximately 150 µL of each antibody sample, concentrated to 1.2 – 2.5 mg/mL, was injected into the NGC system using a Monoject™ Insulin and Tuberculin Safety syringe. After sample application, the column was washed with at least 1 CV of PBS to elute the antibodies while capturing 0.3 mL fractions. The concentrations of the size-excluded antibody samples were determined following the method described in section 2.4.1. To confirm the identity of the peaks seen in the SEC chromatograph, the collected SEC fractions were run on 12% SDS-PAGE gels as described in section 2.4.3. The fractions that corresponded to fully assembled monomeric antibodies were stored at 4 °C for up to two weeks.

2.6 Structural dynamics of allelic variants

2.6.1 Instrument setup and data collection

To study the differences in structural flexibility between the antibody allelic variants with anti-CD20 or anti-AAV5 variable domains, the SAXS/WAXS beamline at the ANSTO Australian Synchrotron in Clayton, Victoria, was used. The beamline is coupled to size exclusion chromatography (SEC) via a co-flow setup. Before loading the antibodies, the samples were concentrated using 10 kDa Amicon Ultra-0.5 Centrifugal Filter Units (Merck Millipore) and centrifuged at 13,000 x *g* for 15 min at 4°C to remove insoluble aggregates. The final concentration of the samples was 4.5 mg/mL. In this project, only anti-CD20 antibodies were used for SAXS. The anti-AAV5 antibodies produced in this study

will be run on the BioSAXS beamline (also at the ANSTO Australian Synchrotron) in the future.

The details of the instrument setup for the SEC-SAXS beamline are shown in Table 2.2. The SEC column used was a 3.2 mL Superdex S200 5/150 (Cytiva) that was equilibrated in PBS, pH 7.4, prior to sample loading. Scattering intensity was measured as a function of momentum transfer (q). Antibody samples of 50 µL were injected into the SEC column at a flow rate of 0.4 mL/mL. The eluted fractions were immediately passed into a 1.5 mm thin-walled glass capillary, where scattering data was collected.

Table 2.2. SEC-SAXS beamline setup and data collection parameters.

Instrument	Australian Synchrotron SAXS/WAXS beamline with a Pilatus detector (Dectris Ltd)
Size exclusion column	Superdex S200 5/150 3.2 mL (Cytiva)
Flow rate (mL/min)	0.4
Flow cell temperature (°C)	22
Detector Z position (mm)	2205
X-ray wavelength (Å)	0.998
***q* range ($Å^{-1}$)**	0.007 - 0.670
Exposure time (s)	1.00
Concentration (mg/mL)	4.5

2.6.2 Data processing

Normalisation and reduction of the data collected from the SEC-SAXS beamline were performed using scatterBrain software. Data processing was performed using software from the ATSAS program suite (version 3.2.1.) (Manalastas-Cantos et al., 2021). To begin, CHROMIXS was used to align the scattering data with the inline SEC traces (Panjkovich & Svergun, 2018). Upstream of the first elution peak, a baseline set of frames of buffer-scattering was selected from the SEC chromatograph to perform the background subtraction. The frames of sample-scattering were selected from the peak corresponding to the monomeric antibody. After subtracting the buffer-scattering from the sample-scattering, the processed

scattering curves were exported to a format (*.dat) readable by other programmes for analysis of scattering data, such as PRIMUS and BioXTAS RAW.

Analysis of the buffer-subtracted scattering data was performed using the PRIMUS software (Manalastas-Cantos et al., 2021). The radius of gyration (R_g) and relative intensity (I(0)) for each sample were calculated using both the "Radius of Gyration" and the "Distance Distribution" analysis functions. The R_g can be used to quantitatively characterise the flexibility of proteins and determine the overall size of the macromolecule (Kikhney & Svergun, 2015). The "Radius of Gyration" function is determined using the Guinier approximation of the scattering at the low-*q* region, which is low-resolution scattering (Putnam, 2016). The values of momentum transfer (*q*) multiplied by R_g were kept below 1.3 to meet the standard criteria for globular proteins (Kikhney & Svergun, 2015; Putnam, 2016). The quality of the fit was assessed based on the fidelity value (from 0.0 to 1.0, 1.0 being the best fit) and the random distribution of residuals, which should average around zero. The presence of aggregates in the samples was evaluated based on the linearity of the Guinier plot. The pair distance distribution function (*P(r)*) from the "Distance Distribution" function can be used to determine the real-space R_g and I(0) values along with the maximum particle dimension (D_{max}). From the "Distance Distribution" function, GNOM (Svergun, 1992) can calculate the distribution of interatomic distances (r). The D_{max} and alpha were adjusted to the lowest value that produced a smooth curve to zero, with *P(r)* above zero and a random distribution of residuals averaging around zero. The data collected from the SAXS beamline was fit to a maximum *q* of approximately 0.2 $Å^{-1}$

To compare the flexibility of the allelic variants, Dimensionless Kratky plots were generated with the R_g from the *P(r)* distribution multiplied by *q*. The intensity I(*q*) was normalised by dividing by I(0) for ease of comparison.

2.7 Propagating and freezing cells for ADCC and ADCP assays

The genome-engineered cell lines used in the ADCC and ADCP assays (see section 2.8) were ordered from Promega. Human B cell-derived Raji and WIL2-S cell lines (Promega) were used as target cells in the ADCC and ADCP assays. All cells were propagated according to the manufacturer's instructions and then stored frozen in

liquid nitrogen. Once frozen, they were only thawed on the day they were used in the assays.

2.7.1 Jurkat ADCC effector cells

The ADCC bioassay effector cells (Promega) are Jurkat cells, a modified T cell line. These cells were used in the ADCC assays (see section 2.8). After thawing for the first time, the cells were centrifuged at 90 x *g* for 10 min. Then, the cells were resuspended in 10 mL of the ADCC cell growth medium (Appendix E1). After resuspension, cells were transferred to a T75 tissue culture flask (Thermo Fisher) and kept in a humidified incubator at 37 °C, 5% CO_2 for 2 - 3 days. For all subsequent passages, the cells were seeded at 2.5 - 4 x 10^5 cells/mL in ADCC cell growth medium. After three passages, the cells were centrifuged at 130 x *g* for 10 min, then resuspended in 1x Dulbecco's phosphate-buffered saline (DPBS) (Gibco). Cells were centrifuged again at 130 x *g* for 10 min and resuspended in chilled (4 °C) ADCC cell freezing medium (Appendix E1). The ADCC effector cells were frozen at 2.01 x 10^7 cells/mL in 325 µL aliquots. The vials were kept in a Mr. Frosty™ Freezing Container (Thermo Fisher) at -80°C for approximately 24 hours before being stored in liquid nitrogen.

2.7.2 Jurkat ADCP effector cells

The FcγRIIa-H effector cells (Promega) are Jurkat cells modified to express the high-affinity H131 allelic variant of FcγRIIa. The cells were removed from liquid nitrogen and thawed in 9 mL of ADCP cell thawing medium (Appendix E2) at 37°C. Cells were centrifuged at 170 x *g* for 5 min, and the supernatant was aspirated. The cell pellet was resuspended in 12 mL of ADCP cell thawing medium at 37°C and transferred to a T75 tissue culture flask (Thermo Fisher). The flask was placed vertically in a humidified incubator at 37 °C, 5% CO_2. On day 2 of propagation, 12 mL of Day 2 cell growth medium (Appendix E2) was added to the T75 flask containing the cells. Subsequently, the T75 flask was grown horizontally. The cells were passaged by seeding at densities of 2.5 - 4 x 10^5 cells/mL in ADCP cell growth medium (Appendix E2). After four passages, the cells were centrifuged at 130 x *g* for 10 min, then resuspended in 1x DPBS. Cells were centrifuged again at 130 x *g* for 10 min and resuspended in chilled (4 °C) ADCP cell freezing medium

(Appendix E2). Finally, ADCP effector cells were frozen at 2.01 x 10^7 cells/mL in 325 µL aliquots. The vials were kept in a Mr. Frosty™ Freezing Container (Thermo Fisher) at -80°C for approximately 24 hours before being stored in liquid nitrogen.

2.7.3 Target cells: Raji and WIL2-S

Cell vials were removed from liquid nitrogen and thawed by adding 9 mL of target cell thawing medium (Appendix E3) at 37°C. The cells were then centrifuged at 130 x *g* for 8 min, and the supernatant was aspirated. After resuspension in 12 mL of target cell thawing medium at 37°C, the cells were transferred to a T75 tissue culture flask (Thermo Fisher) and incubated in a humidified incubator at 37 °C, 5% CO_2. Cells were passaged every 2 – 3 days to maintain a density of between 1 x 10^5 - 1 x 10^6 cells/mL. After three passages, the cells were centrifuged at 130 x *g* for 10 min, then resuspended in 1x DPBS. Cells were centrifuged again at 130 x *g* for 10 min and resuspended in chilled (4 °C) target cell freezing medium (Appendix E3). The Raji cells were frozen at 1 x 10^7 cells/mL, and WIL2-S cells were frozen at 8 x 10^6 cells/mL, each in aliquots of 550 µL. The vials were placed in a Mr. Frosty™ Freezing Container (Thermo Fisher) and kept at -80°C for approximately 24 hours before being stored in liquid nitrogen.

2.8 ADCC and ADCP assays

Assay buffer was composed of 96% RPMI 1640 (L-glutamine) medium (Gibco) and 4% heat-inactivated Low IgG Foetal Bovine Serum (Gibco) and was made fresh on the day of each assay. Before use, the assay buffer was warmed to 37 °C in a water bath.

2.8.1 Preparing target cells (Raji or WIL2-S)

For the ADCC assays, only Raji cells were used as target cells. For ADCP, the majority of the assays were performed using WIL2-S as target cells, but the seven chosen allelic variants were also tested using Raji cells as target cells. On the day of each assay, a vial of target cells was removed from liquid nitrogen and thawed in a water bath at 37 °C.

Thawed cells were centrifuged at 130 x *g* for 10 min, washed with 10 mL of 1x DPBS (Gibco) to remove cell debris, and centrifuged again at 130 x *g* for 10 min, after which the supernatant was aspirated. Raji cells were resuspended in 10 mL and 5.5 mL of fresh assay buffer prewarmed to 37 °C for ADCC and ADCP assays, respectively. In the case of the ADCP assays using WIL2-S cells, they were resuspended in 3.8 mL of assay buffer.

Subsequently, 25 µL of the target cell suspension (approximately 12,500 Raji cells per well for ADCC and 28,900 WIL-2S or 25,000 Raji cells per well for ADCP) was added to each of the inner 60 wells of the assay plates (Figure 2.1). To measure background luminescence, 75 µL of assay buffer was added to wells A1, A2, and A3. The plated target cells were returned to a 37°C, 5% CO2 incubator for approximately 15 min before proceeding with the assay.

	1	2	3	4	5	6	7	8	9	10	11	12
A	B	B	B									
B		UD	Dilu1	Dilu2	Dilu3	Dilu4	Dilu5	Dilu6	Dilu7	Dilu8	No Ab	
C		UD	Dilu1	Dilu2	Dilu3	Dilu4	Dilu5	Dilu6	Dilu7	Dilu8	No Ab	
D		UD	Dilu1	Dilu2	Dilu3	Dilu4	Dilu5	Dilu6	Dilu7	Dilu8	No Ab	
E		UD	Dilu1	Dilu2	Dilu3	Dilu4	Dilu5	Dilu6	Dilu7	Dilu8	No Ab	
F		UD	Dilu1	Dilu2	Dilu3	Dilu4	Dilu5	Dilu6	Dilu7	Dilu8	No Ab	
G		UD	Dilu1	Dilu2	Dilu3	Dilu4	Dilu5	Dilu6	Dilu7	Dilu8	No Ab	
H												

Figure 2.1. Plate layout for the ADCC and ADCP assays. The wells in green were for the reference antibody (triplicates), whereas the wells in blue were for the test antibody (triplicates). “B” shows the wells that were used to measure the background signal. “UD” refers to the wells with undiluted antibodies at 10 µg/mL (ADCC) or 6 µg/mL (ADCP). “Dilu” refers to the antibody dilution series, and “No Ab” refers to the negative control wells, which had no antibodies, only cells.

2.8.2 Antibody dilution series

All the antibodies used in the ADCC and ADCP assays had been through SEC (see section 2.5) within two weeks of the assay and, on the day of each experiment, were diluted to 10 µg/mL and 6 µg/mL with fresh assay buffer for the ADCC and ADCP assays respectively. Antibody serial dilutions were prepared in sterile 96-well

polymerase chain reaction (PCR) plates. The reference antibody (IgG1*01 CD20) and a test antibody were added to each plate in triplicate starting at a concentration of 10 μg/mL (ADCC) or 6 μg/mL (ADCP). Only one ADCP assay was performed using the ADCP Control Antibody (Promega), which is an IgG1 CD20 provided with the FcγRIIa-H Bioassay kit (Promega), and the antibody was prepared according to the manufacturer's instructions. A 1:4 serial dilution was performed for all antibodies as shown in Figure 2.1. Subsequently, 25 μL of antibodies from each well of the dilution series were transferred to their respective wells in the assay plate. Negative control wells in column 11 of the assay plate did not contain any antibodies.

2.8.3 Plating effector cells

For each assay plate, one vial of ADCC effector cells or ADCP effector cells was removed from liquid nitrogen on the day of use. The bottom of the vial was placed in a water bath at 37°C until the cells were just thawed. From the ADCC effector cells vial, 315 μL of cells at 2.01 x 10^7 cells/mL were diluted in 1.8 mL of fresh assay buffer prewarmed to 37 °C. In the case of the ADCP effector cells, 325 μL of cells at 2.01 x 10^7 cells/mL were transferred into a tube containing 2.9 mL of fresh assay buffer at 37°C. Then, 25 μL of resuspended cells was added to the inner 60 wells of the plates, which means the ADCC plates contained approximately 75,000 ADCC effector cells per well, while the ADCP plates contained approximately 50,000 ADCP effector cells per well. Plates were incubated for 6 and 16 hours in a humidified incubator at 37 °C, 5% CO_2, for ADCC and ADCP assays, respectively.

2.8.4 Preparation and addition of Bio-Glo™ Luciferase Assay Reagent

Bio-Glo™ Luciferase Assay Reagent (Promega) was reconstituted according to the manufacturer's instructions and stored in 5 mL aliquots at -20°C. The necessary number of aliquots (one per assay plate) was thawed within 1 hour of use in the assay plates. After the incubation period, plates were equilibrated to ambient temperature (22–25°C) for 15 min. To each of the 60 inner wells, 75 μL of Bio-Glo™ Reagent was added. To measure the background signal, 75 μL of Bio-Glo™ Reagent was added to wells A1, A2, and A3 of each plate. Plates were placed in the SpectraMax M Series Multi-Mode Microplate Reader (Molecular Devices) and left

incubating for 10 min at 25°C. Finally, the luminescence of the plates was measured reading all wavelengths.

2.8.5 Data analysis

The luminescence values collected from the SpectraMax Microplate Reader were processed in Microsoft® Excel. Background luminescence was subtracted from the other luminescence values. To calculate the fold induction (ratio of signal to background), the luminescence values of the wells that contained antibodies were divided by the average of the negative control luminescence of the same plate (Equation 2.1).

$$Fold\ induction = \frac{Luminescence\ of\ well\ with\ test\ antibodies}{Average\ luminescence\ of\ negative\ control\ wells}$$

Equation 2.1. Equation to calculate fold induction of antibodies at each dilution point. The luminescence values used in the equation are background-subtracted.

Results for each sample were normalised across plates based on the fold induction of the reference antibody from the same assay plate. The average fold induction of all the references (from 6 plates) was divided by the average fold induction values of the reference triplicates within each plate to generate a normalisation factor for each dilution point (Equation 2.2). The average fold induction values of the test antibodies were then multiplied by the respective normalisation factor.

$$Normalisation\ factor = \frac{Overall\ average\ fold\ induction\ of\ reference\ Ab}{Average\ fold\ induction\ of\ reference\ of\ respective\ plate}$$

Equation 2.2. Equation to calculate normalisation factor of each sample at each dilution point.

A four-parameter logistic model of the normalised fold induction values with the logarithm of the antibody concentration was plotted using RStudio (Appendix G1). The error bars represent the standard deviation of each sample in the dilution series, which was calculated in Microsoft® Excel. The normalised four-parameter logistic model plots were used to calculate the EC50 (half maximal effective concentration) value of each sample and the standard error of the model in RStudio.

3 Chapter Three

Results and Discussion

3.1 Plasmid cloning and transformation into *E. coli* DH5α cells

Exploring the structural and functional consequences of hinge region variation in human IgG3 constant region alleles requires antibodies to be expressed in a full-length format including variable domains. Variable heavy and light sequences were selected from the anti-CD20 clinical monoclonal Rituximab for structural analysis and functional assays targeting CD20 overexpressing tumour cells lines in ADCP assays. Additionally, anti-AAV5 variable domains from the antibody 9c12 were chosen for future exploration of intracellular anti-viral TRIM21 receptor function.

Plasmids encoding the antibody light chains were ordered directly from Twist Bioscience™ and required no cloning. In parallel, seven gene fragments encoding IGHG alleles with hinge length variations (32, 47, or 62 amino-acid long for IgG3, and 15 and 12 amino-acid long for IgG1 and IgG2 controls, respectively) were ordered from Twist Bioscience™ and were digested with XhoI/NheI and ClaI restriction enzymes to introduce them into plasmids containing the anti-CD20 and anti-AAV5 variable heavy domain sequences. The size of the two bands in the agarose gel confirms that the restriction enzymes digested the plasmid at the correct sites, only resulting in the excision of the CH1, CH2, and CH3 domains (lower band) from the plasmid (upper band) (Figure 3.1).

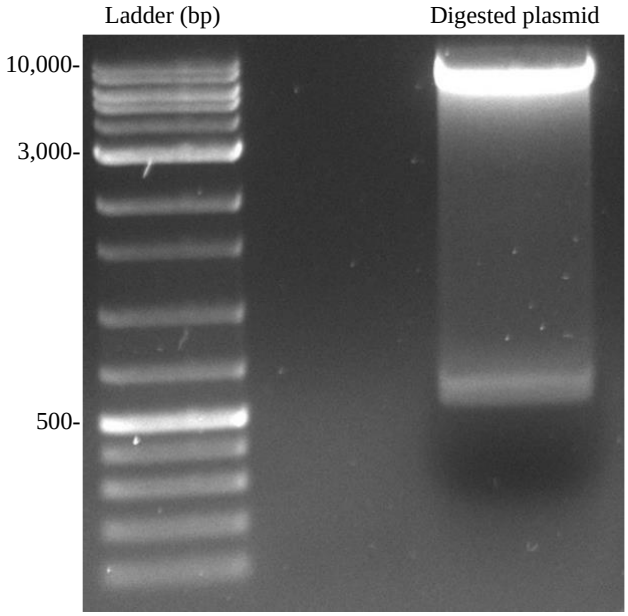

Figure 3.1. 1.5% agarose gel showing plasmid DNA that was digested with XhoI and ClaI (New England BioLabs). SiZer™ 1000 plus DNA Marker Solution was used as the ladder. The top band (around 8,000 base pairs) corresponds to the plasmid backbone including the anti-AAV5 variable domain, and the bottom band (around 500 base pairs) corresponds to the allele fragment.

Sequencing results from the Massey Genome Service (Massey University, New Zealand) of the cloned plasmids were pairwise aligned to the respective allele sequences in Geneious Prime® software version 2024.0.7 (Appendix A4). The alignments confirmed that the cloning was successful and that no erroneous point mutations were introduced during cloning.

Sequence-verified plasmids were purified using the E.Z.N.A.® Endo-free Plasmid DNA Mini Kit II (Omega Bio-Tek) to remove bacterial endotoxins and prepare enough for large-scale mammalian transfections. The plasmids were transfected into HEK293 cells using the Expi293™ Expression System (Gibco). Representative plasmid DNA yields after purification and respective volumes required for each transient transfection are presented in Table 3.1.

Table 3.1. Representative transient transfection of three anti-CD20 allelic variants in 25 mL HEK293 cell cultures. Each IgG heavy chain plasmid (IGHG) was co-transfected with IgG kappa light chain plasmid (IGK) at a mass ratio of 2:1.

Plasmid name	Plasmid concentration (ng/µL)	Plasmid amount required per transfection (µg)	Plasmid volume per transfection (µL)
IGK CD20	1640.0	16.67	10.16
IGHG1*01 CD20	582.5	8.33	14.31
IGHG2*02 CD20	489.5	8.33	17.02
IGHG3*01 CD20	924.0	8.33	9.02

3.2 Antibody purification

Antibody allelic variants were harvested from supernatant of HEK293 cultures and were purified by affinity and/or size exclusion chromatography before being used in structural studies and functional assays.

3.2.1 Gravity feed purification with Protein G Sepharose resin

Initial batches of IgG antibodies produced were purified by gravity feed purification with Protein G Sepharose resin (ThermoFisher). Electrophoresis of each of the purified antibodies showed a band at around 50 kDa and another at around 25 kDa, which corresponded to the IgG heavy and light chains, respectively (Figure 3.2). We noted some additional bands which are likely minor contaminants, except in IgG3*01, where two bands appear near the size of the heavy chain (50 kDa). While this additional band could be related to differences in glycan states, its identity was unclear. Therefore, we adopted size exclusion chromatography (SEC) as a secondary purification step prior to all structural and functional studies.

Due to the low chemical and proteolytic stability of protein G Sepharose, these purification columns could not withstand cleaning procedures with sodium hydroxide or similar sanitising agents (Verdoliva et al., 2002), which eventually led

to contamination issues. Because of this drawback, subsequent antibody purifications were purified using protein L resin columns (see section 3.2.2).

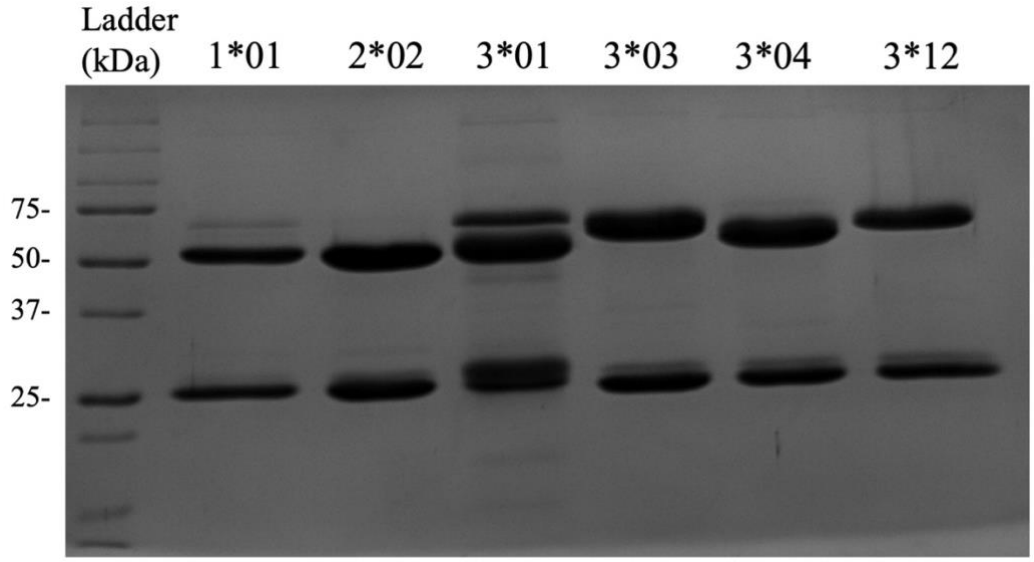

Figure 3.2. SDS-PAGE gel result of six anti-CD20 allelic variants (IgG1*01, IgG2*02, IgG3*01, IgG3*03, IgG3*04, and IgG3*12) purified by gravity feed purification with protein G Sepharose resin. Molecular weights in kDa of Precision Plus Protein™ Standards (Bio-Rad) are labelled. Of the seven anti-CD20 allelic variants included in this project, only IgG3*08 is not shown in this gel because it was purified in a separate attempt.

3.2.2 Affinity chromatography using HiTrap™ MabSelect™ VL Protein L

Most of the antibody variants produced in this project were purified via affinity chromatography using HiTrap™ MabSelect™ VL Protein L resin column (Cytiva). This column can be cleaned with 0.1 M sodium hydroxide without getting damaged, which then reduces the likelihood of column fouling and the growth of biological contaminants over time.

This purification method was robust and effective for both anti-CD20 (Figure 3.3A) and anti-AAV5 (Figure 3.3B) allelic variants. Electrophoresis results show that the purified samples most likely did not contain remaining cell lysates or any other proteins besides antibodies since there are only bands at 50 and 25 kDa for each sample, which correspond to the heavy and light chains, respectively.

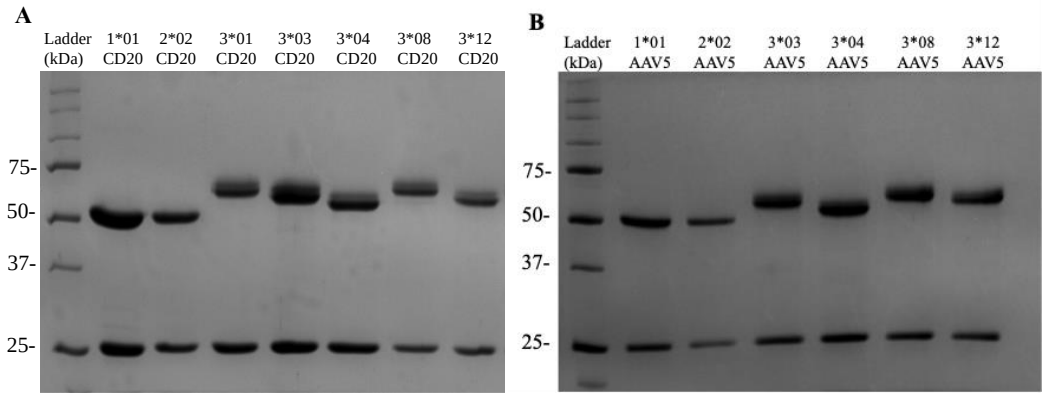

Figure 3.3. SDS-PAGE gel results of allelic variants after purification using HiTrap™ MabSelect™ VL Protein L resin column (Cytiva). Variants with anti-CD20 (A) and anti-AAV5 (B) variable domains were purified. Of the seven anti-CD20 and anti-AAV5 allelic variants included in this project, only IgG3*01 AAV5 is not shown in these images because it was purified in a separate attempt (Appendix C4). Molecular weights in kDa of Precision Plus Protein™ Standards (Bio-Rad) are labelled.

The gel electrophoresis showed a heavy chain band around 60 kDa for the allelic variants IgG3*01 and IgG3*08, while there were heavy chain bands closer to 50 kDa for IgG1*01 and IgG2*02. These results are aligned with the expected differences in hinge length between the antibody subclasses and the IgG3 variants. The variants with longer hinges (i.e., IgG3*01 and IgG3*08 with 62 amino-acid long hinges) had heavy chain bands of higher molecular weight, while IgG1 and IgG2 antibodies had the heavy chain bands of lowest weight due to their short hinges of only 15 and 12 amino acids long, respectively (Vidarsson et al., 2014).

Some of the IgG3 samples show a faint band right above the heavy chain bands, mainly in Figure 3.3A. These faint bands are most likely due to differences in the N-glycosylation profile of the antibodies (Majewska et al., 2020; Nallet et al., 2012).

3.3 SEC of purified antibodies

Purified antibodies were run through size exclusion chromatography (SEC) to remove aggregates and IgG light chains that did not assemble into full antibodies – especially important for the samples that were purified using HiTrap™ MabSelect™ VL Protein L resin column. Additionally, the absorbance traces in the SEC chromatograph were used to inform the peak identity in the elution traces of

the allelic variants after being run in the SEC-coupled SAXS beamline (see section 3.4.1).

For IgG1*01 and IgG2*02 CD20, there was only one peak in the absorbance traces at 280 nm in the SEC chromatograph (Figure 3.4). Gel electrophoresis results confirmed that the peaks correspond to the elution of fully assembled monomeric antibodies (Figure 3.6A, Appendix D1). The fact that there was no higher molecular weight species peak for IgG1*01 and IgG2*02 could be related to the fact that antibodies from these subclasses are more stable and display greater resistance to aggregation than IgG3 antibodies (Warrender et al., 2023).

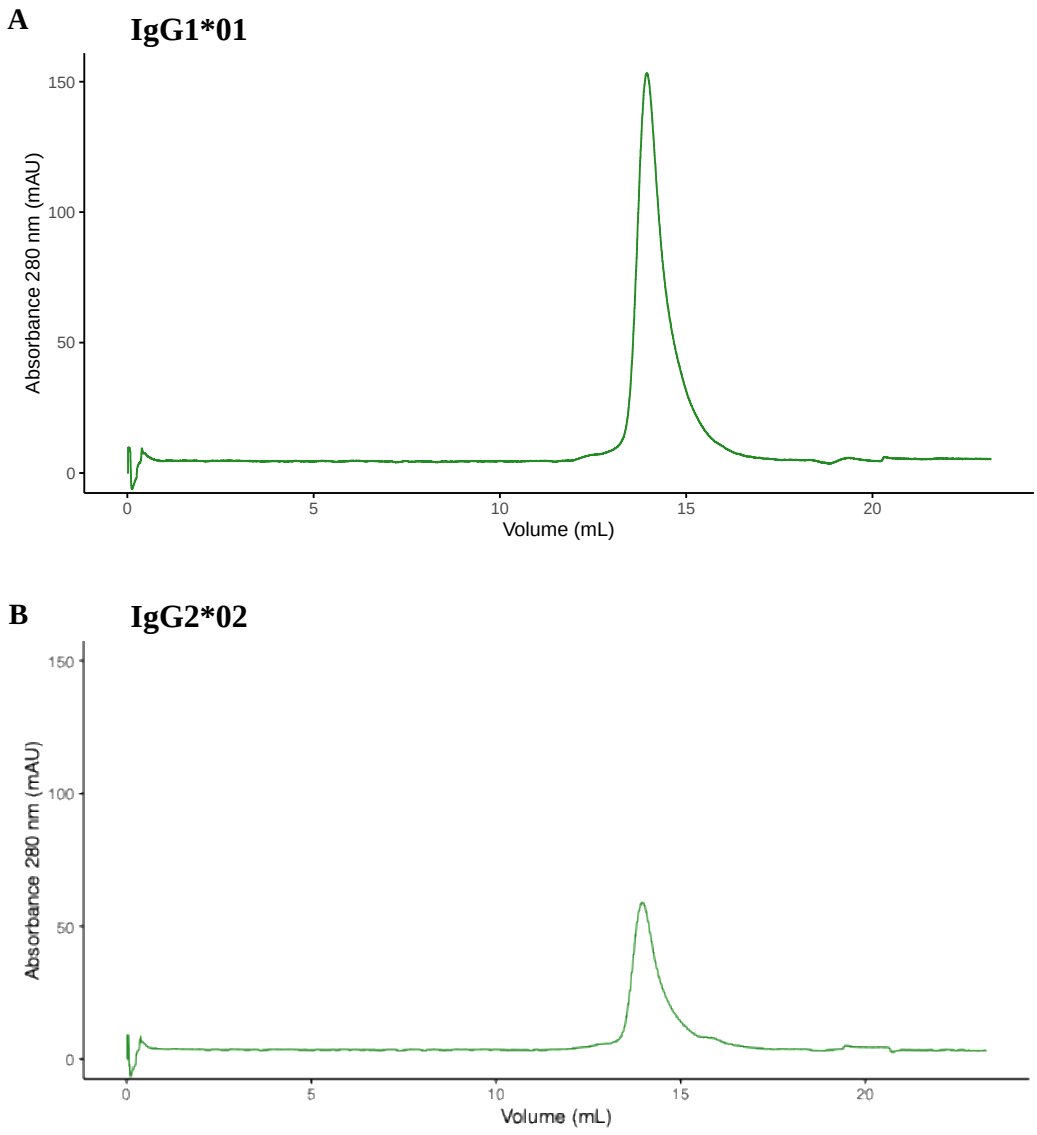

Figure 3.4. Size exclusion chromatographs of IgG1*01 (A) and IgG2*02 (B) CD20 from SEC using ENrich™ SEC 650 10x300 (Bio-Rad) column.

The SEC chromatographs of the IgG3 allelic variants showed two to three absorbance peaks (Figure 3.5, Appendix D2). The collected SEC fractions were run in gel electrophoresis to confirm the identity of the peaks (Figure 3.6). In the case of the antibodies that showed three elution peaks, the peak at the lowest elution volume is suspected to be aggregated antibodies (higher molecular weight species), whereas the one that follows is the monomeric antibody peak. Previous work used mass spectrometry to confirm that the high molecular weight species peak next to the monomeric IgG antibody peak in the SEC chromatograph corresponded to the elution of antibody aggregates (Chakrabarti, 2018; Kükrer et al., 2010). However, some proportion of the peak could also include eluted antibody oligomers, such as trimers, tetramers, hexamers, or reversible aggregates since the SEC fraction resolved in SDS-PAGE gel electrophoresis (Appendix D1).

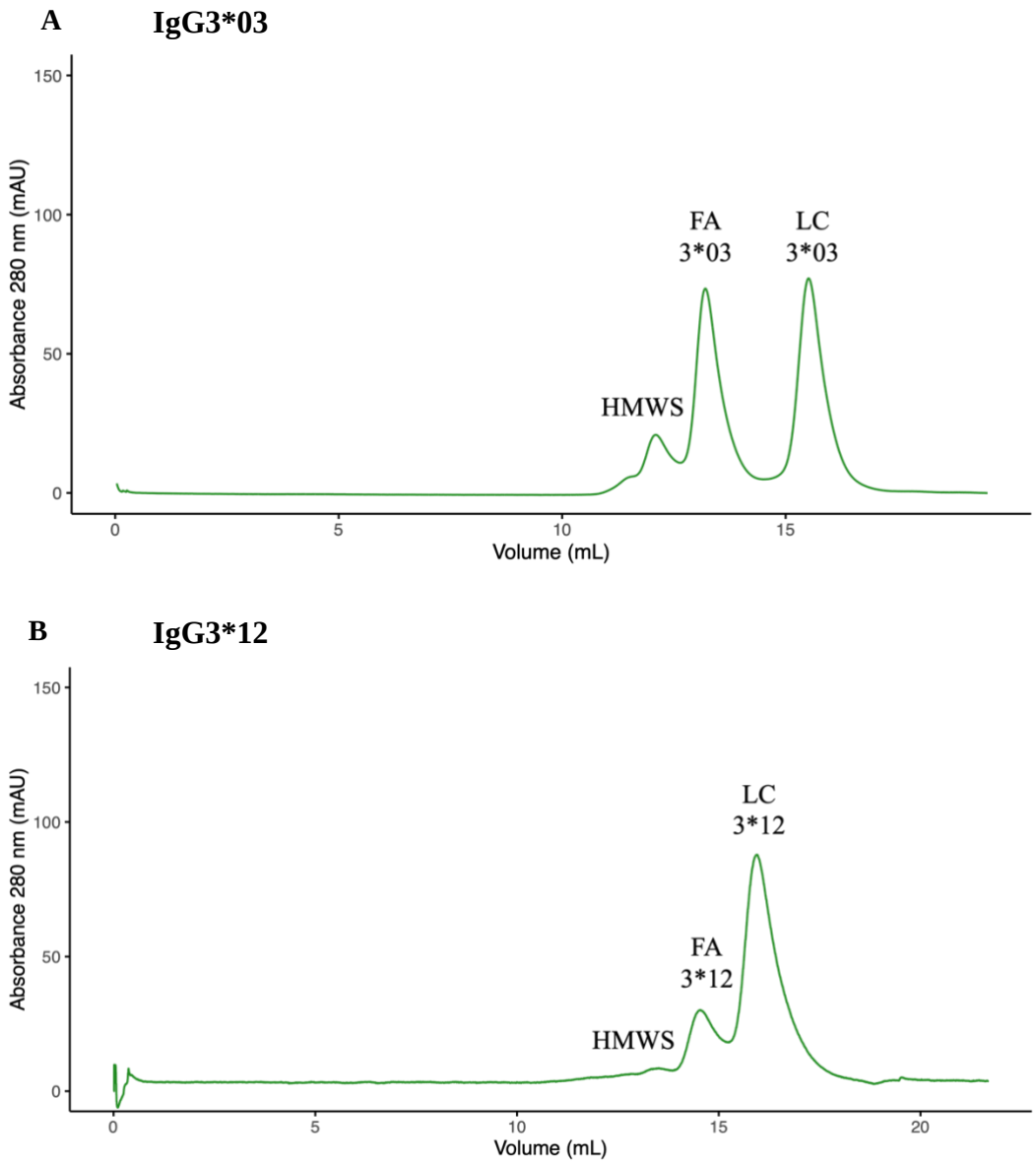

Figure 3.5. Size exclusion chromatographs of IgG3*03 (A) and IgG3*12 (B) CD20 from SEC using ENrich™ SEC 650 10x300 (Bio-Rad) column. "HWMS" corresponds to the high molecular weight species peak, "FA" corresponds to the fully assembled antibody peak, and "LC" corresponds to the light-chain-only peak.

Lastly, the elution peak around 15-18 mL (lower molecular weight species) corresponds to light chain that did not assemble into a full antibody (Figure 3.6B). Since the protein L resin column binds to the kappa light chain of the antibodies, a considerable amount of light chain that did not assemble into full antibody was eluted along with full antibody, as seen by the large peaks after 15 mL of elution. However, this was only observed for SEC with IgG3 antibodies, not with IgG1 and IgG2. This is, potentially, an indication of how easily the antibodies from different

subclasses assemble into full-length tetrameric structures once expressed in the cells. As an attempt to reduce this imbalance in expressed heavy and light chains, the plasmids could have been co-transfected at a 1:1 ratio of light chain to heavy chain instead of 2:1.

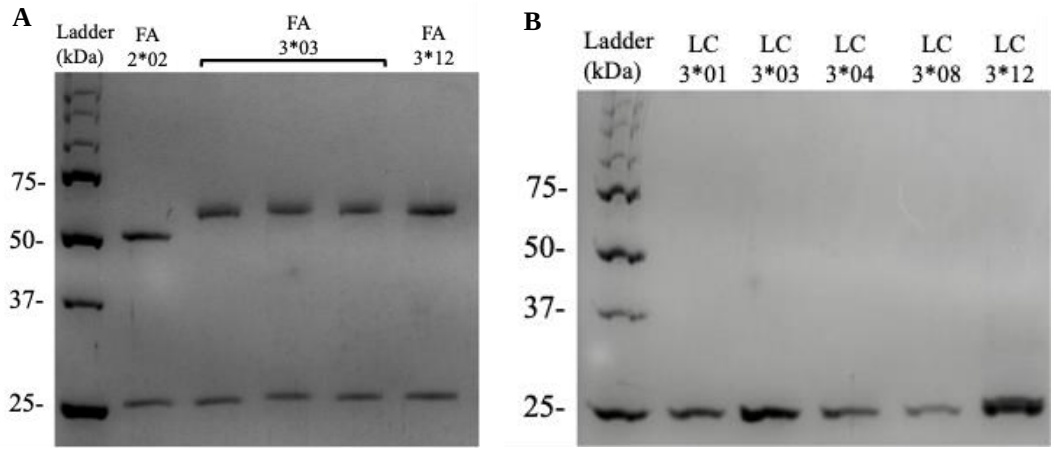

Figure 3.6. 12% SDS-PAGE gel results of collected SEC fractions for some of the anti-CD20 allelic variants. (A) "FA" refers to fully assembled antibody fractions, and (B) "LC" refers to light-chain only fractions. Molecular weights in kDa of Precision Plus Protein™ Standards (Bio-Rad) are labelled. Expected band size for antibody heavy chain is 50-65 kDa, depending on the variant, and 25 kDa for the light chain.

The chromatographs for the SEC runs performed using a Superdex 200 Increase 10/300 GL column (Cytiva) were similar to those in which a ENrich™ SEC 650 column was used. SEC chromatographs of IgG3 antibodies using this column also showed three elution peaks (Figure 3.7). However, with the Superdex 200 column, the full-length monomeric antibodies eluted at a lower volume of around 12 mL instead of at around 14 - 15 mL. The columns have the same bed volume (24 mL) and same bed dimensions (10 x 300 mm) but the ENrich 650 media has a larger pore size and greater separation range of 2 - 1500 kDa, while the Superdex 200 column has a separation range of 10 – 600 kDa. These differences in separation range likely account for the differences in the elution volume of the monomeric antibodies.

The elution profile of IgG3*03 from SEC using the Superdex 200 column showed dual peaks at around 10 mL of elution volume in contrast to other IgG3 alleles (Figure 3.7). This doublet at high molecular weight could correspond to aggregates

or a combination of antibody oligomers such as hexamers, tetramers, or trimers (Chakrabarti, 2018; Kükrer et al., 2010). Since the exclusion limit of Superdex 200 is 600 kDa, tetrameric and hexameric IgG antibodies would not be efficiently separated and would elute together in one peak.

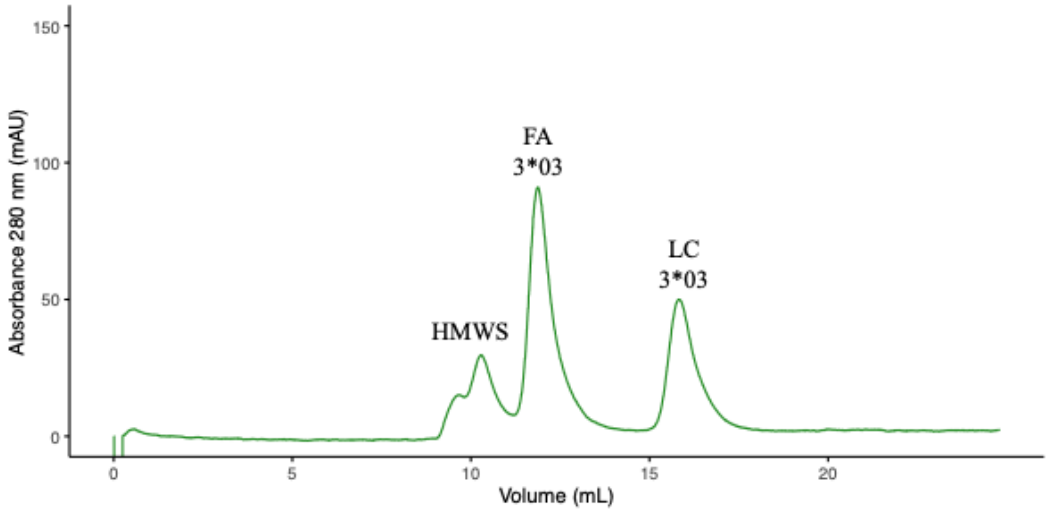

Figure 3.7. Size exclusion chromatograph of IgG3*03 CD20 from SEC using Superdex 200 Increase 10/300 GL (Cytiva). "HWMS" corresponds to the high molecular weight species peak, "FA" corresponds to the fully assembled antibody peak, and "LC" corresponds to the light-chain-only peak.

3.4 Structural dynamics of the allelic variants

Prior to this project, the structural dynamics of a panel of the same trastuzumab IgG3 alleles produced here were evaluated using small angle x-ray scattering (SAXS) by Dr Annmaree Warrender (Warrender, 2023). Here, we aimed to extend this dataset to determine whether the striking differences observed in antibody flexibility are universally applicable for multiple variable domain sequences.

Scattering data was collected for all seven anti-CD20 allelic variants on both the SAXS and Biological SAXS (BioSAXS) beamlines at the ANSTO Australian Synchrotron. The BioSAXS beamline is a newly commissioned beamline designed to replace SAXS but because of technical challenges, the scattering data collected from this new beamline was not of sufficient quality to be included in this thesis. Therefore, the structural dynamics presented here are only from SAXS scattering data.

Additionally, a third set of allelic variants with an anti-AAV5 variable domain was produced in this project, but due to time limitations, they will be tested on the BioSAXS beamlines in the future. From the SAXS data of the anti-CD20 and anti-HER2 allelic variants collected in this project and by Warrender (2023), respectively, we aimed to determine if differences in structural dynamics between the variants aligned with observed variability in ADCC and ADCP effector responses.

3.4.1 Assessing the presence of high molecular weight species

Prior to analysing SAXS scattering data, elution curves from SEC were evaluated by viewing the averaged scattering intensity over time (frame number) using CHROMIXS (Panjkovich & Svergun, 2018). These plots were used to assess the presence of high molecular weight species, such as antibody aggregates, and low molecular weight species, such as light chain molecules that did not assemble into full-length antibodies. Similarly to what was observed in the SEC results presented in section 3.3, the IgG3 samples eluted into two peaks, while IgG1 and IgG2 antibodies eluted into a single peak (Appendix F1). None of the samples presented a third peak (light-chain only peak) because these antibody samples were purified with protein G Sepharose resin (see section 3.2.1), not protein L resin column. The peak of high molecular weight species in the elution profile of IgG3 could correspond to the elution of antibody aggregates, dimers, or trimers. (Chakrabarti, 2018; Kükrer et al., 2010).

The presence of antibody aggregates in the selected sample-scattering frames can be assessed based on the linearity of the Guinier plot at low q (Figure 3.8). The scattering of the samples run in the SAXS beamline was linear and was in alignment with the Guinier fit (Figure 3.8C). This indicates the absence of interparticle attractive interactions, such as aggregates, in the scattering frames where there should only be monomeric antibodies (Putnam, 2016). This analysis provides confidence that the SAXS data should be of high quality.

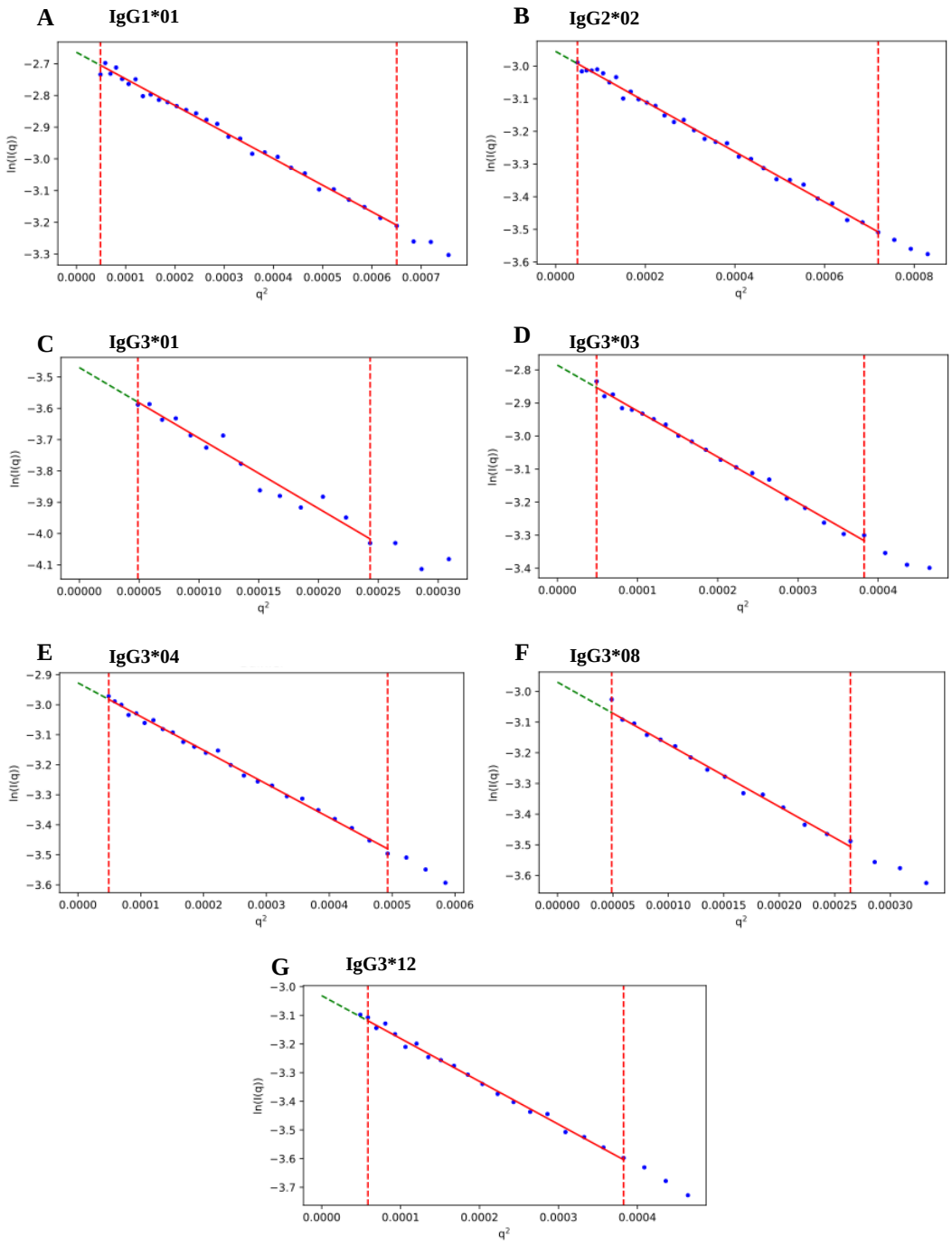

Figure 3.8. Guinier region fits for the seven anti-CD20 allelic variants. The alignment of the scattering (blue dots) with the green and red diagonal lines indicates the linear Guinier fit. Only the scattering in the *q* range between the two vertical red dashed lines was used for Guinier approximation to ensure $qR_g<1.3$.

3.4.2 Influence of hinge length on antibody size

The size of the anti-CD20 allelic variants was compared using radius of gyration (R_g) values and interparticle distance values, which were calculated from the scattering data. R_g provides a measure of the average radii between atoms within the structure, indicating the effective size of the antibody molecules (Putnam, 2016). Guinier analysis was used to calculate the R_g values in reciprocal space, and the pair distance distribution function (*P(r)*) was used to calculate the R_g values in real space (Table 3.2). From the SAXS scattering results, the calculated R_g values were in close agreement (± 2 Å) for each variant, except for IgG3*03, which had approximately ±3 Å of difference between reciprocal and real space values (Table 3.1). The R_g values estimated from the Guinier approximation tended to be smaller compared to those calculated using the real-space values. The Guinier law applies a model that assumes globular-like particles and this approach has been found to underestimate the radius of gyration of unstructured or extended systems (Kikhney & Svergun, 2015; Pérez et al., 2001). Alternatively, the radius of gyration estimated form the *P(r)* distribution is calculate from the entire scattering data. Therefore, the real space estimations are more appropriate for these antibody structures that have extended structures.

From the scattering data, the maximum particle dimensions (D_{max}) and R_g values showed a positive correlation with the hinge length of the allelic variant (Table 3.2). This observation aligns with the conclusions of Warrender (2023) with anti-HER2 variants. In the distance distribution analysis, the tested variant with the shortest hinge, IgG2*02, had a D_{max} of 158.97 Å and R_g of 49.19 (± 0.29) Å, which are the lowest D_{max} and R_g values observed. IgG1*01, with the second shortest hinge, had a D_{max} of 172.14 Å and R_g of 51.49 (± 0.28) Å. Overall, IgG3 antibodies had larger D_{max} and R_g values than IgG1 and IgG2 antibodies. When comparing the IgG3 variants, there were clear differences in the values between variants with different hinge lengths. The IgG3 variant with the shortest hinge, IgG3*04 (32 amino acids long), had a D_{max} of 199.81 Å and an R_g of 58.02 (± 1.0) Å. The variants with slightly longer hinge lengths (47 amino acids), IgG3*03 and IgG3*12, had D_{max} values of 215.00 Å and 212.33 Å, and R_g values of 67.99 (± 0.43) Å and 69.17 (± 0.41) Å, respectively. The variants with a hinge length of 62 amino acids,

IgG3*01 and IgG3*08, had D_{max} of 245.13 Å and 241.40 Å and R_g of 79.96 (± 3.11) Å and 79.28 (± 0.43) Å, respectively, which are the highest D_{max} and R_g values. Even though the R_g value of IgG3*01 is, as expected, very close to that of IgG3*08 because of the same hinge length, it is intriguing that the standard deviation of IgG3*01 is as high as ± 3.11. This is an indication that the quality of the scattering data of IgG3*01 used in the analysis might not be ideal.

The SAXS parameters for the anti-CD20 allelic variants presented in this work were compared to the results of a previous study with anti-HER2 variants (Warrender, 2023). Overall, the anti-CD20 allelic variants presented SAXS parameters that indicate that their size is larger than that of the anti-HER2 variants. Nevertheless, the trend that the variants with longer hinges have higher R_g and D_{max} values than the other variants was consistent across the antibodies of both variable domain sequences. For instance, IgG1*01 anti-CD20 had a D_{max} of 172.14 Å and R_g of 51.49 (± 0.28) Å (Table 3.2), whereas the anti-HER2 variant had a D_{max} of 153.34 Å and R_g of 50.93 (± 0.23) Å (Warrender, 2023). As an example of a variant with a more extended hinge, IgG3*12 anti-CD20 had a D_{max} of 212.33 Å and R_g of 69.17 (± 0.41) Å, while the anti-HER2 variant had a D_{max} of 210.00 Å and R_g of 67.60 (± 0.57) Å. The SAXS parameters for IgG3*12 did not have such a striking difference between anti-CD20 and anti-HER2 as for IgG1*01, but IgG3*12 still showed to be of greater size than the anti-HER2 variant. In both anti-CD20 and anti-HER2, the allelic variants with longer hinges had higher D_{max}, R_g, and V_P values than the other antibodies.

To investigate the causes behind the differences in size between these variants with distinct variable domains, the crystal structures of the variable domains of anti-CD20 and anti-HER2 antibodies were aligned on the PyMOL Molecular Graphics System. The alignment of the two heavy variable domains showed that the anti-CD20 variants present a longer complementarity-determining region 3 (CDR3) loop than the anti-HER2 antibodies (Figure 3.9). The measurement tool in PyMOL indicated that there was 7.7 Å between the two CDR3 loops. This is the most likely cause behind the differences in parameters related to the size of the antibodies of different variable domains.

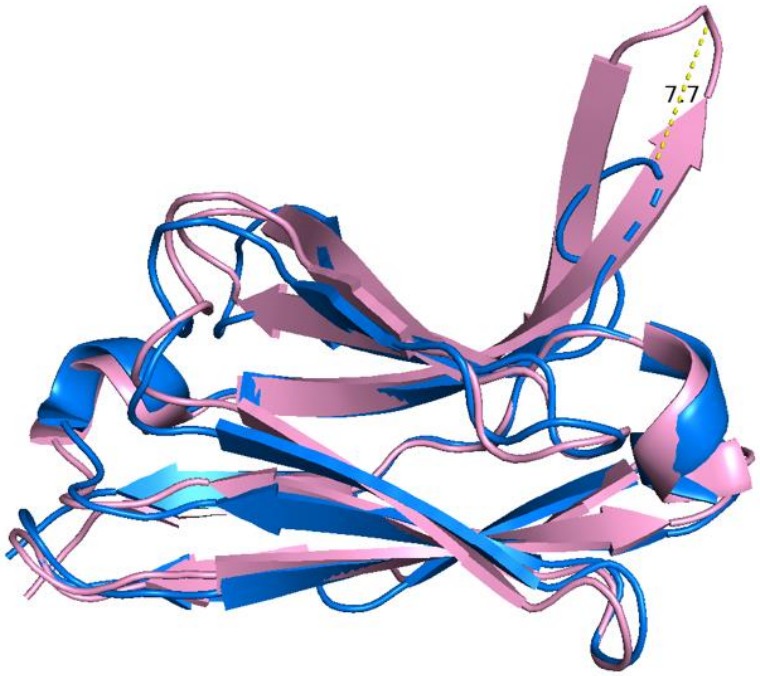

Figure 3.9. Alignment of anti-CD20 (pink) and anti-HER2 (blue) variable heavy domains from Rituximab and Herceptin, respectively. The structure was generated on PyMOL from PDB files of Rituximab Fab arms [PDB: 4KAQ (Bzymek & Williams, 2014)] and Herceptin Fab arms [PDB: 6MH2 (Luthra et al., 2019)]. Yellow dashed lines show there is a distance of 7.7 Å between the pink and blue complementarity-determining region (CDR) loops.

Table 3.2. Calculated SAXS parameters for the anti-CD20 allelic variants.

	IgG1*01	IgG2*02	IgG3*01	IgG3*03	IgG3*04	IgG3*08	IgG3*12
Concentration (mg/mL)	4.5	4.5	4.5	4.5	4.5	4.5	4.5
Hinge length (amino acids)	15	12	62	47	32	62	47
Radius of gyration analysis							
Data point range	2 – 29	1 - 31	1 - 15	2 – 20	1 - 24	2 - 15	1 - 24
I(0) (cm-1) [from Guinier]	0.07 ± 0.0003	0.052 ± 0.0002	0.03 ± 0.0005	0.062 ± 0.0004	0.054 ± 0.0002	0.051 ± 0.0004	0.048 ± 0.0003
R_g (Å) [from Guinier]	50.21 ± 0.36	48.00 ± 0.28	79.32 ± 1.97	64.40 ± 0.61	58.02 ± 0.43	77.41 ± 1.21	67.24 ± 0.63
qR_g limits	0.38 – 1.28	0.34 – 1.29	0.56 – 1.29	0.49 – 1.26	0.41 – 1.29	0.59 – 1.26	0.47 – 1.27
Fidelity	0.82	0.93	0.94	0.91	0.86	0.90	0.89
Distance distribution analysis							
q range ($Å^{-1}$)	0.007 – 0.198	0.007 – 0.178	0.007 – 0.20	0.007 – 0.197	0.007 – 0.188	0.007 – 0.193	0.007 – 0.185
P(r) total quality estimate	0.92	0.82	0.72	0.76	0.83	0.71	0.77
R_g (Å) [from Guinier]	51.46	49.16	79.40	67.83	59.97	78.96	69.00
I(0) (cm^{-1}) [from Guinier]	0.07	0.05	0.03	0.06	0.05	0.05	0.05
R_g (Å) [from *P(r)*]	51.49 ± 0.28	49.19 ± 0.29	79.96 ± 3.11	67.99 ± 0.43	58.02 ± 1.0	79.28 ± 0.43	69.17 ± 0.41
I(0) (cm^{-1}) [from *P(r)*]	0.07 ± 0.0003	0.05 ± 0.0002	0.03 ± 0.0008	0.06 ± 0.0004	0.05 ± 0.0003	0.05 ± 0.0003	0.05 ± 0.0003
Dmax (Å)	172.14	158.97	245.13	215.00	199.81	241.40	212.33
Points	121	124	95	106	112	96	105
Alpha	6.652	8.900	3.478	3.955	6.127	6.137	5.881

3.4.3 Influence of hinge length on structural flexibility

The anti-CD20 allelic variants with different hinge lengths presented distinct curvatures in the *P(r)* distribution (Figure 3.10A). The *P(r)* distribution is a histogram of the interatomic distances (r) present within a structure (Kikhney & Svergun, 2015; Putnam, 2016). Each variant had a *P(r)* distribution containing two or three peaks, which aligns with what is expected for monoclonal antibodies (Belviso et al., 2022; Liu et al., 2019; Lu et al., 2007; Spiteri et al., 2021). Of the three peaks, Peak 1 (maximum r of approximately 40 Å) occurs with the highest frequency in all variants, indicating the most recurring interatomic distances within the predominant conformation adopted by the antibodies (Belviso et al., 2022). This peak most likely corresponds to the width of the Fc region or of a single Fab arm (Figure 3.10B) since these domains are similar in all the IgG variants, regardless of their hinge length (Warrender, 2023). The r values of Peak 1 are approximately the same as the widths of the Fc region and a Fab arm, estimated from x-ray crystallography structures in previous studies (Lu et al., 2007; Saphire et al., 2001; Shah et al., 2017).

A

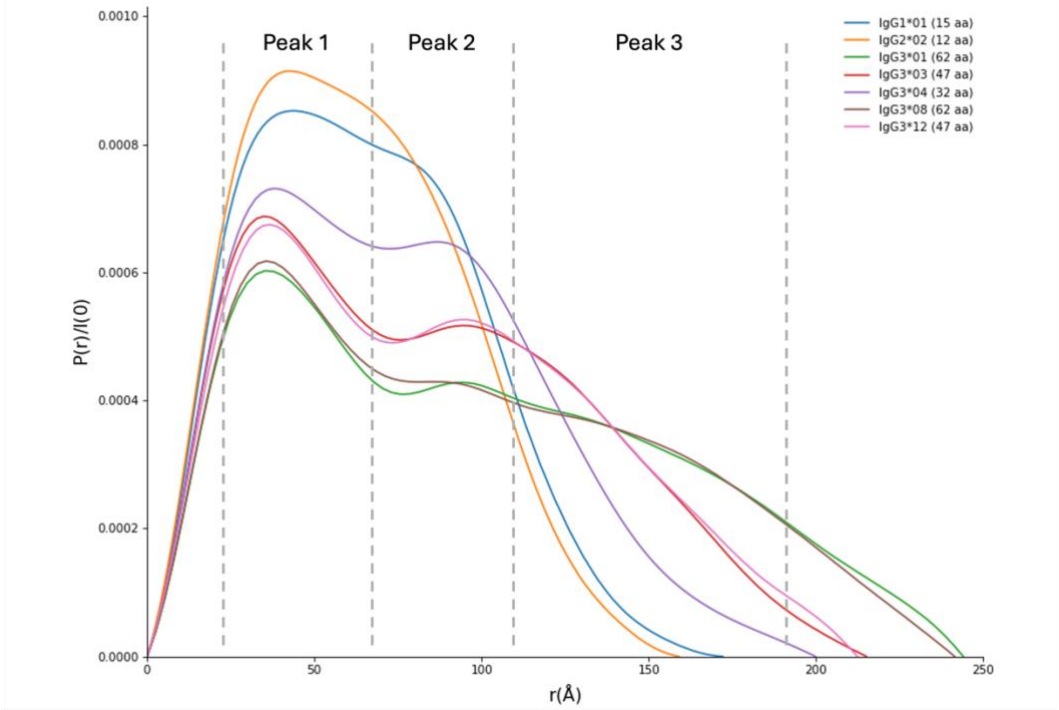

B

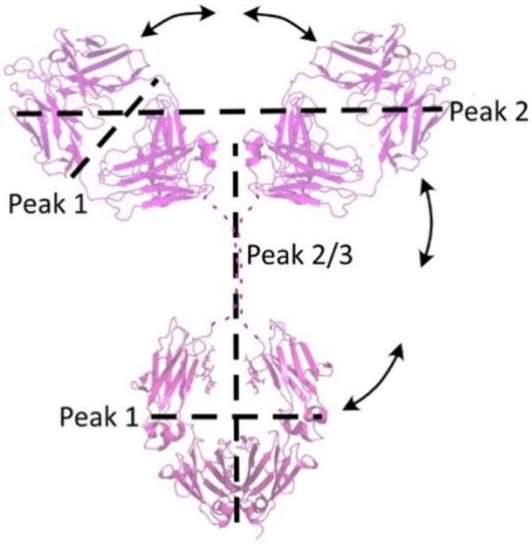

Figure 3.10. (A) Pair distance distribution function (*P(r)*) plot of the anti-CD20 allelic variants. The *P(r)* values are normalised by relative intensity for comparison of all the antibodies on the same scale. The dashed lines indicate the most likely range of the maximum r for each peak. (B) Representative structure of IgG antibody demonstrating the interparticle distances within the structure that correlate to each peak in the *P(r)* distribution. Arrows indicate the potential range of motion exhibited by the antibody domains. The structure was generated on PyMOL with the Fab arms from anti-gp120 IgG1 [PDB: 1hzh (Saphire et al., 2001)] and the Fc region from human IgG3 [PDB: 5w38 (Shah et al., 2017)]. Figure B from Warrender (2023).

In contrast to Peak 1, Peak 2 of the *P(r)* had a variable maximum r for the variants of different hinge lengths, mainly when comparing IgG1*01 and IgG2*02 with the IgG3 variants (Figure 3.10A). This variability in maximum r was also observed with the anti-HER2 allelic variants (Warrender, 2023). Peak 2 most likely corresponds to the distance between the Fab arms and to the distance between the Fab and Fc domains (Belviso et al., 2022; Lu et al., 2007). Possibly due to its shorter hinge, IgG2*02 did not have a clear Peak 2 present, which indicates that the distances between the two Fab arms and between the Fab and Fc domains in this variant are similar to the width of the Fc region and of a Fab arm (Peak 1). Consequently, the frequency of Peak 2 for IgG2*02 is shown together with the frequency of Peak 1. On the other hand, all the IgG3 variants had maximum r values between approximately 89 – 94 Å. The lowest r maximum is of IgG3*04, the IgG3 variant with the shortest hinge (32 amino acids), and the highest r values are of IgG3*01 and IgG3*08, with hinges of 62 amino acids long.

The width of the *P(r)* distribution curves seems to be associated with the hinge length of the anti-CD20 antibodies, and this trend was also observed with the anti-HER2 variants (Warrender, 2023). IgG2*02 of both anti-CD20 and anti-HER2 variable domains displayed the narrowest *P(r)* distribution among the variants, probably because it has the shortest hinge (12 amino acids). IgG1*01, with a hinge of 15 amino acids, had a slightly broader distribution than IgG2*02 and showed more distinct Peaks 1 and 2. The IgG3 variants with the same hinge length had very similar *P(r)* distributions and similar maximum r values. IgG3*03, which has the shortest hinge among the IgG3 variants, had a narrower *P(r)* distribution than the other IgG3. The variants with the longest hinges of 62 amino acids, IgG3*01 and IgG3*08, had the broadest *P(r)* distributions. Possibly because of their extended hinges, IgG3*01 and IgG3*08 display a third intraparticle distance of higher r values (approximately 150 Å), which corresponds to Peak 3. The other variants, mainly IgG1*01, IgG2*02, and IgG3*04, display very low frequencies of high intraparticle distances, most likely due to their shorter hinges. These results indicate that differences in *P(r)* distribution and SAXS parameters (Table 3.2) between the variants could be attributed to the variability in hinge length rather than the single amino acid polymorphisms present in the Fc region.

Flexible structures commonly adopt more extended conformations with higher interatomic distance values within the structure (Liu et al., 2019). Warrender (2023) demonstrated that the anti-HER2 allelic variants with the longest hinges (IgG3*01 and IgG3*08) had the highest r values in the *P(r)* distributions, as seen by the right-shifted curves. Therefore, extended hinges contributed towards higher flexibility. The *P(r)* distributions of the anti-CD20 allelic variants support this conclusion.

As another method to assess flexibility, Dimensionless Kratky plots were used to compare the structural flexibility of the allelic variants. All tested anti-CD20 and anti-HER2 variants, independently of the hinge length, presented a curvature that was approaching zero at higher qR_g values (Figure 3.11) (Warrender, 2023). This behaviour is expected for extended structures with relatively well-ordered domains (Fab arms and Fc region) tethered by a flexible linker region, which would be the hinge (Receveur-Brechot & Durand, 2012). If the structures were disordered, the intensity would increase with the qR_g values. The high variability in intensity values for IgG3*01 at high qR_g is most likely because this sample had noisier scattering at wider *q* than the other samples (Appendix F1).

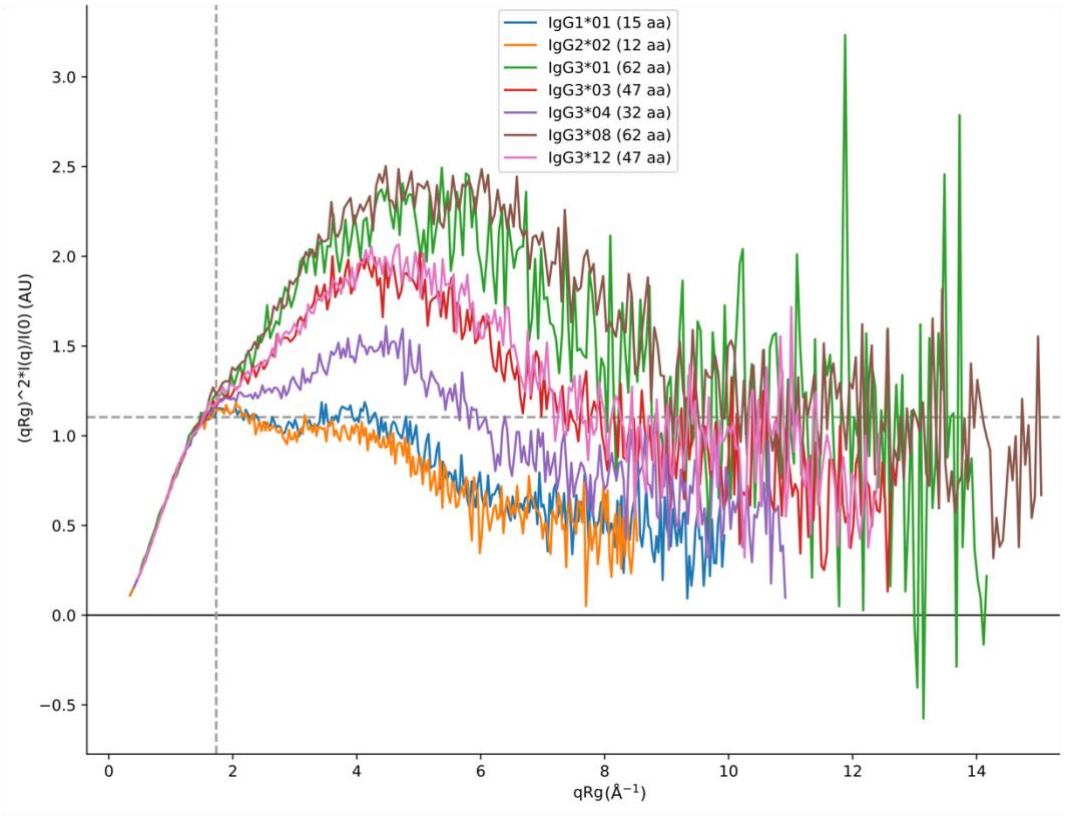

Figure 3.11. Dimensionless Kratky plot of the allelic variants. Intensity is normalised, and q is multiplied by R_g to remove the effects of protein size and molecular weight. The grey dashed lines represent the expected peak maxima for folded, globular proteins, where $(qR_g)^2I(q)/I(0) = 1.104$ in a q range of 0.05 – 0.1 $Å^{-1}$ (Receveur-Bréchot & Durand, 2012).

For both anti-CD20 and anti-HER2 antibodies, the allelic variants that share the same hinge length had similar behaviours in the Dimensionless Kratky plots (Figure 3.11) (Warrender, 2023). The variants with longer hinges, such as IgG3*01 and IgG3*08, had more prominent curves and extended further in the y-axis, which is a reflection of their more elongated structure. The broader peak for the longest hinge variants is an indication of the larger separation of the Fab and Fc domains (Spiteri et al., 2021). IgG1*01 and IgG2*02, which have the shortest hinges, exhibited lower peak maxima than the IgG3 variants. The peak maxima seem to be correlated with the hinge length of the variants, regardless of their variable domain sequence.

The comparison of the SAXS parameters of the anti-CD20 and anti-HER2 allelic variants shows that the differences in sequence and size of the variable domain did not affect the overall flexibility trends associated with the hinge length. The overall size of the variants seems to be larger or smaller in approximately the same

proportion depending on the variable domain sequence. The effects of the hinge length on antibody size and SAXS parameters are consistent across antibodies of different variable domains.

3.5 Influence of hinge length on ADCC and ADCP responses

To study how our observed differences in allelic variant flexibility might affect antibody Fc-mediated functions, we developed methods using genome-engineered reporter cells to detect Fc receptor engagement and activation. This approach is designed to mimic antibody effector functions mediated by the immune system. For ADCC, the Fc receptor with the largest purported contribution to ADCC is FcγRIIIa (Richards et al., 2018), whereas, for ADCP, FcγRIIa is responsible (Brady et al., 2023). Jurkat T cells have been engineered to express each of these receptors in isolation and drive luciferase expression when activated. By using an engineered cell line, we can isolate the effects of specific antibody mechanisms without the interference of multiple Fc receptors on the cell surface.

3.5.1 ADCC response

Three anti-CD20 allelic variants (IgG1*01, IgG3*03, and IgG3*04) were first tested in ADCC assays using CD20 expressing Raji cells to assess whether the results using genome-engineered reporter cells aligned with the conclusions from previous studies (de Taeye et al., 2020; Niwa et al., 2005). The magnitude of the ADCC activity for each antibody was quantified based on the luminescence at each antibody concentration relative to the luminescence of the negative control (no antibody). The luminescence of the wells containing antibodies was divided by the average luminescence of the negative control to determine the fold induction of each sample. The values of fold induction and half maximum effective concentration (EC50) were used to quantify the strength of the ADCC response of each antibody variant.

In the ADCC assays, IgG1*01 triggered stronger ADCC at lower concentration than the other two variants. The variants with shorter hinges (IgG1*01 and IgG3*04) displayed higher fold induction values and lower EC50 than the variant with a longer hinge (IgG3*03) (Figure 3.12, Table 3.3). These results show that IgG1*01, which has the shortest hinge (15 amino acids), led to stronger ADCC than both

IgG3 antibodies and that the IgG3 variant with a shorter hinge (IgG3*04) had stronger ADCC than the one with a longer hinge (IgG3*03). These observations are aligned with what was presented in previous studies (de Taeye et al., 2020; Niwa et al., 2005). Similarly to the results presented here, de Taeye et al. (2020) demonstrated that IgG3*04 had the strongest ADCC activity among the tested IgG3 variants and that IgG1 had the strongest ADCC, mainly when compared to the longer-hinged IgG3 variants.

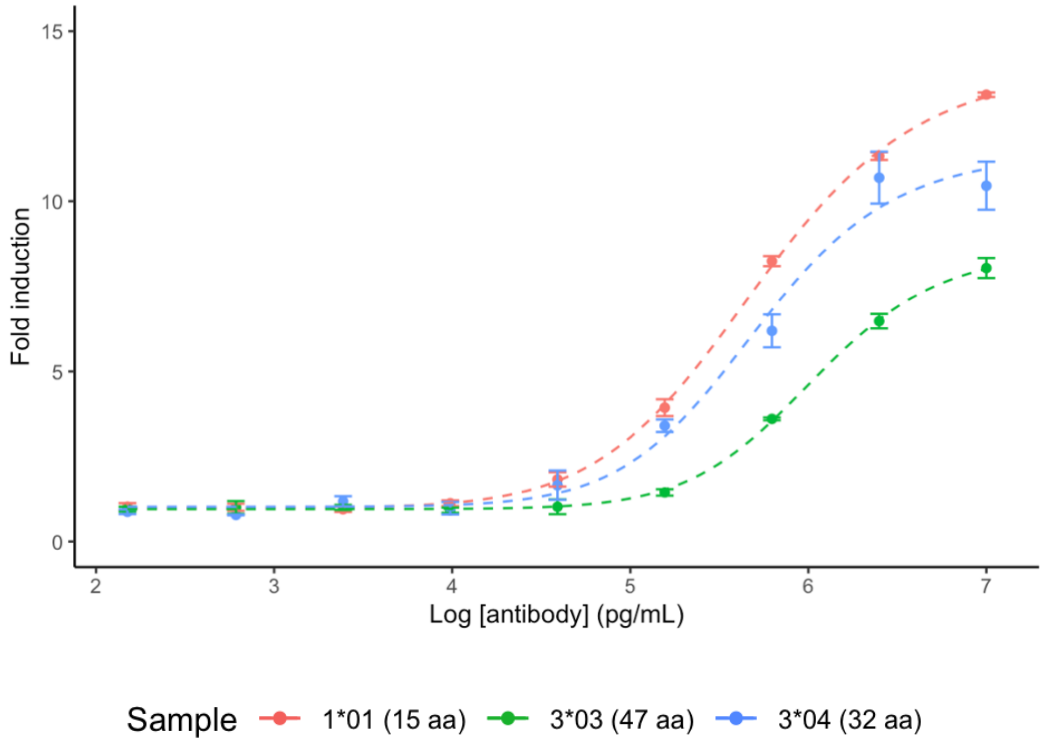

Figure 3.12. Four-parameter logistic model of fold induction values IgG1*01, IgG3*03, and IgG3*04 CD20 in ADCC assay. Each sample was tested in triplicate on the assay plate. Next to the sample name, there is the hinge length of the antibodies in number of amino acid residues.

Table 3.3. EC50 values (pg/mL) and standard error of the four-parameter logistic model for the ADCC assay with IgG1*01, IgG3*03, and IgG3*04 CD20.

Allelic variant	EC50 values	Standard error
IgG1*01	5.71	0.02
IgG3*03	6.03	0.02
IgG3*04	5.71	0.10

In previous research, differences in ADCC response between allelic variants (more specifically, allotypes) have been tested using peripheral blood mononuclear cells (PBMCs) as effector cells and using Raji, Wien-133, and red blood cells as target cells (de Taeye et al., 2020). Antibodies of anti-CD20, anti-CD52, anti-RhD, and anti-TNP variable domains were tested, and the results indicated that the effects of the hinge length and constant domain (CH2, more specifically) sequence on the ADCC response were consistent across the target cells and were antigen-independent. Moreover, the study concluded that the glycosylation profile of the IgG3 variants had minimal effect on ADCC.

In light of the conclusions of previous studies around the effects of the hinge length on ADCC response, the results presented here are in alignment with the observation that allelic variants of shorter hinges trigger stronger ADCC response. Although the assay method used here is different from previous research, the results we presented corroborate what has been shown in the literature. This validates the assay method used in this work, which was mainly applied to assess differences in ADCP response between allelic variants.

3.5.2 ADCP response

Having successfully optimised methods for the ADCC assay, we next sought to apply our approach to ADCP assays, for which high-resolution allelic data is missing from the literature. The Anti-CD20 Control antibody included in the FcγRIIa-H ADCP Bioassay kit (Promega) was tested along with the IgG1*01 CD20 produced for this project to determine if these antibodies display comparable fold induction (Figure 3.13).

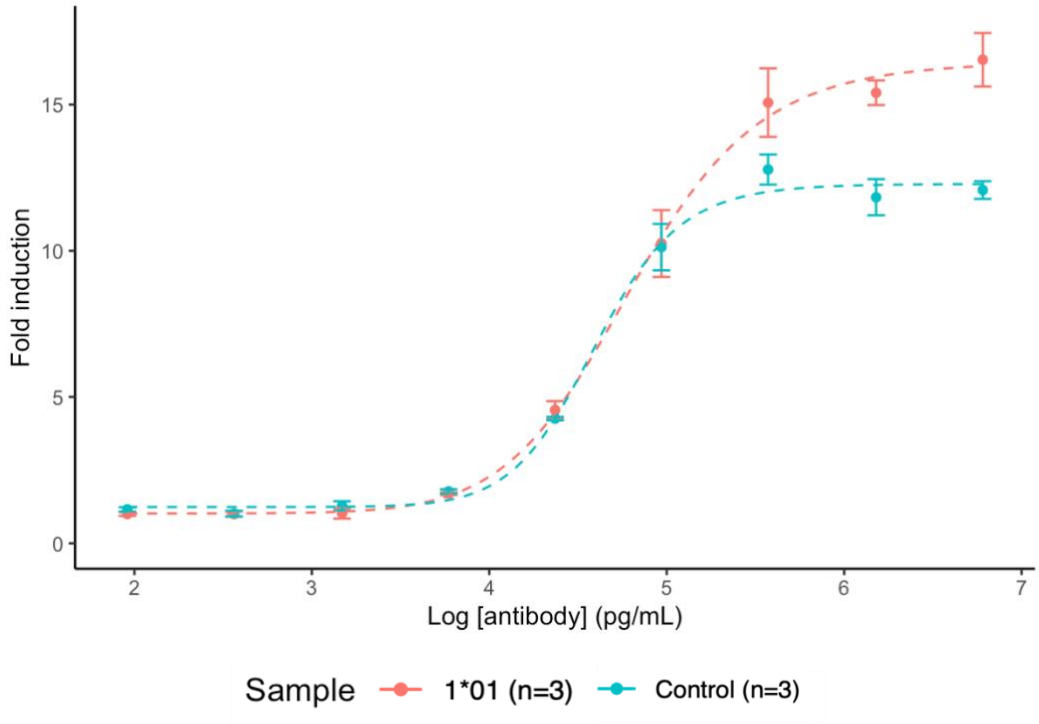

Figure 3.13. Four-parameter logistic model of fold induction values from ADCP assay with IgG1*01 CD20 and Anti-CD20 Control antibody. Each sample was tested in triplicate on the assay plate.

The antibodies had similar (±0.21) EC50 values after fitting a four-parameter logistic model (Table 3.4). However, IgG1*01 displayed higher maximal luminescence above background than the control antibody (Figure 3.13). This difference in fold induction could be due to differences in variable domain between the two antibodies. Even though both bind to CD20 antigen, the antibodies could have different variable domain sequences, which could then lead to differences in binding affinity to the target cells. In spite of these differences, IgG1*01 and the control displayed similar behaviour in the ADCC assay. Therefore, following this test, IgG1*01 was used as a reference sample for all the ADCP assays done in this work and was used to normalise the fold induction of the test antibodies across assay plates. This allowed us to produce the internal controls on a larger scale to ensure consistency across the ADCP assays.

Table 3.4. EC50 values (pg/mL) and standard error of the four-parameter logistic model for ADCP assay with IgG1*01 and the Anti-CD20 Control antibody from Promega.

Sample	EC50 values	Standard error
IgG1*01	4.80	0.04
Control	4.59	0.04

Next, we undertook ADCP assays for each of the individual allelic variants. The strategy was to perform two independent replicates (each containing three technical replicates) where the antibodies were expressed and purified in different batches. These antibodies were purified via the same affinity chromatography method (using protein L resin column) and were size-excluded via equivalent SEC methods.

Each allelic variant displayed similar fold induction curves in the replicate ADCP assays (Figure 3.14). One of the few differences between the results of the assay replicates is that the maximal luminescence values above background of the second ADCP assay with WIL2-S cells were overall higher than the first assay. For instance, the maximal fold induction value for the overall average of IgG1*01 was higher in the second assay (8.3) than in the first (5.2). The higher luminescence is possibly due to the use of Bio-Glo™ Luciferase Assay Reagent (Promega) that was reconstituted more recently (fewer days) before the second assays compared to the first assays with WIL2-S cells. Normalisation across plates helps to alleviate this variability, but the results show that it was not enough to remove these differences completely.

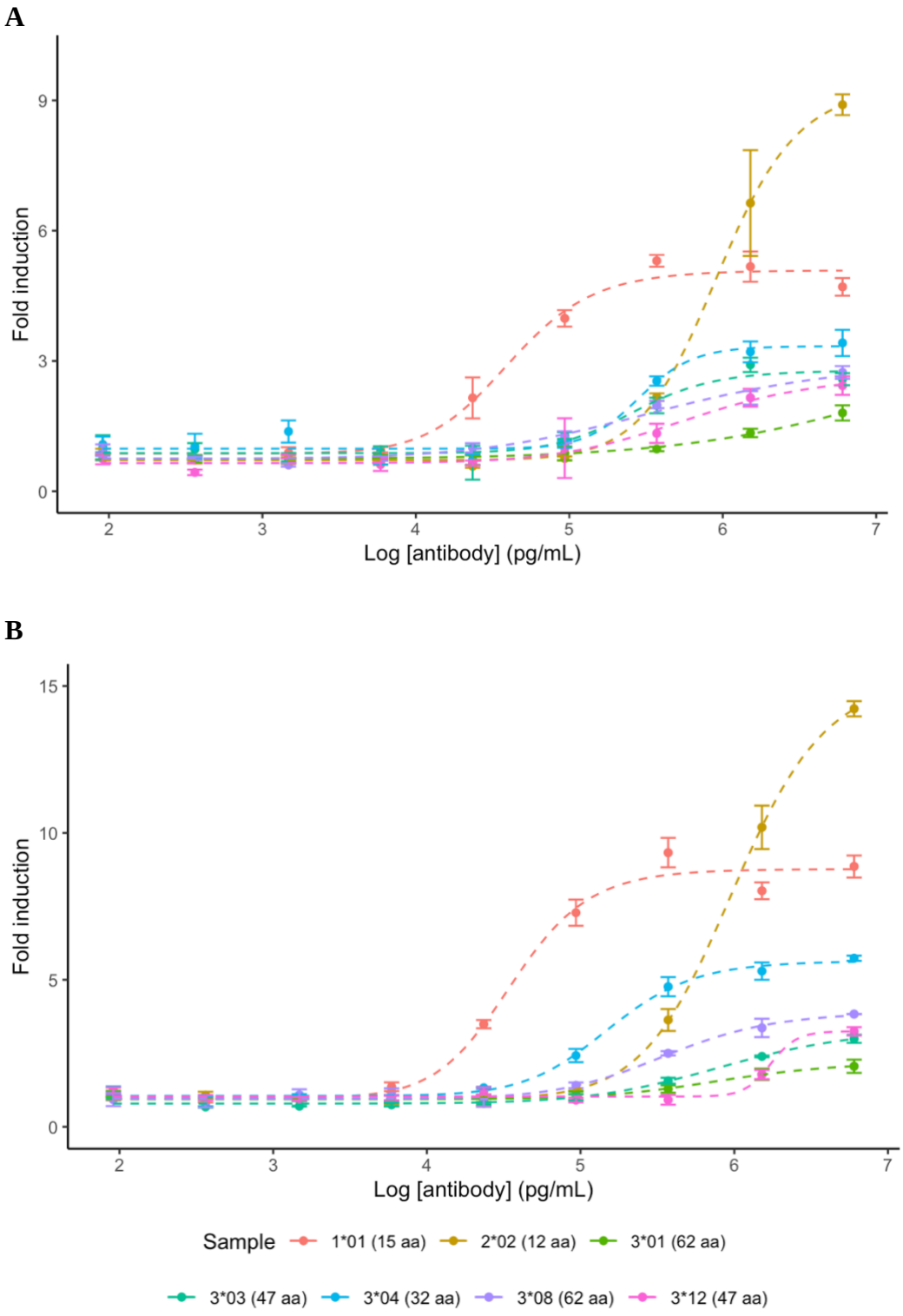

Figure 3.14. Four-parameter logistic models of fold induction values of the seven selected anti-CD20 allelic variants from first (A) and second (B) ADCP assays using WIL2-S as target cells. The first and second assays were tested with a different antibody expression batch. Each sample was tested in triplicate on the assay plates. Next to the sample name, there is the hinge length of the antibodies in number of amino acid residues.

In both independent replicates using WIL2-S cells, IgG1*01 showed high luminescence values at a considerably lower concentration compared to the other samples. IgG2*02, the variant with the shortest hinge, achieved the highest fold induction values at high concentrations. IgG3*01 and IgG3*12, which have the longest hinge, presented very low fold induction in comparison to the other variants. In contrast, IgG3*04, which contains the shortest hinge among the IgG3, displayed the highest fold induction of the subclass in both assays.

To determine whether the trends we observed were cell line dependent, the ADCP assays were repeated using a second CD20-expressing target cell line (Raji). In the ADCP assays using Raji as target cells (Figure 3.15), the fold induction trends for the allelic variants were very similar to what was observed for the assays with WIL2-S cells. The only variants that behaved differently were IgG3*01 and IgG3*08, which presented higher and lower fold induction values, respectively, than what was observed in the assays using WIL2-S cells.

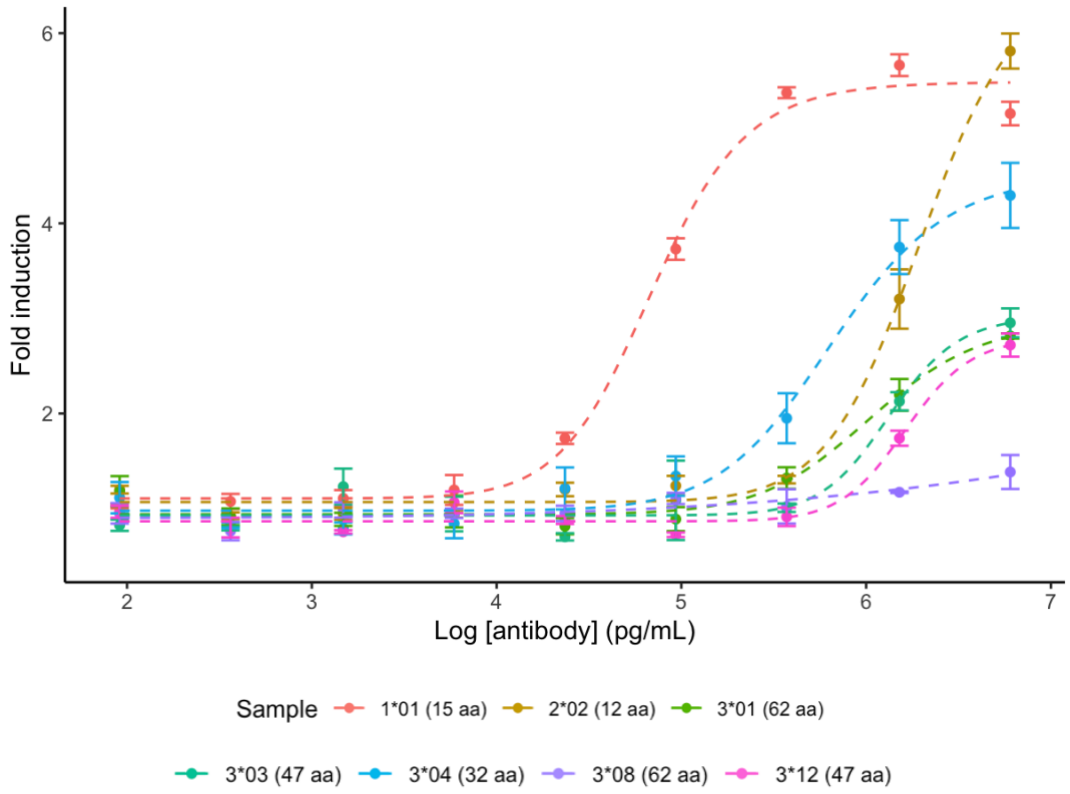

Figure 3.15. Four-parameter logistic model of fold induction values from ADCP assays of the seven chosen anti-CD20 allelic variants using Raji as target cells. Each sample was tested in triplicate on the assay plate. Next to the sample name, there is the hinge length of the antibodies in number of amino acid residues.

For each of the plots (Figure 3.14, Figure 3.15), the fold induction of IgG1*01 from one of the assay plates was selected to represent the variant since all the plates tested this sample. The representative IgG1*01 has the fold induction values closest to the overall average for this variant and has the lowest standard deviation between its triplicates. In the first assay with WIL2-S cells, the fold induction values for IgG1*01 were chosen from the plate where IgG3*08 was tested, whereas for the second assay with these cells, the IgG1*01 fold induction was chosen from the plate where IgG2*02 was tested. For the graph of the assays with Raji cells, the IgG1*01 fold induction is from the plate where IgG3*01 was tested.

The negative control wells of some of the ADCP assay plates (the first assay with IgG3*12, the second assay with IgG2*02, and the assays with IgG3*03, IgG3*08, and IgG3*12 using Raji cells) showed unusually high luminescence values, while the wells that contained antibodies at the lowest concentration had normal (low)

luminescence values. Because of this issue, the fold induction of these assay plates was calculated using the wells with the lowest antibody concentration as the negative control instead of the wells that did not contain any antibody - the actual negative control. The only exception was the first assay with IgG3*12 using WIL2-S cells, in which the wells with the lowest antibody concentration and the negative control were used in combination to calculate the fold induction. The fold induction values for IgG1*01 (reference) of this plate would be either considerably higher or lower than the average if only the negative control wells or the most dilute wells, respectively, were used to calculate the fold induction. This assay will be repeated to generate publication-quality data.

A four-parameter logistic model was fit to the assays. This model assumes that the data is symmetric and fits in the four-parameter logistic regression equation (Appendix G1). However, in the case of the first assay of IgG3*01 using WIL2-S cells, the four-parameter model had a high standard error, indicating that this model did not properly fit the data (Table 3.5). A five-parameter logistic model, which assumes that the data forms an asymmetric curve, fit the data better than the four-parameter model. Using a four-parameter model, the EC50 of IgG3*01 for the first assay would be 8.39 pg/mL with a standard error of 4.94, compared to an EC50 of 6.16 pg/mL with a standard error of 0.29 with the five-parameter model. Comparing these two values, the EC50 from the five-parameter logistic model for this test is more similar to the EC50 of the other two assays (from the four-parameter logistic model). The most likely reason for the poor fitting to the four-parameter model is the low fold induction values of IgG3*01, which hinder the fitting of the data to a symmetric curve. Future assays could test IgG3*01 at higher concentrations with the aim of achieving saturation, which would then facilitate the fitting of the data to the logistic regression.

Table 3.5. EC50 values (pg/mL) and standard error of the four-parameter logistic model for the allelic variants tested in the ADCP assays. The seven variants were tested twice with WIL2-S cells and once with Raji cells. Along with the name of the allelic variants, there is the hinge length in number of amino acid residues. *Only the fold induction of IgG3*01 in the first assay with WIL2-S cells was fit to a five-parameter logistic model.

	1st assay with WIL-2S		2nd assay with WIL2-S		Assay with Raji	
Allelic variant	**EC50 Value**	**Std error**	**EC50 Value**	**Std error**	**EC50 Value**	**Std error**
1*01 (15 aa)	4.61	0.08	4.55	0.07	4.84	0.06
2*02 (12 aa)	5.97	0.02	6.00	0.02	6.30	0.11
3*01 (62 aa)	6.16*	0.29	5.92	0.22	6.03	0.13
3*03 (47 aa)	5.42	0.14	5.95	0.22	6.13	0.09
3*04 (32 aa)	5.46	0.10	5.19	0.05	5.82	0.10
3*08 (62 aa)	5.62	0.45	5.56	0.12	14.96	26.07
3*12 (47 aa)	5.78	0.21	6.24	0.14	6.22	0.10

Neither five- nor four-parameter logistic models generated a good fit for the normalised results of the assay with IgG3*08 using Raji cells. This is partly due to the fact that the fold induction values for IgG1*01 (reference) in the same assay plate were higher than usual (~11.0 at the highest antibody concentration) (Appendix G3). Consequently, the normalised fold induction values for the ADCP assay of IgG3*08 with Raji cells were scaled down considerably, leading to issues in the fit of the logistic models (Table 3.5). For means of comparison, the EC50 of IgG3*08 from the pre-normalisation fold induction of the assay with Raji cells is 5.98 pg/mL, which is close to the normalised EC50 values from the other two assays with this variant (5.62 pg/mL and 5.56 pg/mL). As mentioned for IgG3*01, testing IgG3*08 at a higher concentration could help avoid issues of data fitting to logistic regression.

The EC50 values for the two ADCP assays with WIL2-S as target cells were similar (standard deviations of up to 0.37). The EC50 values from the assays with Raji as target cells were higher than the ones from the assays with WIL2-S cells, but only by up to 0.7 (except for IgG3*08). Distinctions in the EC50 values between the assays with different target cell lines were expected, partly because of differences in antigen density between WIL2-S and Raji cells. WIL2-S cells have higher CD20 density on their surface compared to Raji (Gurjar et al., 2017), which contributes to the binding of the anti-CD20 antibodies in the ADCP assays. With a higher antigen density, more antibodies can bind to each cell, and therefore, there will be a higher Fc region density around the target cells for FcγRs to bind to (Figure 3.16). The more antibody-binding to FcγRs and FcγR-crosslinking (ITAM engagement), the more luminescence is generated from the effector cells, which corresponds to stronger ADCP. Moreover, there were more WIL2-S cells per well in the assay plates than Raji (28,900 and 25,000 cells, respectively) due to differences in how the cells were diluted from frozen. The manufacturer's recommendation is 25,000 target cells per well. The differences in antigen density and cell numbers are the most likely causes behind lower EC50 values for the assays with WIL2-S cells compared to the ones with Raji.

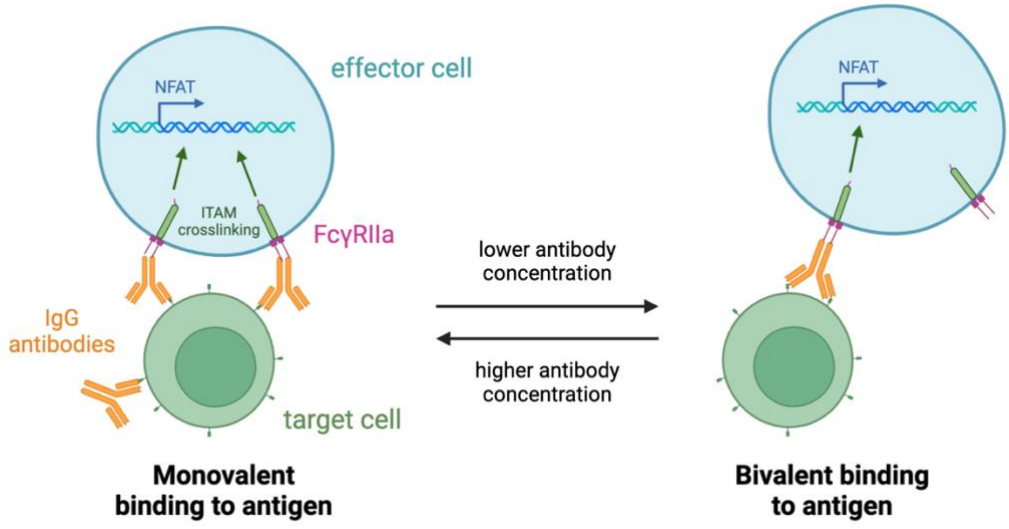

Figure 3.16. Variability in monovalent and bivalent binding of IgG antibodies to antigen on target cell is dependent on antibody concentration and influences crosslinking of FcγRs via ITAM in effector cells. Greater receptor engagement contributes to the activation of the NFAT pathway. Figure made using BioRender: https://www.biorender.com/.

When comparing the allelic variants, the three assays showed a similar pattern: IgG1*01 had the lowest EC50 among the variants, IgG3*04 had the lowest (or close second-lowest) EC50 among the IgG3 samples, and IgG3*12 was among the three variants with highest EC50. IgG3*01, IgG3*03, and IgG3*08 had fluctuating positions when being ranked based on EC50 values. Curiously, IgG2*02 had the second-highest EC50 values among the seven variants, even though it achieved the highest fold induction values at the highest antibody concentrations. This finding was consistent across the three assays (Figure 3.14, Figure 3.15). The fold induction of IgG2*02 demonstrates that this variant requires higher antibody concentration to achieve luminescence above background, but it also triggers the strongest ADCP among the variants at the highest tested concentration. This behaviour could be an indication that IgG2*02 binds bivalently to CD20 at low concentrations but shifts to primarily monovalent binding at higher concentrations (Figure 3.16). At high antibody concentrations, the shorter hinge of IgG2*02 could be facilitating the monovalent binding to antigen and FcγRIIa, allowing for higher FcγR engagement via ITAM crosslinking and, thus, higher luminescence generation than the other allelic variants. Testing allelic variants with different variable domain sequences along with different target cell lines could provide further insight into this hypothesis.

In contrast to previous studies (Chu et al., 2020; Crowley et al., 2022; Richards et al., 2008; Richardson et al., 2019), the ADCP assay method used in this work involved effector cells that only expressed one type of FcγR, the FcγRIIa/CD32a. It is pertinent to note that only the polymorphic variant FcγRIIa-H (histidine at position 131) is present on the cells, which is the higher affinity variant of FcγRIIa. This removes the possibility of different types of FcγRs or polymorphic variants for the receptor, such as FcγRIIa-R, affecting the results due to differences in binding affinity to IgG (Bruhns et al., 2009; Talathi et al., 2019).

The binding affinity of IgG2 to FcγRIIa is considerably lower than that of IgG1 and IgG3 (Patel et al., 2013), which is possibly one of the reasons why a higher concentration of IgG2*02 is required to achieve luminescence values above background compared to IgG1*01 and some of the IgG3. The FcγRIIa-H variant, used in the ADCP assays, has a higher affinity for IgG2 than FcγRIIa-R (Bruhns et

al., 2009; Crowley et al., 2023). Nonetheless, even though binding affinity to FcγR influences the magnitude of the effector functions triggered, higher affinity to the receptor does not necessarily correlate to stronger effector functions (Chu et al., 2020; Richards et al., 2008).

There were clear differences in the magnitude of ADCP response between the allelic variants, as seen by the fold induction curves and the EC50 values (Figure 3.14, Figure 3.15, Table 3.5). The hinge length of the variants appears to have influenced these results, as there seems to be a trend that variants with shorter hinges trigger stronger ADCP (lower EC50). However, the association between hinge length and EC50 value is not statistically significant (p-value > 0.05) when comparing the variants across all three subclasses (Figure 3.17A). The main cause behind the lack of correlation is the fact that IgG2*02, the variant with the shortest hinge, consistently displayed one of the highest EC50 values. To remove the influence of subclass-specific characteristics, variants from the IgG3 subclass only were compared (Fig 3.17B), but this comparison also demonstrated no significant correlation between hinge length and EC50. For contrast, the p-value for the correlation of hinge length and EC50 between IgG1*01 and the IgG3 variants (excluding IgG2*02) is 0.0002. Overall, the assay results and the correlation plots indicate that the variability in the magnitude of the ADCP response between the allelic variants may not be fully attributed to the differences in hinge length despite a moderate trend. Testing with more replicates could help resolve this uncertainty.

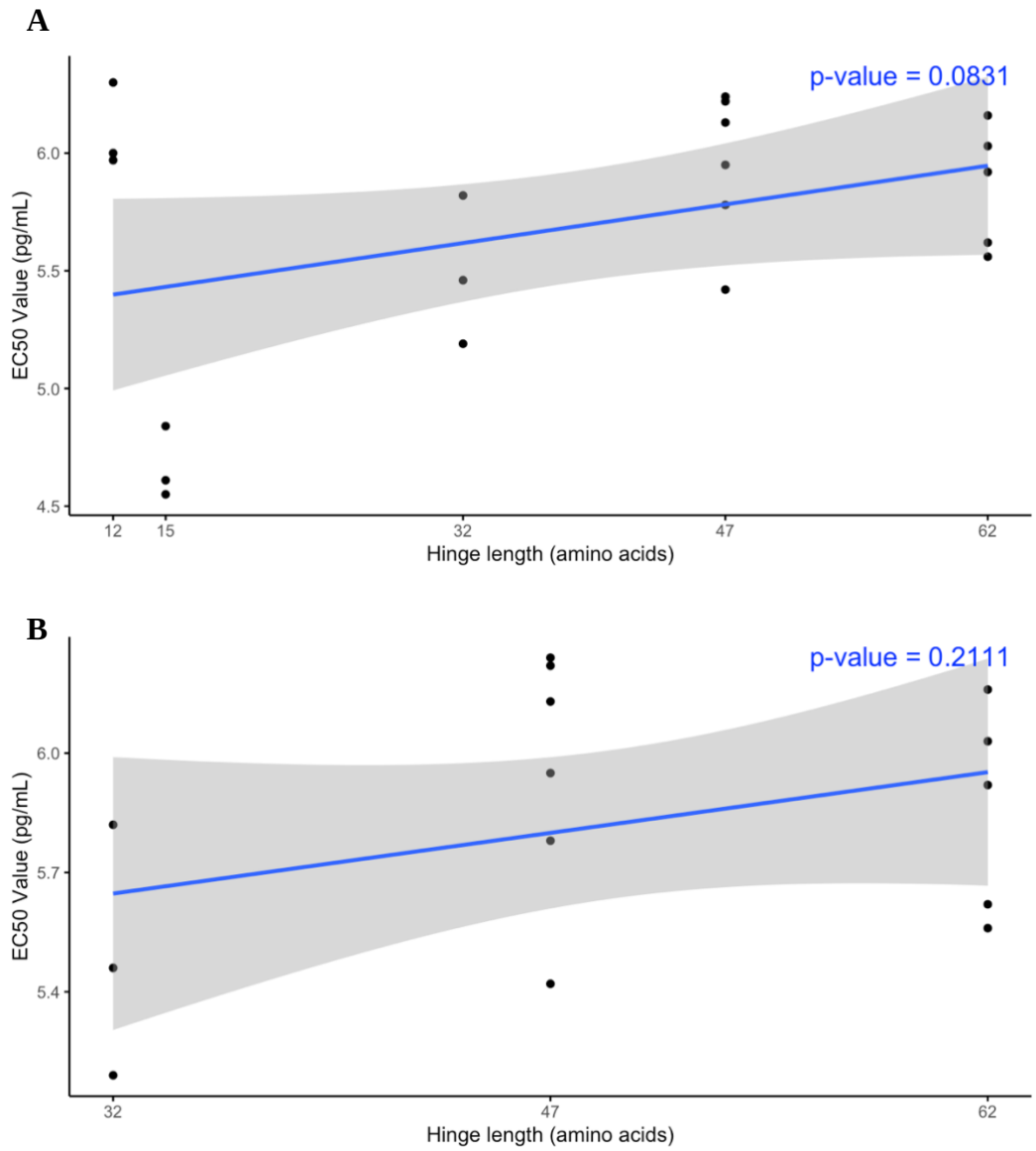

Figure 3.17. Correlation plots of hinge length in number of amino acids with EC50 value (pg/mL) from the four-parameter logistic model. The calculated p-value is shown on the right. The shaded area shows the confidence interval. The EC50 values are from the replicate assays with WIL2-S and the assay with Raji. The only EC50 value from a five-parameter model is for IgG3*01 from the first assay with WIL2-S. The EC50 of IgG3*08 from the assay with Raji cells was not included due to the very poor fitting to the logistic models. (A) Correlation plot with EC50 and hinge lengths of the seven allelic variants. (B) Correlation plot of EC50 and hinge lengths of IgG3 variants only.

Since variants of the same hinge length did not exhibit matching fold induction curves, it is possible that the few amino acid polymorphisms in the Fc region of the selected IgG3 variants influenced the results, possibly by altering the binding affinity to FcγRIIa (Crowley et al., 2023). For instance, the Y296F mutation present

in IgG3*12, but also in all IgG2, has been associated with lower affinity to FcγRIIIa and weaker ADCC response (de Taeye et al., 2020), which shows that polymorphisms in the Fc region between the variants could be influencing their EC50 values. In contrast, the results of Crowley et al. (2023) demonstrated that the genetic variability in the Fc region of allotypes alone (without the influence of the hinge length) did not appreciably alter FcγR-mediated effector functions.

Variability in N-linked glycosylation profiles of the Fc region between the variants could also be influencing the results by affecting their binding affinity to FcγRIIa (Forthal et al., 2010; Subedi & Barb, 2016). For example, IgG2 antibodies and IgG3*12 have an equal ratio of G1 Fa and G1 Fb glycan isoforms, which differ in the position of the terminal galactose residue, while the other allelic variants have up to four times more G1 Fa (Warrender et al., 2023). These differences are related to the presence of phenylalanine instead of tyrosine at position 296 in IgG2 antibodies and IgG3*12. On the other hand, prior work has shown that differences in glycosylation profile between allotypes have minimal effect on ADCC (de Taeye et al., 2020), which may also hold true for ADCP.

Interestingly, the conclusions of this work in regard to the effects of the hinge length on the ADCP response are not aligned with the observations from previous studies. Chu et al. (2020), a study with HIV-specific antibodies that were designed with IgG1 backbone and IgG3 hinges, demonstrated that the IgG1 antibodies designed with longer hinges triggered greater ADCP responses, while the results we presented here indicate that variants with shorter hinges tend to trigger stronger ADCP. Furthermore, Richardson et al. (2019) demonstrated that HIV-specific broadly neutralising antibodies of the IgG3 subclass that were engineered with IgG1 hinges (15 amino acids) showed significantly reduced ADCP compared to variants with hinges of 47 and 62 amino acids, indicating that IgG3 variants with longer hinges could trigger stronger ADCP than the ones of shorter hinges. Both these studies used HIV-specific antibodies and the monocytic cell line THP-1, and these factors may be part of the cause behind the contrast with the findings presented here. Results obtained with HIV-specific antibodies are not necessarily observed with antibodies of different variable domains, partly due to differences in epitope features (Griffith & McCoy, 2021). Differences in antibody target and variable

domain may lead to differences in the spatial conformation of the IgG around the target cells, affecting how the Fc region of each antibody is displayed and, thus, how easily it binds to FcγRs (Hadzhieva et al., 2017). The contrast in observations presented here with previous research highlights the need for further ADCP assays with different antigen targets being tested.

Many variables still remain to be tested in order to have more clarity on the extent of the influence of the hinge length on the magnitude of ADCP responses. It would be valuable, for instance, to test the allelic variants in ADCP assays with effector cells that express FcγRIIa-R, the lower affinity variant of the receptor, and with target cells that express CD20 at a different density than Raji and WIL2-S cells. In addition, different antigens could be tested along with antibodies of different variable domains, possibly including more allelic variants as well.

4 Chapter Four

Conclusions and Future Directions

The extent of the genetic diversity in the constant region of human IgG is yet to be determined. The number of allelic variants that have already been identified has been growing with the improvement of sequencing techniques (Ford et al., 2023). Along with the identification of different polymorphic variants, there is a need to understand the evolutionary drivers behind these differences in genetic composition. This study provided insight into the scope of the influence of constant region polymorphisms on human IgG antibody structure and Fc-mediated effector functions.

Due to the genetic polymorphisms in the constant region of IgG antibodies, their structural dynamics, thermal stability, and immune function vary considerably within the subclasses, mainly among the IgG3. This variability is one of the reasons why the outcome of disease and responsiveness to therapeutics and vaccines can be different from one person to the next (Kratochvil et al., 2017; Richardson et al., 2019; Rodriguez et al., 2023). The expanding documentation of the effects of allelic variation on IgG antibody properties could be applied to improve therapeutic antibodies, making them more effective in the treatment of cancer, autoimmunity, and infectious diseases. For example, therapeutic mAbs could be developed with a combination of naturally occurring constant region sequences that have been associated with desirable properties, such as stronger effector function and higher thermal stability. There is a growing body of evidence on the influence of the hinge length on these antibody properties (Canfield & Morrison, 1991; Chu et al., 2020; Warrender et al., 2023), and this work aimed to contribute to the understanding of the effects of allelic hinge variation on IgG3 effector functions. Furthermore, we aimed to determine if the differences in structural dynamics between polymorphic variants aligned with observed variability in Fc-mediated effector functions, more specifically, ADCC and ADCP.

The findings of this work support the evidence that constant region diversity, primarily around hinge length, among IgG3 antibodies affects their structural

dynamics and some Fc-mediated effector functions, such as ADCC. The results from SAXS analysis show a clear trend of hinge length with size and flexibility of the allelic variants of anti-CD20 and anti-HER variable domains, in which variants with longer hinges had larger and more flexible structures. This variability in structural dynamics seems to contribute to differences in the magnitude of ADCC effector function, as variants with shorter hinges, and thus with greater molecular rigidity, tended to display stronger responses. ADCP responses were less clear, and while a moderate trend was observed with longer hinges promoting stronger reporter cell activation, this correlation did not reach a statistical significance of $p < 0.05$. The exact reason for the weak correlation is unclear, and therefore, we suggest performing further tests with more replicates in order to get more clarity on the influence of the hinge length on ADCP. It is likely that other variables, such as polymorphisms in the Fc region, differences in affinity to FcγRs, and antigen density on target cells along with spatial conformations of the IgG around these cells, affect the strength of the immune response in conjunction with the hinge length (Chu et al., 2020; Crowley et al., 2023; Hadzhieva et al., 2017; Richards et al., 2008).

To complement the structural analysis done with anti-CD20 and anti-HER2 allelic variants, the anti-AAV5 antibody variants produced in this work will be used for BioSAXS in the near future. Moreover, the anti-CD20 variants will be analysed again on the BioSAXS beamline, with the aim of collecting scattering data of higher quality and greater q range than the SAXS data presented here. Nevertheless, the structural data that was presented in this work, in combination with the findings of Warrender (2023), provides a strong basis for us to be confident of some of the effects of the hinge length on IgG3 antibody size and flexibility.

The observations of the SAXS structural analysis in this work support further investigation of conformational dynamics of the allelic variants by using higher resolution techniques. Future work could include the application of molecular dynamic (MD) simulations to help provide further insight into the differences in conformational dynamics between the variants. MD can be used to generate an ensemble of structural models at atomic resolution, demonstrating multiple conformations that antibodies can adopt in solution (Yamashita, 2018). In addition,

negative-stain electron microscopy (EM) can be utilised as a complementary tool to SAXS and can be used to assess both protein structure and protein-protein interactions from relatively low sample amounts (Gallagher et al., 2019; Rames et al., 2014).

Multiple variables remain to be tested in ADCP assays with IgG allelic variants. Future work should assess whether using target cells with different antigens and at different densities would lead to a distinct pattern of strength of ADCP response. This would include using allelic variants with different variable domains, which is also a variable to be assessed. Testing the other polymorphic variant of FcγRIIa, FcγRIIa-R, could also give useful insights into antibody function since it displays different binding affinities to IgG (Bruhns et al., 2009). Additionally, it would be valuable to assess the differences in ADCP function using PBMCs such as monocytes and NK cells, which would provide a more similar setting to the *in vivo* environment, partly due to the availability of several different Fc receptors on the cells.

Overall, this work has contributed to a greater understanding of the influence of constant region polymorphisms of IgG antibodies on their structural dynamics and Fc-mediated effector functions. The data presented here is the basis for future research on the influence of IgG constant region polymorphisms on antibody structural dynamics and immune effector functions, which could contribute to improvements and innovations in the design of therapeutic antibodies.

References

Ackerman, M. E., Moldt, B., Wyatt, R. T., Dugast, A.-S., McAndrew, E., Tsoukas, S., Jost, S., Berger, C. T., Sciaranghella, G., Liu, Q., Irvine, D. J., Burton, D. R., & Alter, G. (2011). A robust, high-throughput assay to determine the phagocytic activity of clinical antibody samples. *Journal of Immunological Methods*, *366*(1–2), 8–19. https://doi.org/10.1016/j.jim.2010.12.016

Anderson, C. L., Shen, L., Eicher, D. M., Wewers, M. D., & Gill, J. K. (1990). Phagocytosis mediated by three distinct Fc gamma receptor classes on human leukocytes. *The Journal of Experimental Medicine*, *171*(4), 1333–1345. https://doi.org/10.1084/jem.171.4.1333

Arthur, G. K., & Cruse, G. (2022). Regulation of Trafficking and Signaling of the High Affinity IgE Receptor by FcεRIβ and the Potential Impact of FcεRIβ Splicing in Allergic Inflammation. *International Journal of Molecular Sciences*, *23*(2), 788. https://doi.org/10.3390/ijms23020788

Ashish, Solanki, A. K., Boone, C. D., & Krueger, J. K. (2010). Global structure of HIV-1 neutralizing antibody IgG1 b12 is asymmetric. *Biochemical and Biophysical Research Communications*, *391*(1), 947–951. https://doi.org/10.1016/j.bbrc.2009.11.170

Bashirova, A. A., Zheng, W., Akdag, M., Augusto, D. G., Vince, N., Dong, K. L., O'hUigin, C., & Carrington, M. (2021). Population-specific diversity of the immunoglobulin constant heavy G chain (IGHG) genes. *Genes & Immunity*, *22*(7–8), 327–334. https://doi.org/10.1038/s41435-021-00156-2

Bassing, C. H., Swat, W., & Alt, F. W. (2002). The Mechanism and Regulation of Chromosomal V(D)J Recombination. *Cell*, *109*(2), S45–S55. https://doi.org/10.1016/S0092-8674(02)00675-X

Belviso, B. D., Mangiatordi, G. F., Alberga, D., Mangini, V., Carrozzini, B., & Caliandro, R. (2022). Structural Characterization of the Full-Length Anti-CD20 Antibody Rituximab. *Frontiers in Molecular Biosciences*, *9*, 823174. https://doi.org/10.3389/fmolb.2022.823174

Beppler, J., Koehler-Santos, P., Pasqualim, G., Matte, U., Alho, C. S., Dias, F. S., Kowalski, T. W., Velasco, I. T., Monteiro, R. C., & Pinheiro Da Silva, F. (2016). Fc Gamma Receptor IIA (CD32A) R131 Polymorphism as a Marker of Genetic Susceptibility to Sepsis. *Inflammation*, *39*(2), 518–525. https://doi.org/10.1007/s10753-015-0275-1

Berón, W., Alvarez-Dominguez, C., Mayorga, L., & Stahl, P. D. (1995). Membrane trafficking along the phagocytic pathway. *Trends in Cell Biology*, *5*(3), 100–104. https://doi.org/10.1016/S0962-8924(00)88958-8

BioRender. (n.d.). https://www.biorender.com/

Björkström, N. K., Gonzalez, V. D., Malmberg, K.-J., Falconer, K., Alaeus, A., Nowak, G., Jorns, C., Ericzon, B.-G., Weiland, O., Sandberg, J. K., & Ljunggren, H.-G. (2008). Elevated Numbers of FcγRIIIA+ (CD16+) Effector CD8 T Cells with NK Cell-Like Function in Chronic Hepatitis C Virus Infection. *The Journal of Immunology*, *181*(6), 4219–4228. https://doi.org/10.4049/jimmunol.181.6.4219

Bottermann, M., Lode, H. E., Watkinson, R. E., Foss, S., Sandlie, I., Andersen, J. T., & James, L. C. (2016). Antibody-antigen kinetics constrain intracellular humoral immunity. *Scientific Reports*, *6*(1), 37457. https://doi.org/10.1038/srep37457

Bournazos, S., & Ravetch, J. V. (2017). Diversification of IgG effector functions. *International Immunology*, *29*(7), 303–310. https://doi.org/10.1093/intimm/dxx025

Brady, T., Cayatte, C., Roe, T. L., Speer, S. D., Ji, H., Machiesky, L., Zhang, T., Wilkins, D., Tuffy, K. M., & Kelly, E. J. (2023). Fc-mediated functions of nirsevimab complement direct respiratory syncytial virus neutralization but are not required for optimal prophylactic protection. *Frontiers in Immunology*, *14*, 1283120. https://doi.org/10.3389/fimmu.2023.1283120

Bruhns, P., Frémont, S., & Daëron, M. (2005). Regulation of allergy by Fc receptors. *Current Opinion in Immunology*, *17*(6), 662–669. https://doi.org/10.1016/j.coi.2005.09.012

Bruhns, P., Iannascoli, B., England, P., Mancardi, D. A., Fernandez, N., Jorieux, S., & Daëron, M. (2009). Specificity and affinity of human Fcγ receptors and their polymorphic variants for human IgG subclasses. *Blood*, *113*(16), 3716–3725. https://doi.org/10.1182/blood-2008-09-179754

Bzymek, K. P., & Williams, J. C. (2014, December 24). *Structure of Rituximab Fab*. RCSB PDB. https://doi.org/10.2210/pdb4KAQ/pdb

Calonga-Solís, V., Malheiros, D., Beltrame, M. H., Vargas, L. D. B., Dourado, R. M., Issler, H. C., Wassem, R., Petzl-Erler, M. L., & Augusto, D. G. (2019). Unveiling the Diversity of Immunoglobulin Heavy Constant Gamma (IGHG) Gene Segments in Brazilian Populations Reveals 28 Novel Alleles and Evidence of Gene Conversion and Natural Selection. *Frontiers in Immunology*, *10*, 1161. https://doi.org/10.3389/fimmu.2019.01161

Canfield, S. M., & Morrison, S. L. (1991). The binding affinity of human IgG for its high affinity Fc receptor is determined by multiple amino acids in the CH2 domain and is modulated by the hinge region. *The Journal of Experimental Medicine*, *173*(6), 1483–1491. https://doi.org/10.1084/jem.173.6.1483

Capone, M., & Matthew, J. (2016). Fc Receptor-Like Proteins in Pathophysiology of B-cell Disorder. *Journal of Clinical & Cellular Immunology*, *7*(3). https://doi.org/10.4172/2155-9899.1000427

Carter, P. J. (2006). Potent antibody therapeutics by design. *Nature Reviews Immunology*, *6*(5), 343–357. https://doi.org/10.1038/nri1837

Catici, D. A. M., Amos, H. E., Yang, Y., Van Den Elsen, J. M. H., & Pudney, C. R. (2016). The red edge excitation shift phenomenon can be used to unmask protein structural ensembles: Implications for NEMO–ubiquitin interactions. *The FEBS Journal*, *283*(12), 2272–2284. https://doi.org/10.1111/febs.13724

Chakrabarti, A. (2018). Separation of Monoclonal Antibodies by Analytical Size Exclusion Chromatography. In T. Böldicke (Ed.), *Antibody Engineering*. InTech. https://doi.org/10.5772/intechopen.73321

Cheng, Z. J., Garvin, D., Paguio, A., Moravec, R., Engel, L., Fan, F., & Surowy, T. (2014). Development of a robust reporter-based ADCC assay with frozen, thaw-and-use cells to measure Fc effector function of therapeutic antibodies. *Journal of Immunological Methods*, *414*, 69–81. https://doi.org/10.1016/j.jim.2014.07.010

Chowdhury, P. S., & Wu, H. (2005). Tailor-made antibody therapeutics. *Methods*, *36*(1), 11–24. https://doi.org/10.1016/j.ymeth.2005.01.002

Chu, T. H., Crowley, A. R., Backes, I., Chang, C., Tay, M., Broge, T., Tuyishime, M., Ferrari, G., Seaman, M. S., Richardson, S. I., Tomaras, G. D., Alter, G., Leib, D., & Ackerman, M. E. (2020). Hinge length contributes to the phagocytic activity of HIV-specific IgG1 and IgG3 antibodies. *PLOS Pathogens*, *16*(2), e1008083. https://doi.org/10.1371/journal.ppat.1008083

Cleary, K. L. S., Chan, H. T. C., James, S., Glennie, M. J., & Cragg, M. S. (2017). Antibody Distance from the Cell Membrane Regulates Antibody Effector Mechanisms. *The Journal of Immunology*, *198*(10), 3999–4011. https://doi.org/10.4049/jimmunol.1601473

Coënon, L., & Villalba, M. (2022). From CD16a Biology to Antibody-Dependent Cell-Mediated Cytotoxicity Improvement. *Frontiers in Immunology*, *13*, 913215. https://doi.org/10.3389/fimmu.2022.913215

Constantinides, M., Fayd'herbe De Maudave, A., Potier-Cartereau, M., Campos-Mora, M., Cartron, G., & Villalba, M. (2023). Direct Cell Death Induced by CD20 Monoclonal Antibodies on B Cell Lymphoma Cells Revealed by New Protocols of Analysis. *Cancers*, *15*(4), 1109. https://doi.org/10.3390/cancers15041109

Crowley, A. R., Richardson, S. I., Tuyishime, M., Jennewein, M., Bailey, M. J., Lee, J., Alter, G., Ferrari, G., Morris, L., & Ackerman, M. E. (2023). Functional consequences of allotypic polymorphisms in human immunoglobulin G subclasses. *Immunogenetics*, *75*(1), 1–16. https://doi.org/10.1007/s00251-022-01272-7

Daëron, M. (1997). Fc RECEPTOR BIOLOGY. *Annual Review of Immunology*, *15*(Volume 15, 1997), 203–234. https://doi.org/10.1146/annurev.immunol.15.1.203

Damelang, T., Brinkhaus, M., Van Osch, T. L. J., Schuurman, J., Labrijn, A. F., Rispens, T., & Vidarsson, G. (2024). Impact of structural modifications of IgG antibodies on effector functions. *Frontiers in Immunology*, *14*, 1304365. https://doi.org/10.3389/fimmu.2023.1304365

de Taeye, S. W., Bentlage, A. E. H., Mebius, M. M., Meesters, J. I., Lissenberg-Thunnissen, S., Falck, D., Sénard, T., Salehi, N., Wuhrer, M., Schuurman, J., Labrijn, A. F., Rispens, T., & Vidarsson, G. (2020). FcγR Binding and ADCC Activity of Human IgG Allotypes. *Frontiers in Immunology*, *11*. https://www.frontiersin.org/articles/10.3389/fimmu.2020.00740

Delidakis, G., Kim, J. E., George, K., & Georgiou, G. (2022). Improving Antibody Therapeutics by Manipulating the Fc Domain: Immunological and Structural Considerations. *Annual Review of Biomedical Engineering*, *24*(1), 249–274. https://doi.org/10.1146/annurev-bioeng-082721-024500

Duchemin, A. M., Ernst, L. K., & Anderson, C. L. (1994). Clustering of the high affinity Fc receptor for immunoglobulin G (Fc gamma RI) results in phosphorylation of its associated gamma-chain. *The Journal of Biological Chemistry*, *269*(16), 12111–12117.

Dudley, D. D., Chaudhuri, J., Bassing, C. H., & Alt, F. W. (2005). Mechanism and Control of V(D)J Recombination versus Class Switch Recombination: Similarities and Differences. In *Advances in Immunology* (Vol. 86, pp. 43–112). Elsevier. https://doi.org/10.1016/S0065-2776(04)86002-4

Ernst, L. K., Duchemin, A. M., & Anderson, C. L. (1993). Association of the high-affinity receptor for IgG (Fc gamma RI) with the gamma subunit of the IgE receptor. *Proceedings of the National Academy of Sciences*, *90*(13), 6023–6027. https://doi.org/10.1073/pnas.90.13.6023

Eryilmaz, E., Janda, A., Kim, J., Cordero, R. J. B., Cowburn, D., & Casadevall, A. (2013). Global structures of IgG isotypes expressing identical variable regions. *Molecular Immunology*, *56*(4), 588–598. https://doi.org/10.1016/j.molimm.2013.06.006

Expasy—ProtParam. (n.d.). https://web.expasy.org/protparam/

Fang, R., Wey, A., Bobbili, N. K., Leke, R. F. G., Taylor, D. W., & Chen, J. J. (2017). An analytical approach to reduce between-plate variation in multiplex assays that measure antibodies to Plasmodium falciparum antigens. *Malaria Journal*, *16*(1), 287. https://doi.org/10.1186/s12936-017-1933-6

Ferrante, A., Beard, L. J., & Feldman, R. G. (1990). IgG subclass distribution of antibodies to bacterial and viral antigens: *The Pediatric Infectious Disease Journal*, *9*(Supplement), 516–524. https://doi.org/10.1097/00006454-199008001-00004

Ford, E. E., Tieri, D., Rodriguez, O. L., Francoeur, N. J., Soto, J., Kos, J. T., Peres, A., Gibson, W. S., Silver, C. A., Deikus, G., Hudson, E., Woolley, C. R., Beckmann, N., Charney, A., Mitchell, T. C., Yaari, G., Sebra, R. P., Watson, C. T., & Smith, M. L. (2023). FLAIRR-Seq: A Method for Single-Molecule Resolution of Near Full-Length Antibody H Chain Repertoires. *The Journal of Immunology*, *210*(10), 1607–1619. https://doi.org/10.4049/jimmunol.2200825

Forthal, D. N., Gach, J. S., Landucci, G., Jez, J., Strasser, R., Kunert, R., & Steinkellner, H. (2010). Fc-Glycosylation Influences Fcγ Receptor Binding and Cell-Mediated Anti-HIV Activity of Monoclonal Antibody 2G12. *The Journal of Immunology*, *185*(11), 6876–6882. https://doi.org/10.4049/jimmunol.1002600

Foss, S., Jonsson, A., Bottermann, M., Watkinson, R., Lode, H. E., McAdam, M. B., Michaelsen, T. E., Sandlie, I., James, L. C., & Andersen, J. T. (2022). Potent TRIM21 and complement-dependent intracellular antiviral immunity requires the IgG3 hinge. *Science Immunology*, *7*(70), eabj1640. https://doi.org/10.1126/sciimmunol.abj1640

Foss, S., Watkinson, R. E., Grevys, A., McAdam, M. B., Bern, M., Høydahl, L. S., Dalhus, B., Michaelsen, T. E., Sandlie, I., James, L. C., & Andersen, J. T. (2016). TRIM21 Immune Signaling Is More Sensitive to Antibody Affinity Than Its Neutralization Activity. *The Journal of Immunology*, *196*(8), 3452–3459. https://doi.org/10.4049/jimmunol.1502601

Fric, J., Zelante, T., Wong, A. Y. W., Mertes, A., Yu, H.-B., & Ricciardi-Castagnoli, P. (2012). NFAT control of innate immunity. *Blood*, *120*(7), 1380–1389. https://doi.org/10.1182/blood-2012-02-404475

Gallagher, J. R., Kim, A. J., Gulati, N. M., & Harris, A. K. (2019). Negative-Stain Transmission Electron Microscopy of Molecular Complexes for Image Analysis by 2D Class Averaging. *Current Protocols in Microbiology*, *54*(1), e90. https://doi.org/10.1002/cpmc.90

Gasteiger, E., Hoogland, C., Gattiker, A., Duvaud, S., Wilkins, M. R., Appel, R. D., & Bairoch, A. (2005). Protein Identification and Analysis Tools on the ExPASy Server. In J. M. Walker (Ed.), *The Proteomics Protocols Handbook* (pp. 571–607). Humana Press. https://doi.org/10.1385/1-59259-890-0:571

Ghetie, V., Hubbard, J. G., Kim, J., Tsen, M., Lee, Y., & Ward, E. S. (1996). Abnormally short serum half-lives of IgG in β2-microglobulin-deficient mice. *European Journal of Immunology*, *26*(3), 690–696. https://doi.org/10.1002/eji.1830260327

Giudicelli, V. (2006). IMGT/LIGM-DB, the IMGT(R) comprehensive database of immunoglobulin and T cell receptor nucleotide sequences. *Nucleic Acids Research*, *34*(90001), D781–D784. https://doi.org/10.1093/nar/gkj088

Goebl, N. A., Babbey, C. M., Datta-Mannan, A., Witcher, D. R., Wroblewski, V. J., & Dunn, K. W. (2008). Neonatal Fc Receptor Mediates Internalization of Fc in Transfected Human Endothelial Cells. *Molecular Biology of the Cell*, *19*(12), 5490–5505. https://doi.org/10.1091/mbc.e07-02-0101

Granoff, D. M., & Holmes, S. J. (1992). G2m(23) Immunoglobulin Allotype and Immunity to Haemophilus influenzae Typeb. *Journal of Infectious Diseases*, *165*(Supplement 1), S66–S69. https://doi.org/10.1093/infdis/165-Supplement_1-S66

Griffith, S. A., & McCoy, L. E. (2021). To bnAb or Not to bnAb: Defining Broadly Neutralising Antibodies Against HIV-1. *Frontiers in Immunology*, *12*, 708227. https://doi.org/10.3389/fimmu.2021.708227

Grubb, R. (1956). AGGLUTINATION OF ERYTHROCYTESCOATED WITH "INCOMPLETE" ANTI-RH BY CERTAIN RHEUMATOID ARTHRITIC SERA AND SOME OTHER SERA: The Existence of Human Serum Groups. *Acta Pathologica Microbiologica Scandinavica*, *39*(3), 195–197. https://doi.org/10.1111/j.1699-0463.1956.tb03392.x

Gül, N., Babes, L., Siegmund, K., Korthouwer, R., Bögels, M., Braster, R., Vidarsson, G., Ten Hagen, T. L. M., Kubes, P., & Van Egmond, M. (2014). Macrophages eliminate circulating tumor cells after monoclonal antibody therapy. *Journal of Clinical Investigation*, *124*(2), 812–823. https://doi.org/10.1172/JCI66776

Gurjar, S. A., Derrick, J. P., Dearman, R. J., Thorpe, R., Hufton, S., Kimber, I., & Wadhwa, M. (2017). Surrogate CD16-expressing effector cell lines for determining the bioactivity of therapeutic monoclonal antibodies. *Journal of Pharmaceutical and Biomedical Analysis*, *143*, 188–198. https://doi.org/10.1016/j.jpba.2017.06.004

Hadzhieva, M., Pashov, A. D., Kaveri, S., Lacroix-Desmazes, S., Mouquet, H., & Dimitrov, J. D. (2017). Impact of Antigen Density on the Binding Mechanism of IgG Antibodies. *Scientific Reports*, *7*(1), 3767. https://doi.org/10.1038/s41598-017-03942-z

Hamilton, R. G. (1987). Human IgG subclass measurements in the clinical laboratory. *Clinical Chemistry*, *33*(10), 1707–1725.

Hine, B. C., Hunt, P. W., Beasley, A. M., Windon, R. G., Glover, S. A., & Colditz, I. G. (2010). Selective transport of IgE into ovine mammary secretions. *Research in Veterinary Science*, *89*(2), 184–190. https://doi.org/10.1016/j.rvsc.2010.02.010

Hui, G. K., Gardener, A. D., Begum, H., Eldrid, C., Thalassinos, K., Gor, J., & Perkins, S. J. (2019). The solution structure of the human IgG2 subclass is distinct from those for human IgG1 and IgG4 providing an explanation for their discrete functions. *Journal of Biological Chemistry*, *294*(28), 10789–10806. https://doi.org/10.1074/jbc.RA118.007134

Ito, T., & Tsumoto, K. (2013). Effects of subclass change on the structural stability of chimeric, humanized, and human antibodies under thermal stress. *Protein Science*, *22*(11), 1542–1551. https://doi.org/10.1002/pro.2340

Izadi, A., Hailu, A., Godzwon, M., Wrighton, S., Olofsson, B., Schmidt, T., Söderlund-Strand, A., Elder, E., Appelberg, S., Valsjö, M., Larsson, O., Wendel-Hansen, V., Ohlin, M., Bahnan, W., & Nordenfelt, P. (2023). Subclass-switched anti-spike IgG3 oligoclonal cocktails strongly enhance Fc-mediated opsonization. *Proceedings of the National Academy of Sciences*, *120*(15), e2217590120. https://doi.org/10.1073/pnas.2217590120

Jay, J., Bray, B., Qi, Y., Igbinigie, E., Wu, H., Li, J., & Ren, G. (2018). IgG Antibody 3D Structures and Dynamics. *Antibodies*, *7*(2), 18. https://doi.org/10.3390/antib7020018

Jefferis, R., & Lefranc, M.-P. (2009). Human immunoglobulin allotypes: Possible implications for immunogenicity. *mAbs*, *1*(4), 332–338. https://doi.org/10.4161/mabs.1.4.9122

Jefferis, R., Lund, J., & Pound, J. D. (1998). IgG-Fc-mediated effector functions: Molecular definition of interaction sites for effector ligands and the role of glycosylation. *Immunological Reviews*, *163*(1), 59–76. https://doi.org/10.1111/j.1600-065X.1998.tb01188.x

Johnson, W. E., Kohn, P. H., & Steinberg, A. G. (1977). Population genetics of the human allotypes Gm, Inv, and A2m. *Clinical Immunology and Immunopathology*, *7*(1), 97–113. https://doi.org/10.1016/0090-1229(77)90034-4

Jones, P. T., Dear, P. H., Foote, J., Neuberger, M. S., & Winter, G. (1986). Replacing the complementarity-determining regions in a human antibody with those from a mouse. *Nature*, *321*(6069), 522–525. https://doi.org/10.1038/321522a0

Karshikoff, A., Nilsson, L., & Ladenstein, R. (2015). Rigidity versus flexibility: The dilemma of understanding protein thermal stability. *The FEBS Journal*, *282*(20), 3899–3917. https://doi.org/10.1111/febs.13343

Kikhney, A. G., & Svergun, D. I. (2015). A practical guide to small angle X-ray scattering (SAXS) of flexible and intrinsically disordered proteins. *FEBS Letters*, *589*(19PartA), 2570–2577. https://doi.org/10.1016/j.febslet.2015.08.027

Kikuno, K., Kang, D.-W., Tahara, K., Torii, I., Kubagawa, H. M., Ho, K. J., Baudino, L., Nishizaki, N., Shibuya, A., & Kubagawa, H. (2007). Unusual biochemical features and follicular dendritic cell expression of human Fcalpha/mu receptor. *European Journal of Immunology*, *37*(12), 3540–3550. https://doi.org/10.1002/eji.200737655

Knight, M. J., Woolley, R. E., Kwok, A., Parsons, S., Jones, H. B. L., Gulácsy, C. E., Phaal, P., Kassaar, O., Dawkins, K., Rodriguez, E., Marques, A., Bowsher, L., Wells, S. A., Watts, A., Van Den Elsen, J. M. H., Turner, A., O'Hara, J., & Pudney, C. R. (2020). Monoclonal antibody stability can be usefully monitored using the excitation-energy-dependent fluorescence edge-shift. *Biochemical Journal*, *477*(18), 3599–3612. https://doi.org/10.1042/BCJ20200580

Ko, S., Park, S., Sohn, M. H., Jo, M., Ko, B. J., Na, J.-H., Yoo, H., Jeong, A. L., Ha, K., Woo, J. R., Lim, C., Shin, J. H., Lee, D., Choi, S.-Y., & Jung, S. T. (2022). An Fc variant with two mutations confers prolonged serum half-life and enhanced effector functions on IgG antibodies. *Experimental & Molecular Medicine*, *54*(11), 1850–1861. https://doi.org/10.1038/s12276-022-00870-5

Köhler, G., & Milstein, C. (1975). Continuous cultures of fused cells secreting antibody of predefined specificity. *Nature*, *256*(5517), 495–497. https://doi.org/10.1038/256495a0

Kratochvil, S., McKay, P. F., Chung, A. W., Kent, S. J., Gilmour, J., & Shattock, R. J. (2017). Immunoglobulin G1 Allotype Influences Antibody Subclass Distribution in Response to HIV gp140 Vaccination. *Frontiers in Immunology*, *8*, 1883. https://doi.org/10.3389/fimmu.2017.01883

Kubagawa, H., Oka, S., Kubagawa, Y., Torii, I., Takayama, E., Kang, D.-W., Gartland, G. L., Bertoli, L. F., Mori, H., Takatsu, H., Kitamura, T., Ohno, H., & Wang, J.-Y. (2009). Identity of the elusive IgM Fc receptor (FcμR) in humans. *Journal of Experimental Medicine*, *206*(12), 2779–2793. https://doi.org/10.1084/jem.20091107

Kükrer, B., Filipe, V., Van Duijn, E., Kasper, P. T., Vreeken, R. J., Heck, A. J. R., & Jiskoot, W. (2010). Mass Spectrometric Analysis of Intact Human Monoclonal Antibody Aggregates Fractionated by Size-Exclusion Chromatography. *Pharmaceutical Research*, *27*(10), 2197–2204. https://doi.org/10.1007/s11095-010-0224-5

Lau, A. W., & Brink, R. (2020). Selection in the germinal center. *Current Opinion in Immunology*, *63*, 29–34. https://doi.org/10.1016/j.coi.2019.11.001

Lefranc, M.-P., Giudicelli, V., Ginestoux, C., Jabado-Michaloud, J., Folch, G., Bellahcene, F., Wu, Y., Gemrot, E., Brochet, X., Lane, J., Regnier, L., Ehrenmann, F., Lefranc, G., & Duroux, P. (2009). IMGT(R), the international ImMunoGeneTics information system(R). *Nucleic Acids Research*, *37*(Database), D1006–D1012. https://doi.org/10.1093/nar/gkn838

Lefranc, M.-P., & Lefranc, G. (2020). Immunoglobulins or Antibodies: IMGT® Bridging Genes, Structures and Functions. *Biomedicines*, *8*(9), 319. https://doi.org/10.3390/biomedicines8090319

Li, B., Xu, L., Tao, F., Xie, K., Wu, Z., Li, Y., Li, J., Chen, K., Pi, C., Mendelsohn, A., Larrick, J. W., Gu, H., & Fang, J. (2017). Simultaneous exposure to FcγR and FcαR on monocytes and macrophages enhances antitumor activity *in vivo*. *Oncotarget*, *8*(24), 39356–39366. https://doi.org/10.18632/oncotarget.17000

Liu, X., Zhao, Y., Shi, H., Zhang, Y., Yin, X., Liu, M., Zhang, H., He, Y., Lu, B., Jin, T., & Li, F. (2019). Human immunoglobulin G hinge regulates agonistic anti-CD40 immunostimulatory and antitumour activities through biophysical flexibility. *Nature Communications*, *10*(1), 4206. https://doi.org/10.1038/s41467-019-12097-6

Lu, L. L., Suscovich, T. J., Fortune, S. M., & Alter, G. (2018). Beyond binding: Antibody effector functions in infectious diseases. *Nature Reviews Immunology*, *18*(1), 46–61. https://doi.org/10.1038/nri.2017.106

Lu, Y., Harding, S. E., Michaelsen, T. E., Longman, E., Davis, K. G., Ortega, Á., Grossmann, J. G., Sandlie, I., & García De La Torre, J. (2007). Solution Conformation of Wild-Type and Mutant IgG3 and IgG4 Immunoglobulins Using Crystallohydrodynamics: Possible Implications for Complement Activation. *Biophysical Journal*, *93*(11), 3733–3744. https://doi.org/10.1529/biophysj.107.108993

Luthra, A., Langley, D. B., Schofield, P., Jackson, J., Abdelatti, M., Rouet, R., Nevoltris, D., Mazigi, O., Crossett, B., Christie, M., & Christ, D. (2019). Human Antibody Bispecifics through Phage Display Selection. *Biochemistry*, *58*(13), 1701–1704. https://doi.org/10.1021/acs.biochem.9b00037

Lyu, X., Zhao, Q., Hui, J., Wang, T., Lin, M., Wang, K., Zhang, J., Shentu, J., Dalby, P. A., Zhang, H., & Liu, B. (2022). The global landscape of approved antibody therapies. *Antibody Therapeutics*, *5*(4), 233–257. https://doi.org/10.1093/abt/tbac021

Macian, F. (2005). NFAT proteins: Key regulators of T-cell development and function. *Nature Reviews Immunology*, *5*(6), 472–484. https://doi.org/10.1038/nri1632

Majewska, N. I., Tejada, M. L., Betenbaugh, M. J., & Agarwal, N. (2020). *N*-Glycosylation of IgG and IgG-Like Recombinant Therapeutic Proteins: Why Is It Important and How Can We Control It? *Annual Review of Chemical and Biomolecular Engineering*, *11*(1), 311–338. https://doi.org/10.1146/annurev-chembioeng-102419-010001

Maloney, D. G., Grillo-López, A. J., White, C. A., Bodkin, D., Schilder, R. J., Neidhart, J. A., Janakiraman, N., Foon, K. A., Liles, T.-M., Dallaire, B. K., Wey, K., Royston, I., Davis, T., & Levy, R. (1997). IDEC-C2B8 (Rituximab) Anti-CD20 Monoclonal Antibody Therapy in Patients With Relapsed Low-Grade Non-Hodgkin's Lymphoma. *Blood*, *90*(6), 2188–2195. https://doi.org/10.1182/blood.V90.6.2188

Manalastas-Cantos, K., Konarev, P. V., Hajizadeh, N. R., Kikhney, A. G., Petoukhov, M. V., Molodenskiy, D. S., Panjkovich, A., Mertens, H. D. T., Gruzinov, A., Borges, C., Jeffries, C. M., Svergun, D. I., & Franke, D. (2021). ATSAS 3.0: Expanded functionality and new tools for small-angle scattering data analysis. *Journal of Applied Crystallography*, *54*(Pt 1), 343–355. https://doi.org/10.1107/S1600576720013412

Mancardi, D., & Daëron, M. (2014). Fc Receptors in Immune Responses. *Reference Module in Biomedical Sciences*, B9780128012383001197. https://doi.org/10.1016/B978-0-12-801238-3.00119-7

Manis, J. P., Tian, M., & Alt, F. W. (2002). Mechanism and control of class-switch recombination. *Trends in Immunology*, *23*(1), 31–39. https://doi.org/10.1016/S1471-4906(01)02111-1

Masuda, M., & Roos, D. (1993). Association of all three types of Fc gamma R (CD64, CD32, and CD16) with a gamma-chain homodimer in cultured human monocytes. *Journal of Immunology (Baltimore, Md.: 1950)*, *151*(12), 7188–7195.

Merle, N. S., Noe, R., Halbwachs-Mecarelli, L., Fremeaux-Bacchi, V., & Roumenina, L. T. (2015). Complement System Part II: Role in Immunity. *Frontiers in Immunology*, *6*. https://doi.org/10.3389/fimmu.2015.00257

Miyake, K., & Karasuyama, H. (2021). The Role of Trogocytosis in the Modulation of Immune Cell Functions. *Cells*, *10*(5), 1255. https://doi.org/10.3390/cells10051255

Mkaddem, S. B., Benhamou, M., & Monteiro, R. C. (2019). Understanding Fc Receptor Involvement in Inflammatory Diseases: From Mechanisms to New Therapeutic Tools. *Frontiers in Immunology*, *10*, 811. https://doi.org/10.3389/fimmu.2019.00811

Monteiro, R. C., & Van De Winkel, J. G. J. (2003). IgA Fc Receptors. *Annual Review of Immunology*, *21*(1), 177–204. https://doi.org/10.1146/annurev.immunol.21.120601.141011

Morrison, S. L., Johnson, M. J., Herzenberg, L. A., & Oi, V. T. (1984). Chimeric human antibody molecules: Mouse antigen-binding domains with human constant region domains. *Proceedings of the National Academy of Sciences of the United States of America*, *81*(21), 6851–6855. https://doi.org/10.1073/pnas.81.21.6851

Nallet, S., Fornelli, L., Schmitt, S., Parra, J., Baldi, L., Tsybin, Y. O., & Wurm, F. M. (2012). Glycan variability on a recombinant IgG antibody transiently produced in HEK-293E cells. *New Biotechnology*, *29*(4), 471–476. https://doi.org/10.1016/j.nbt.2012.02.003

Nimmerjahn, F., & Ravetch, J. V. (2008). Fcγ receptors as regulators of immune responses. *Nature Reviews Immunology*, *8*(1), 34–47. https://doi.org/10.1038/nri2206

Niwa, R., Natsume, A., Uehara, A., Wakitani, M., Iida, S., Uchida, K., Satoh, M., & Shitara, K. (2005). IgG subclass-independent improvement of antibody-dependent cellular cytotoxicity by fucose removal from Asn297-linked oligosaccharides. *Journal of Immunological Methods*, *306*(1–2), 151–160. https://doi.org/10.1016/j.jim.2005.08.009

Otten, M. A., & van Egmond, M. (2004). The Fc receptor for IgA (FcαRI, CD89). *Immunology Letters*, *92*(1–2), 23–31. https://doi.org/10.1016/j.imlet.2003.11.018

Pandey, J. P., Kistner-Griffin, E., Iwasaki, M., Bu, S., Deepe, R., Black, L., Kasuga, Y., Hamada, G. S., & Tsugane, S. (2012). Genetic markers of immunoglobulin G and susceptibility to breast cancer. *Human Immunology*, *73*(11), 1155–1158. https://doi.org/10.1016/j.humimm.2012.07.340

Pandey, J. P., & Namboodiri, A. M. (2014). Genetic variants of IgG1 antibodies and FcγRIIIa receptors influence the magnitude of antibody-dependent cell-mediated cytotoxicity against prostate cancer cells. *OncoImmunology*, *3*(1), e27317. https://doi.org/10.4161/onci.27317

Panjkovich, A., & Svergun, D. I. (2018). CHROMIXS: Automatic and interactive analysis of chromatography-coupled small-angle X-ray scattering data. *Bioinformatics*, *34*(11), 1944–1946. https://doi.org/10.1093/bioinformatics/btx846

Parekh, B. S., Berger, E., Sibley, S., Cahya, S., Xiao, L., LaCerte, M. A., Vaillancourt, P., Wooden, S., & Gately, D. (2012). Development and validation of an antibody-dependent cell-mediated cytotoxicity-reporter gene assay. *mAbs*, *4*(3), 310–318. https://doi.org/10.4161/mabs.19873

Patel, R., Johnson, K. K., Andrien, B. A., & Tamburini, P. P. (2013). IGG SUBCLASS VARIATION OF A MONOCLONAL ANTIBODY BINDING TO HUMAN FC-GAMMA RECEPTORS. *American Journal of Biochemistry and Biotechnology*, *9*(3), 206–218. https://doi.org/10.3844/ajbbsp.2013.206.218

Pérez, J., Vachette, P., Russo, D., Desmadril, M., & Durand, D. (2001). Heat-induced unfolding of neocarzinostatin, a small all-β protein investigated by small-angle X-ray scattering 1 1Edited by M. F. Moody. *Journal of Molecular Biology*, *308*(4), 721–743. https://doi.org/10.1006/jmbi.2001.4611

Preud'homme, J.-L., Petit, I., Barra, A., Morel, Jean-Claude Lecron, F., & Lelièvre, E. (2000). Structural and functional properties of membrane and secreted IgD. *Molecular Immunology*, *37*(15), 871–887. https://doi.org/10.1016/S0161-5890(01)00006-2

Putnam, C. D. (2016). Guinier peak analysis for visual and automated inspection of small-angle X-ray scattering data. *Journal of Applied Crystallography*, *49*(5), 1412–1419. https://doi.org/10.1107/S1600576716010906

Ra, C., Jouvin, M.-H. E., Blank, U., & Kinet, J.-P. (1989). A macrophage Fcγ receptor and the mast cell receptor for IgE share an identical subunit. *Nature*, *341*(6244), 752–754. https://doi.org/10.1038/341752a0

Rambo, R. P., & Tainer, J. A. (2011). Characterizing flexible and intrinsically unstructured biological macromolecules by SAS using the Porod-Debye law. *Biopolymers*, *95*(8), 559–571. https://doi.org/10.1002/bip.21638

Rames, M., Yu, Y., & Ren, G. (2014). Optimized Negative Staining: A High-throughput Protocol for Examining Small and Asymmetric Protein Structure by Electron Microscopy. *Journal of Visualized Experiments*, *90*, 51087. https://doi.org/10.3791/51087

Rao, A., Luo, C., & Hogan, P. G. (1997). TRANSCRIPTION FACTORS OF THE NFAT FAMILY:Regulation and Function. *Annual Review of Immunology*, *15*(1), 707–747. https://doi.org/10.1146/annurev.immunol.15.1.707

Ravetch, J. V., & Perussia, B. (1989). Alternative membrane forms of Fc gamma RIII(CD16) on human natural killer cells and neutrophils. Cell type-specific expression of two genes that differ in single nucleotide substitutions. *The Journal of Experimental Medicine*, *170*(2), 481–497. https://doi.org/10.1084/jem.170.2.481

Receveur-Brechot, V., & Durand, D. (2012). How Random are Intrinsically Disordered Proteins? A Small Angle Scattering Perspective. *Current Protein & Peptide Science*, *13*(1), 55–75. https://doi.org/10.2174/138920312799277901

Richards, J. O., Karki, S., Lazar, G. A., Chen, H., Dang, W., & Desjarlais, J. R. (2008). Optimization of antibody binding to FcγRIIa enhances macrophage phagocytosis of tumor cells. *Molecular Cancer Therapeutics*, *7*(8), 2517–2527. https://doi.org/10.1158/1535-7163.MCT-08-0201

Richardson, S. I., Lambson, B. E., Crowley, A. R., Bashirova, A., Scheepers, C., Garrett, N., Abdool Karim, S., Mkhize, N. N., Carrington, M., Ackerman, M. E., Moore, P. L., & Morris, L. (2019). IgG3 enhances neutralization potency and Fc effector function of an HIV V2-specific broadly neutralizing antibody. *PLOS Pathogens*, *15*(12), e1008064. https://doi.org/10.1371/journal.ppat.1008064

Robbie, G. J., Criste, R., Dall'Acqua, W. F., Jensen, K., Patel, N. K., Losonsky, G. A., & Griffin, M. P. (2013). A Novel Investigational Fc-Modified Humanized Monoclonal Antibody, Motavizumab-YTE, Has an Extended Half-Life in Healthy Adults. *Antimicrobial Agents and Chemotherapy*, *57*(12), 6147–6153. https://doi.org/10.1128/AAC.01285-13

Rodriguez, O. L., Safonova, Y., Silver, C. A., Shields, K., Gibson, W. S., Kos, J. T., Tieri, D., Ke, H., Jackson, K. J. L., Boyd, S. D., Smith, M. L., Marasco, W. A., & Watson, C. T. (2023). Genetic variation in the immunoglobulin heavy chain locus shapes the human antibody repertoire. *Nature Communications*, *14*(1), 4419. https://doi.org/10.1038/s41467-023-40070-x

Romain, G., Senyukov, V., Rey-Villamizar, N., Merouane, A., Kelton, W., Liadi, I., Mahendra, A., Charab, W., Georgiou, G., Roysam, B., Lee, D. A., & Varadarajan, N. (2014). Antibody Fc engineering improves frequency and promotes kinetic boosting of serial killing mediated by NK cells. *Blood*, *124*(22), 3241–3249. https://doi.org/10.1182/blood-2014-04-569061

Roth, D. B. (2014). V(D)J Recombination: Mechanism, Errors, and Fidelity. *Microbiology Spectrum*, *2*(6), 2.6.18. https://doi.org/10.1128/microbiolspec.MDNA3-0041-2014

Roux, K. H., Strelets, L., Brekke, O. H., Sandlie, I., & Michaelsen, T. E. (1998). Comparisons of the Ability of Human IgG3 Hinge Mutants, IgM, IgE, and IgA2, to Form Small Immune Complexes: A Role for Flexibility and Geometry. *The Journal of Immunology*, *161*(8), 4083–4090. https://doi.org/10.4049/jimmunol.161.8.4083

Saphire, E. O., Parren, P. W. H. I., Pantophlet, R., Zwick, M. B., Morris, G. M., Rudd, P. M., Dwek, R. A., Stanfield, R. L., Burton, D. R., & Wilson, I. A. (2001). Crystal Structure of a Neutralizing Human IgG Against HIV-1: A Template for Vaccine Design. *Science*, *293*(5532), 1155–1159. https://doi.org/10.1126/science.1061692

Schmitz, S., Schmitz, E. A., Crowe, J. E., & Meiler, J. (2022). The human antibody sequence space and structural design of the V, J regions, and CDRH3 with Rosetta. *mAbs*, *14*(1), 2068212. https://doi.org/10.1080/19420862.2022.2068212

Shah, I. S., Lovell, S., Mehzabeen, N., Battaile, K. P., & Tolbert, T. J. (2017). Structural characterization of the Man5 glycoform of human IgG3 Fc. *Molecular Immunology*, *92*, 28–37. https://doi.org/10.1016/j.molimm.2017.10.001

Shibuya, A., Sakamoto, N., Shimizu, Y., Shibuya, K., Osawa, M., Hiroyama, T., Eyre, H. J., Sutherland, G. R., Endo, Y., Fujita, T., Miyabayashi, T., Sakano, S., Tsuji, T., Nakayama, E., Phillips, J. H., Lanier, L. L., & Nakauchi, H. (2000). Fcα/μ receptor mediates endocytosis of IgM-coated microbes. *Nature Immunology*, *1*(5), 441–446. https://doi.org/10.1038/80886

Sondermann, P., Kaiser, J., & Jacob, U. (2001). Molecular Basis for Immune Complex Recognition: A Comparison of Fc-Receptor Structures. *Journal of Molecular Biology*, *309*(3), 737–749. https://doi.org/10.1006/jmbi.2001.4670

Spiteri, V. A., Goodall, M., Doutch, J., Rambo, R. P., Gor, J., & Perkins, S. J. (2021). Solution structures of human myeloma IgG3 antibody reveal extended Fab and Fc regions relative to the other IgG subclasses. *Journal of Biological Chemistry*, *297*(3), 100995. https://doi.org/10.1016/j.jbc.2021.100995

Stavnezer, J. (1996). Immunoglobulin class switching. *Current Opinion in Immunology*, *8*(2), 199–205. https://doi.org/10.1016/S0952-7915(96)80058-6

Stavnezer, J., Guikema, J. E. J., & Schrader, C. E. (2008). Mechanism and Regulation of Class Switch Recombination. *Annual Review of Immunology*, *26*(1), 261–292. https://doi.org/10.1146/annurev.immunol.26.021607.090248

Subedi, G. P., & Barb, A. W. (2016). The immunoglobulin G1 N-glycan composition affects binding to each low affinity Fc γ receptor. *mAbs*, *8*(8), 1512–1524. https://doi.org/10.1080/19420862.2016.1218586

Svergun, D. I. (1992). Determination of the regularization parameter in indirect-transform methods using perceptual criteria. *Journal of Applied Crystallography*, *25*(4), 495–503. https://doi.org/10.1107/S0021889892001663

Takai, T. (2002). Roles of Fc receptors in autoimmunity. *Nature Reviews Immunology*, *2*(8), 580–592. https://doi.org/10.1038/nri856

Talathi, S. P., Shaikh, N. N., Pandey, S. S., Saxena, V. A., Mamulwar, M. S., & Thakar, M. R. (2019). FcγRIIIa receptor polymorphism influences NK cell mediated ADCC activity against HIV. *BMC Infectious Diseases*, *19*(1), 1053. https://doi.org/10.1186/s12879-019-4674-z

Temming, A. R., De Taeye, S. W., De Graaf, E. L., De Neef, L. A., Dekkers, G., Bruggeman, C. W., Koers, J., Ligthart, P., Nagelkerke, S. Q., Zimring, J. C., Kuijpers, T. W., Wuhrer, M., Rispens, T., & Vidarsson, G. (2019). Functional Attributes of Antibodies, Effector Cells, and Target Cells Affecting NK Cell–Mediated Antibody-Dependent Cellular Cytotoxicity. *The Journal of Immunology*, *203*(12), 3126–3135. https://doi.org/10.4049/jimmunol.1900985

Tian, X., Vestergaard, B., Thorolfsson, M., Yang, Z., Rasmussen, H. B., & Langkilde, A. E. (2015). In-depth analysis of subclass-specific conformational preferences of IgG antibodies. *IUCrJ*, *2*(1), 9–18. https://doi.org/10.1107/S205225251402209X

Toyama, H., Okada, S., Hatano, M., Takahashi, Y., Takeda, N., Ichii, H., Takemori, T., Kuroda, Y., & Tokuhisa, T. (2002). Memory B Cells without Somatic Hypermutation Are Generated from Bcl6-Deficient B Cells. *Immunity*, *17*(3), 329–339. https://doi.org/10.1016/S1074-7613(02)00387-4

Unkeless, J. C., Shen, Z., Lin, C.-W., & DeBeus, E. (1995). Function of human FcγRIIA and FcγRIIIB. *Seminars in Immunology*, *7*(1), 37–44. https://doi.org/10.1016/1044-5323(95)90006-3

van der Horst, H. J., Nijhof, I. S., Mutis, T., & Chamuleau, M. E. D. (2020). Fc-Engineered Antibodies with Enhanced Fc-Effector Function for the Treatment of B-Cell Malignancies. *Cancers*, *12*(10), 3041. https://doi.org/10.3390/cancers12103041

Van Erp, E. A., Luytjes, W., Ferwerda, G., & Van Kasteren, P. B. (2019). Fc-Mediated Antibody Effector Functions During Respiratory Syncytial Virus Infection and Disease. *Frontiers in Immunology*, *10*, 548. https://doi.org/10.3389/fimmu.2019.00548

Van Loghem, E., Aalberse, R. C., & Matsumoto, H. (1984). A Genetic Marker of Human IgE Heavy Chains, Em(1) [1]. *Vox Sanguinis*, *46*(4), 195–206. https://doi.org/10.1111/j.1423-0410.1984.tb00075.x

Verdoliva, A., Pannone, F., Rossi, M., Catello, S., & Manfredi, V. (2002). Affinity purification of polyclonal antibodies using a new all-D synthetic peptide ligand: Comparison with protein A and protein G. *Journal of Immunological Methods*, *271*(1–2), 77–88. https://doi.org/10.1016/S0022-1759(02)00341-1

Vidarsson, G., Dekkers, G., & Rispens, T. (2014). IgG Subclasses and Allotypes: From Structure to Effector Functions. *Frontiers in Immunology*, *5*. https://doi.org/10.3389/fimmu.2014.00520

Vorobjeva, N. V., & Chernyak, B. V. (2020). NETosis: Molecular Mechanisms, Role in Physiology and Pathology. *Biochemistry (Moscow)*, *85*(10), 1178–1190. https://doi.org/10.1134/S0006297920100065

Wang, W. (2015). NK cell-mediated antibody-dependent cellular cytotoxicity in cancer immunotherapy. *Frontiers in Immunology*, *6*. https://doi.org/10.3389/fimmu.2015.00368

Warrender, A. K. (2023). *The Influence of Constant Region Polymorphisms on Antibody Stability and Structural Dynamics*. University of Waikato.

Warrender, A. K., & Kelton, W. (2020). Beyond Allotypes: The Influence of Allelic Diversity in Antibody Constant Domains. *Frontiers in Immunology*, *11*. https://www.frontiersin.org/articles/10.3389/fimmu.2020.02016

Warrender, A. K., Pan, J., Pudney, C. R., Arcus, V. L., & Kelton, W. (2023). Constant domain polymorphisms influence monoclonal antibody stability and dynamics. *Protein Science*, *32*(3), e4589. https://doi.org/10.1002/pro.4589

Wilson, T. J., Fuchs, A., & Colonna, M. (2012). Cutting edge: Human FcRL4 and FcRL5 are receptors for IgA and IgG. *Journal of Immunology (Baltimore, Md.: 1950)*, *188*(10), 4741–4745. https://doi.org/10.4049/jimmunol.1102651

Woof, J. M., & Russell, M. W. (2011). Structure and function relationships in IgA. *Mucosal Immunology*, *4*(6), 590–597. https://doi.org/10.1038/mi.2011.39

Yamashita, T. (2018). Toward rational antibody design: Recent advancements in molecular dynamics simulations. *International Immunology*, *30*(4), 133–140. https://doi.org/10.1093/intimm/dxx077

Yang, H., Jiang, H., Song, Y., Chen, D. J., Shen, X. J., & Chen, J. H. (2018). Neutrophil CD16b crosslinking induces lipid raft-mediated activation of SHP-2 and affects cytokine expression and retarded neutrophil apoptosis. *Experimental Cell Research*, *362*(1), 121–131. https://doi.org/10.1016/j.yexcr.2017.11.009

Yang, P.-C., Berin, M. C., Yu, L. C. H., Conrad, D. H., & Perdue, M. H. (2000). Enhanced intestinal transepithelial antigen transport in allergic rats is mediated by IgE and CD23 (FcεRII). *Journal of Clinical Investigation*, *106*(7), 879–886. https://doi.org/10.1172/JCI9258

Yogo, R., Yamaguchi, Y., Watanabe, H., Yagi, H., Satoh, T., Nakanishi, M., Onitsuka, M., Omasa, T., Shimada, M., Maruno, T., Torisu, T., Watanabe, S., Higo, D., Uchihashi, T., Yanaka, S., Uchiyama, S., & Kato, K. (2019). The Fab portion of immunoglobulin G contributes to its binding to Fcγ receptor III. *Scientific Reports*, *9*(1), 11957. https://doi.org/10.1038/s41598-019-48323-w

Appendices

Appendix A: Plasmid cloning information

A1: Amino acid sequences of the selected allelic variants

Table 4.1. Heavy chain sequences for the selected allelic variants (not including variable domain sequence).

>IGHG1*01	ASTKGPSVFPLAPSSKSTSGGTAALGCLVKDYFPEPVTVSWNS GALTSGVHTFPAVLQSSGLYSLSSVVTVPSSSLGTQTYICNVN HKPSNTKVDKKVEPKSCDKTHTCPPCPAPELLGGPSVFLFPPK PKDTLMISRTPEVTCVVVDVSHEDPEVKFNWYVDGVEVHNA KTKPREEQYNSTYRVVSVLTVLHQDWLNGKEYKCKVSNKAL PAPIEKTISKAKGQPREPQVYTLPPSRDELTKNQVSLTCLVKGF YPSDIAVEWESNGQPENNYKTTPPVLDSDGSFFLYSKLTVDKS RWQQGNVFSCSVMHEALHNHYTQKSLSLSPGK
>IGHG2*02	ASTKGPSVFPLAPCSRSTSESTAALGCLVKDYFPEPVTVSWNS GALTSGVHTFPAVLQSSGLYSLSSVVTVTSSNFGTQTYTCNVD HKPSNTKVDKTVERKCCVECPPCPAPPVAGPSVFLFPPKPKDT LMISRTPEVTCVVVDVSHEDPEVQFNWYVDGMEVHNAKTKP REEQFNSTFRVVSVLTVVHQDWLNGKEYKCKVSNKGLPAPIE KTISKTKGQPREPQVYTLPPSREEMTKNQVSLTCLVKGFYPSD IAVEWESNGQPENNYKTTPPMLDSDGSFFLYSKLTVDKSRWQ QGNVFSCSVMHEALHNHYTQKSLSLSPGK
>IGHG3*01	ASTKGPSVFPLAPCSRSTSGGTAALGCLVKDYFPEPVTVSWNS GALTSGVHTFPAVLQSSGLYSLSSVVTVPSSSLGTQTYTCNVN HKPSNTKVDKRVELKTPLGDTTHTCPRCPEPKSCDTPPPCPRC PEPKSCDTPPPCPRCPEPKSCDTPPPCPRCPAPELLGGPSVFLFP PKPKDTLMISRTPEVTCVVVDVSHEDPEVQFKWYVDGVEVH NAKTKPREEQYNSTFRVVSVLTVLHQDWLNGKEYKCKVSNK ALPAPIEKTISKTKGQPREPQVYTLPPSREEMTKNQVSLTCLV KGFYPSDIAVEWESSGQPENNYNTTPPMLDSDGSFFLYSKLTV DKSRWQQGNIFSCSVMHEALHNRFTQKSLSLSPGK
> IGHG3*03	ASTKGPSVFPLAPCSRSTSGGTAALGCLVKDYFPEPVTVSWNS GALTSGVHTFPAVLQSSGLYSLSSVVTVPSSSLGTQTYTCNVN HKPSNTKVDKRVELKTPLGDTTHTCPRCPEPKSCDTPPPCPRC PEPKSCDTPPPCPRCPAPELLGGPSVFLFPPKPKDTLMISRTPEV TCVVVDVSHEDPEVQFKWYVDGVEVHNAKTKPREEQYNSTF RVVSVLTVLHQDWLNGKEYKCKVSNKALPAPIEKTISKTKGQ PREPQVYTLPPSREEMTKNQVSLTCLVKGFYPSDIAVEWESSG QPENNYNTTPPVLDSDGSFFLYSRLTVDKSRWQEGNVFSCSV MHEALHNRFTQKSLSLSPGK
> IGHG3*04	ASTKGPSVFPLAPCSRSTSGGTAALGCLVKDYFPEPVTVSWNS GALTSGVHTFPAVLQSSGLYSLSSVVTVPSSSLGTQTYTCNVN HKPSNTKVDKRVELKTPLGDTTHTCPRCPEPKSCDTPPPCPRC

	PAPELLGGPSVFLFPPKPKDTLMISRTPEVTCVVVDVSHEDPE VQFKWYVDGVEVHNAKTKPREEQYNSTFRVVSVLTVLHQD WLNGKEYKCKVSNKALPAPIEKTISKTKGQPREPQVYTLPPSR EEMTKNQVSLTCLVKGFYPSDIAVEWESSGQPENNYNTTPPM LDSDGSFFLYSKLTVDKSRWQQGNIFSCSVMHEALHNRFTQK SLSLSPGK
> IGHG3*08	ASTKGPSVFPLAPCSRSTSGGTAALGCLVKDYFPEPVTVSWNS GALTSGVHTFPAVLQSSGLYSLSSVVTVPSSSLGTQTYTCNVN HKPSNTKVDKRVELKTPLGDTTHTCPRCPEPKSCDTPPPCPRC PEPKSCDTPPPCPRCPEPKSCDTPPPCPRCPAPELLGGPSVFLFP PKPKDTLMISRTPEVTCVVVDVSHEDPEVQFKWYVDGVEVH NAKTKPREEQYNSTFRVVSVLTVLHQDWLNGKEYKCKVSNK ALPAPIEKTISKTKGQPREPQVYTLPPSREEMTKNQVSLTCLV KGFYPSDIAVEWESNGQPENNYNTTPPMLDSDGSFFLYSKLT VDKSRWQQGNIFSCSVMHEALHNRFTQKSLSLSPGK
> IGHG3*12	ASTKGPSVFPLAPCSRSTSGGTAALGCLVKDYFPEPVTVSWNS GALTSGVHTFPAVLQSSGLYSLSSVVTVPSSSLGTQTYTCNVN HKPSNTKVDKRVELKTPLGDTTHTCPRCPEPKSCDTPPPCPRC PEPKSCDTPPPCPRCPAPELLGGPSVFLFPPKPKDTLMISRTPEV TCVVVDVSHEDPEVQFKWYVDGVEVHNAKTKPREEQFNSTF RVVSVLTVLHQDWLNGKEYKCKVSNKALPAPIEKTISKTKGQ PREPQVYTLPPSREEMTKNQVSLTCLVKGFYPSDIAVEWESSG QPENNYNTTPPMLDSDGSFFLYSKLTVDKSRWQQGNIFSCSV MHEALHNRFTQKSLSLSPGK

A2: Amino acid sequences for light chain and signal peptide

Kappa light chain sequence without the variable domain:

TAAAPSVFIFPPSDEQLKSGTASVVCLLNNFYPREAKVQWKVDNALQSGN
SQESVTEQDSKDSTYSLSSTLTLSKADYEKHKVYACEVTHQGLSSPVTKSF
NRGEC

Rabbit IGKC signal peptide:

MDTRAPTQLLGLLLLWLPGARCA

Rabbit IGHG signal peptide:

METGLRWLLLVAVLKGVQC

A3: Amino acid sequences for anti-CD20 and anti-AAV5 variable domains

Anti-CD20 heavy variable domain:

QVQLQQPGAELVKPGASVKMSCKASGYTFTSYNMHWVKQTPGRGLEWI
GAIYPGNGDTSYNQKFKGKATLTADKSSSTAYMQLSSLTSEDSAVYYCA
RSTYYGGDWYFNVWGAGTTVTVSA

Anti-CD20 light variable domain:

QIVLSQSPAILSASPGEKVTMTCRASSSVSYIHWFQQKPGSSPKPWIYATSN
LASGVPVRFSGSGSGTSYSLTISRVEAEDAATYYCQQWTSNPPTFGGGTK
LEIKR

Anti-AAV5 heavy variable domain:

VQLKQSGPGLLQPSQRLSITCTVSGFSLGRYGVHWIRQSPGKGLEWLGVI
WRGGTTDYNAVFMSRLSINKDDSKSQVFFTMNSLRPDDTAIYYCARQGS
NFPLAYWGQGTLVTVSA

Anti-AAV5 light variable domain:

NIVMTQTPKFLLVSIGDSITITCKASQSVTNDAAWYQKKPGQSPQLLIYQA
STRYTGVPDRFSGSGYGTDFTFTISAVQAEDLAVYFCHQDYSSPLTFGAGT
KLELK

A4: Pairwise alignment of sequencing results to expected sequence

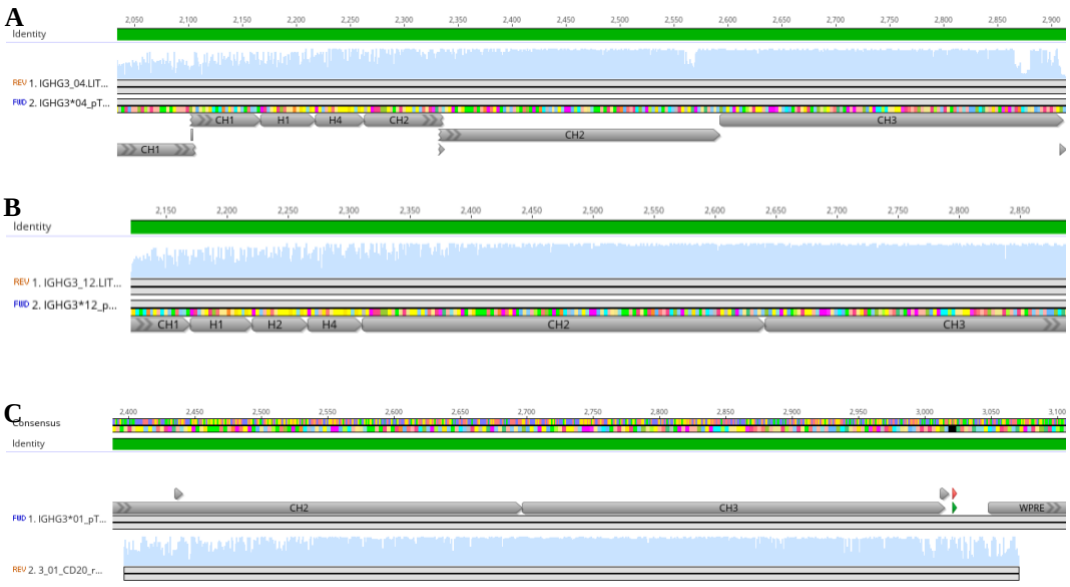

Figure 4.1. Alignment of sequencing results of IgG3*04 AAV5 (A), IgG3*12 AAV5 (B), and IgG3*01 CD20 (C) with the expected plasmid DNA sequence.

Appendix B: Agarose gel electrophoresis information

Agarose Gel Buffer Composition

40 mL 1xTAE Buffer

0.6 g Agarose

Microwave (30-second bursts until dissolved)

Cool with running water over the flask

4 µL 10,000x thiazole orange

Pour into OWL electrophoresis gel caster (Thermo Fisher)

Tris-acetate-EDTA (TAE) Buffer (50x)

242 g Tris-base

700 mL MQ H_2O

57 mL 100% glacial acetic acid

100 mL 0.5 M EDTA (pH 8.0)

Make up to 1 L with MQ H_2O

EDTA Buffer (1x)

93.05 g EDTA disodium salt

400 mL MQ H_2O

pH to 8.0 with NaOH

Make up to 500 ml with MQ H_2O

Appendix C: Antibody purification information

C1: Gravity feed purification with Protein G Sepharose resin

25x Phosphate-buffered saline (PBS)

3.24 M NaCl

67.5 mM KCl

250 mM Na_2HPO_4

45 mM KH_2PO_4

Diluted 1:10 with milli-Q water to make up 1x PBS

pH to 7.4 with HCl

C2: Extinction coefficients of antibody allelic variants expressed

Table 4.2. Extinction coefficients of anti-CD20 allelic variants.

Allelic variant	Extinction coefficient (all cysteine residues are reduced)
IgG1*01	1.469
IgG2*02	1.434
IgG3*01	1.340
IgG3*03	1.367
IgG3*04	1.393
IgG3*08	1.340
IgG3*12	1.348

Table 4.3. Extinction coefficients of anti-AAV5 allelic variants.

Allelic variant	Extinction coefficient (all cysteine residues are reduced)
IgG1*01	1.396
IgG2*02	1.358
IgG3*01	1.264
IgG3*03	1.291
IgG3*04	1.319
IgG3*08	1.263
IgG3*12	1.271

C3: SDS-PAGE gel

4x SDS-Loading Dye

250 mM Tris (pH 6.8)

20% glycerol (v/v)

4% SDS (w/v)

10% beta-2-mercaptoethanol (w/v)

0.025% bromophenol blue (w/v)

Tris-glycine SDS Buffer

25 mM Tris (pH 8.5)

250 mM glycine

0.1% SDS (w/v)

Fairbanks Staining Solution

0.05% Coomassie blue

25% isopropanol

10% acetic acid

Destaining Solution

10% acetic acid

C4: Purification data

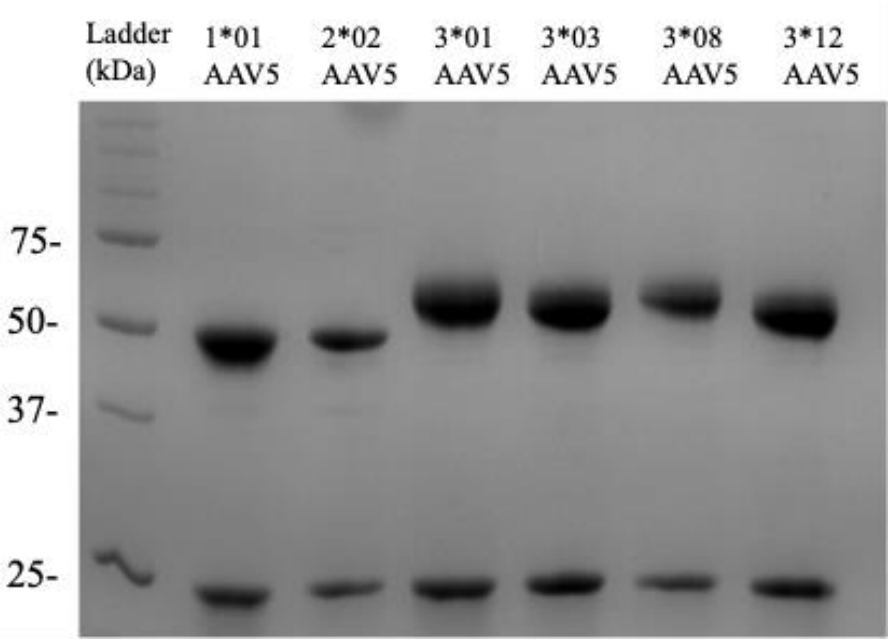

Figure 4.2. 12% SDS-PAGE gel result of anti-AAV5 allelic variants (except for IgG3*04) after purification using HiTrap™ MabSelect™ VL Protein L. Molecular weights in kDa of Precision Plus Protein™ Standards (Bio-Rad) are labelled. Expected band size for the antibody heavy chain is 50-65 kDa, depending on the variant, and 25 kDa for the light chain.

Appendix D: Size exclusion chromatography information

D1: Electrophoresis results from SEC

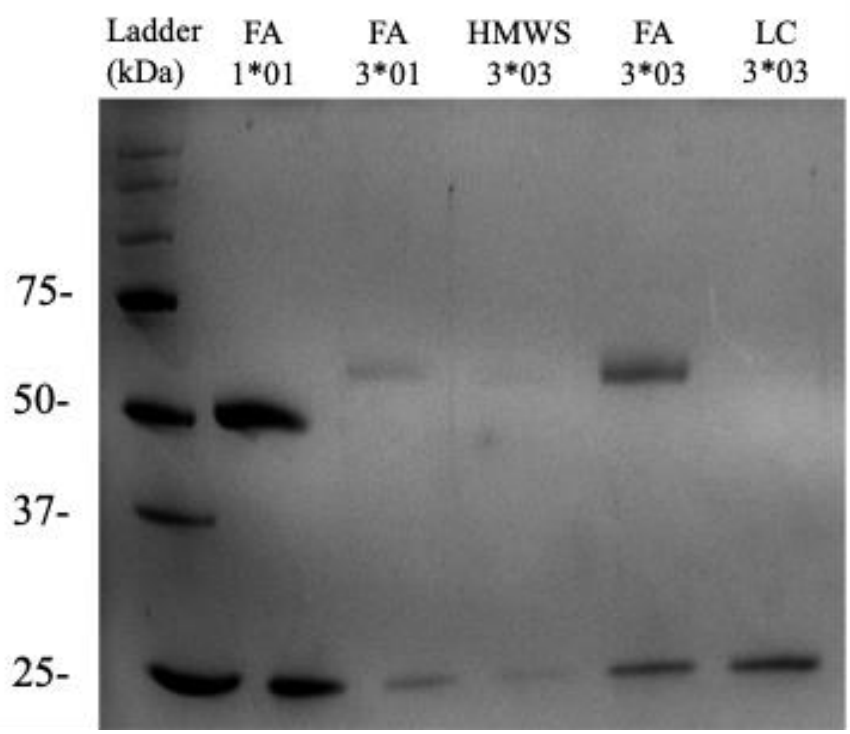

Figure 4.3. SDS-PAGE gel showing collected SEC fractions for IgG1*01, IgG3*01, and IgG3*03 CD20. "FA" corresponds to fully assembled antibody fractions, "HMWS" corresponds to high molecular weight species fractions, and "LC" corresponds to light-chain only fractions. Molecular weights in kDa of Precision Plus Protein™ Standards (Bio-Rad) are labelled. Expected band size for the antibody heavy chain is 50-65 kDa, depending on the variant, and 25 kDa for the light chain.

D2: Absorbance traces in SEC chromatographs

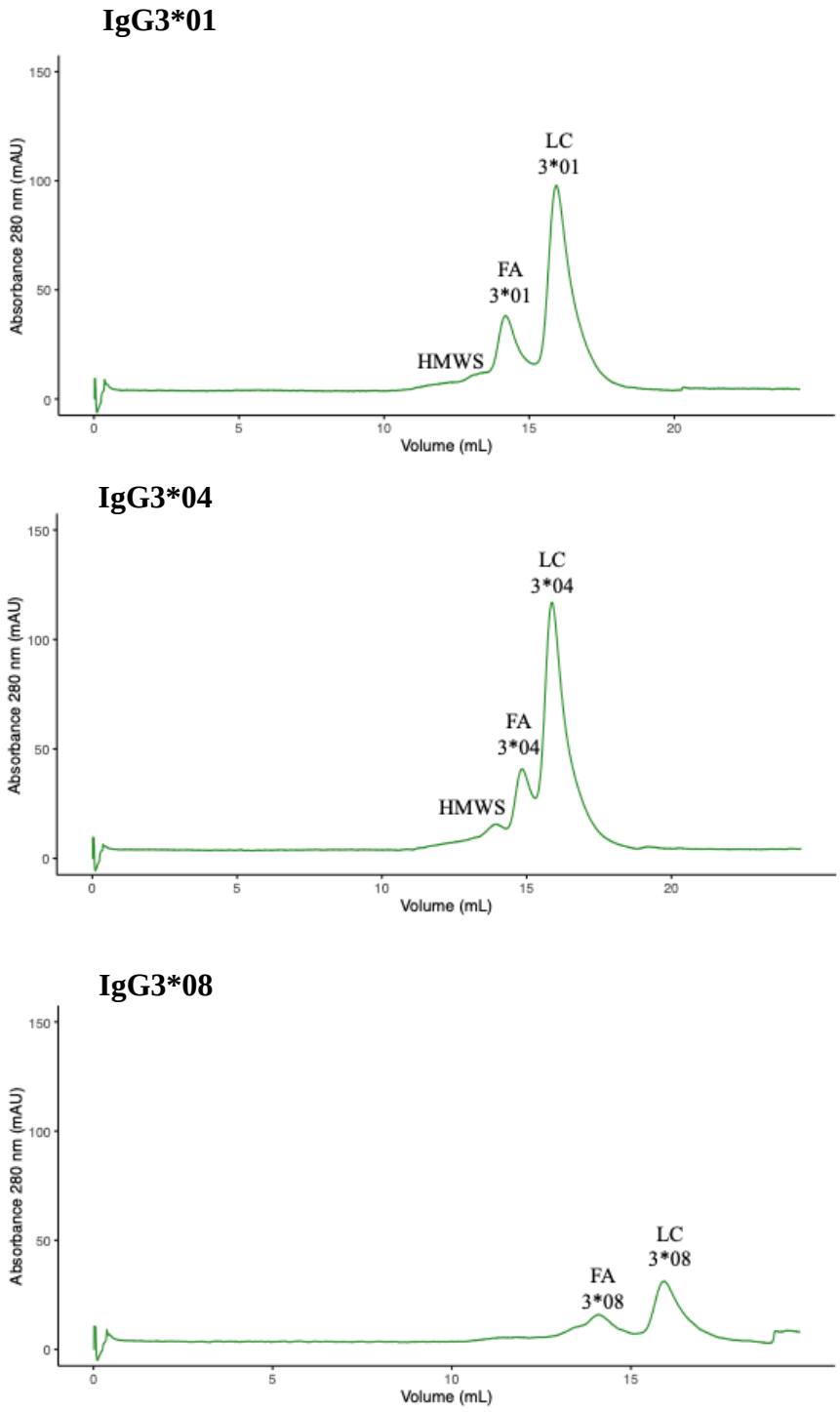

Figure 4.4. Size exclusion chromatographs of IgG3*01, IgG3*04, and IgG3*08 CD20 from SEC using ENrich™ SEC 650 10x300 (Bio-Rad) column. "HWMS" corresponds to high molecular weight species peak, "FA" corresponds to fully assembled antibody peak, and "LC" corresponds to light-chain only peak.

Appendix E: Cell propagation and freezing information

E1: ADCC effector cells

ADCC Cell growth medium

90% RPMI 1640 L-glutamine (Gibco)

10% heat-inactivated foetal bovine serum (FBS) (Gibco)

100 μg/mL hygromycin (Gibco)

250 μg/mL Geneticin™ (G-418 sulphate) (Gibco)

1 mM pyruvate

0.1 mM MEM amino acids.

ADCC Cell freezing medium

85% RPMI 1640 L-glutamine (Gibco)

10% Low IgG FBS

5% DMSO

E2: ADCP effector cells

ADCP Cell thawing medium

89% RPMI 1640 ATCC modification (Gibco)

10% heat-inactivated FBS

1% MEM amino acids

Day 2 Cell growth medium

89% RPMI 1640 ATCC modification

10% heat-inactivated FBS

1% MEM amino acids

400 μg/mL hygromycin (Gibco)

1 mg/mL Geneticin™ (G-418 sulphate) (Gibco)

ADCP Cell growth medium (day 3 and beyond)

89% RPMI 1640 ATCC modification

10% heat-inactivated FBS

1% MEM amino acids

500 μg/mL hygromycin (Gibco)

200 μg/mL Geneticin™ (G-418 sulphate) (Gibco)

ADCP Cell freezing medium

79% RPMI 1640 ATCC modification

14% Low IgG FBS (Gibco)

7% DMSO

E3: Raji and WIL2-S cells

Target cell growth medium

RPMI 1640 ATCC modification (Gibco)

10% heat-inactivated FBS

Target cell freezing medium

79% RPMI 1640 ATCC modification

14% heat-inactivated FBS

7% DMSO

Appendix F: SAXS data analysis information

F1: Elution profiles of the samples from SEC coupled to SAXS beamline

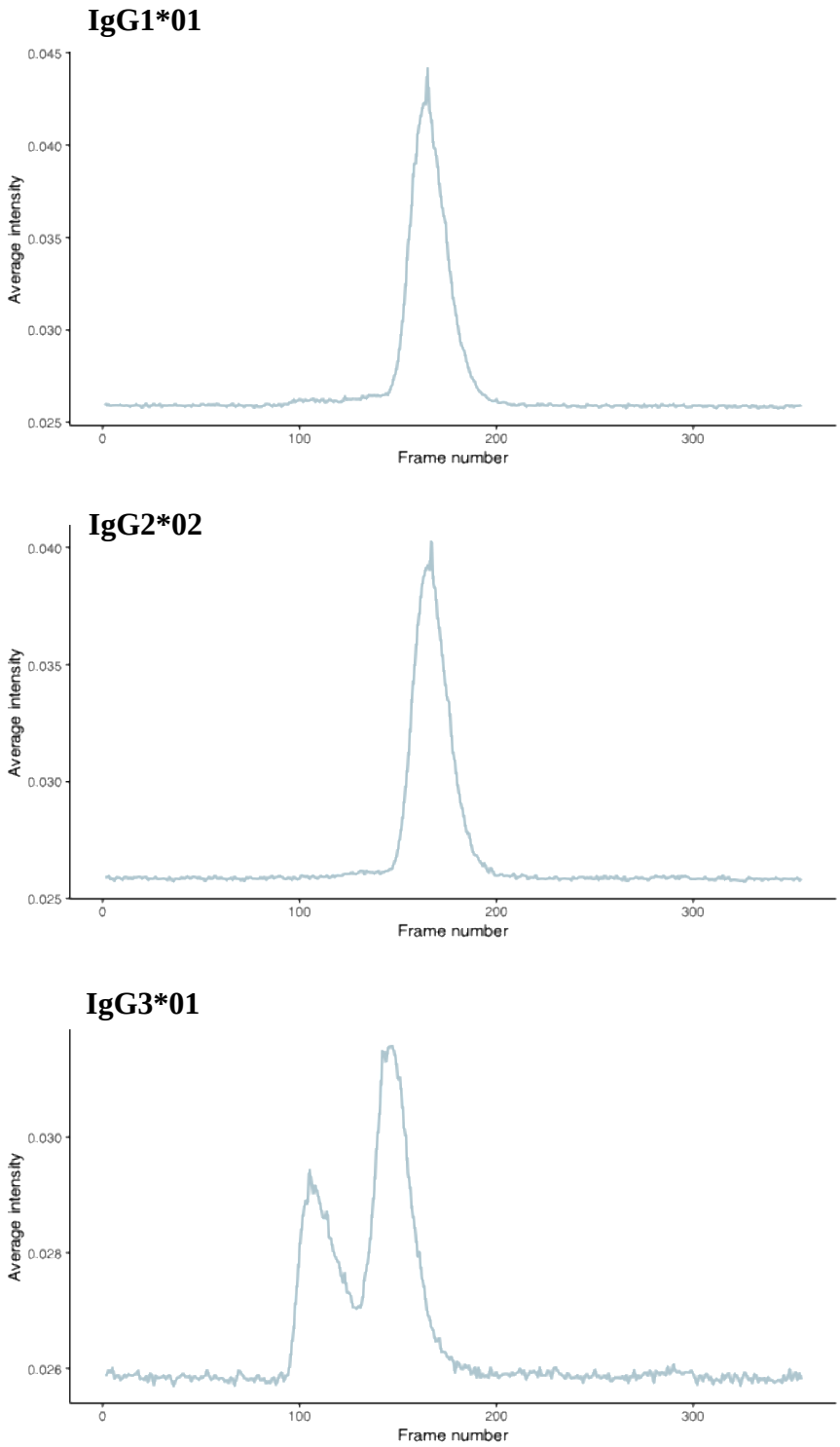

Figure 4.5. Elution peaks of IgG1*01, IgG2*02, IgG3*01 CD20 in the SEC-SAXS beamline as averaged scattering intensity versus frame number.

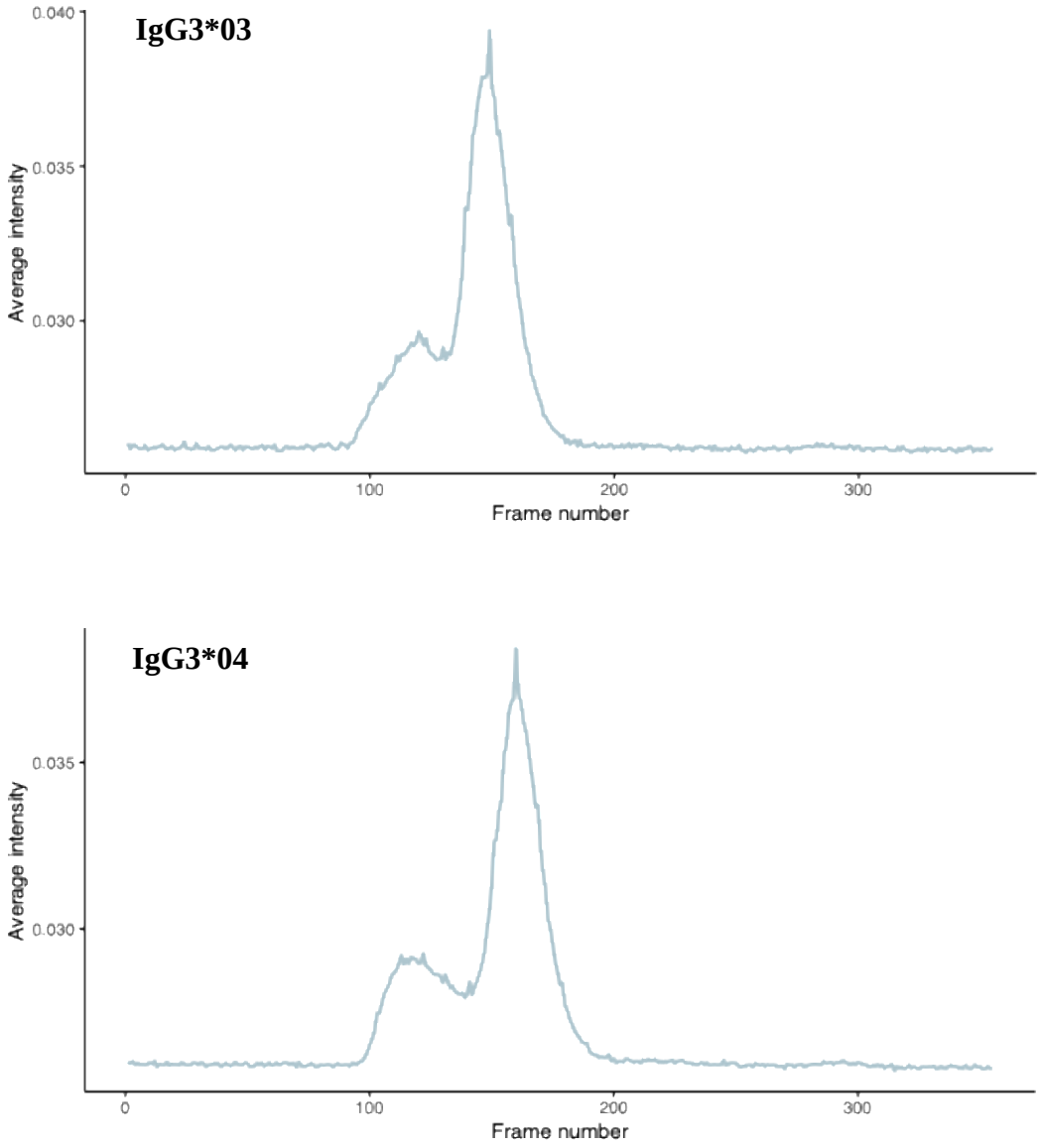

Figure 4.6. Elution peaks of IgG3*03 and IgG3*04 CD20 in the SEC-SAXS beamline as averaged scattering intensity versus frame number.

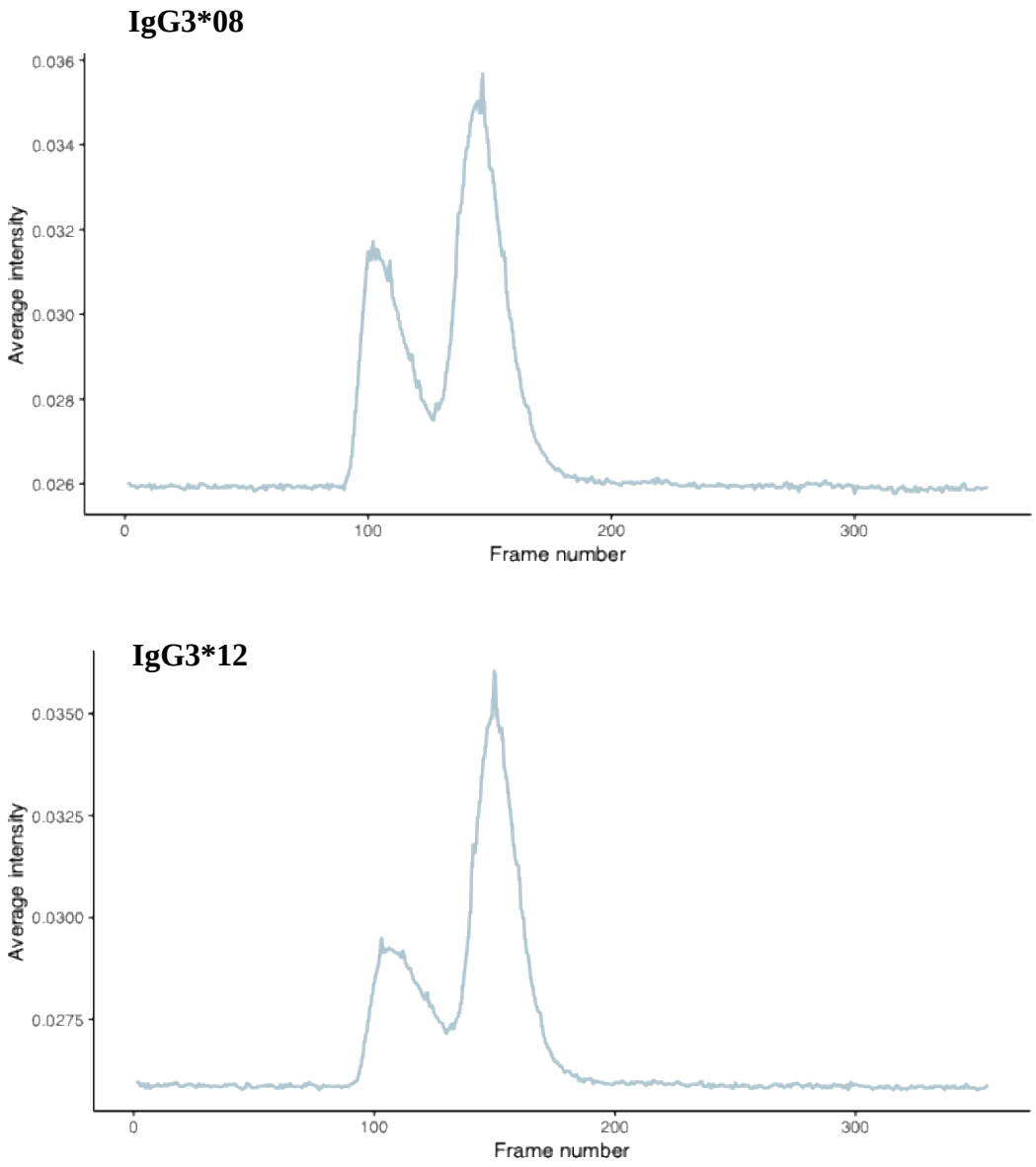

Figure 4.7. Elution peaks of IgG3*08 and IgG3*12 CD20 in the SEC-SAXS beamline as averaged scattering intensity versus frame number.

F2: Data analysis on BioXTAS RAW

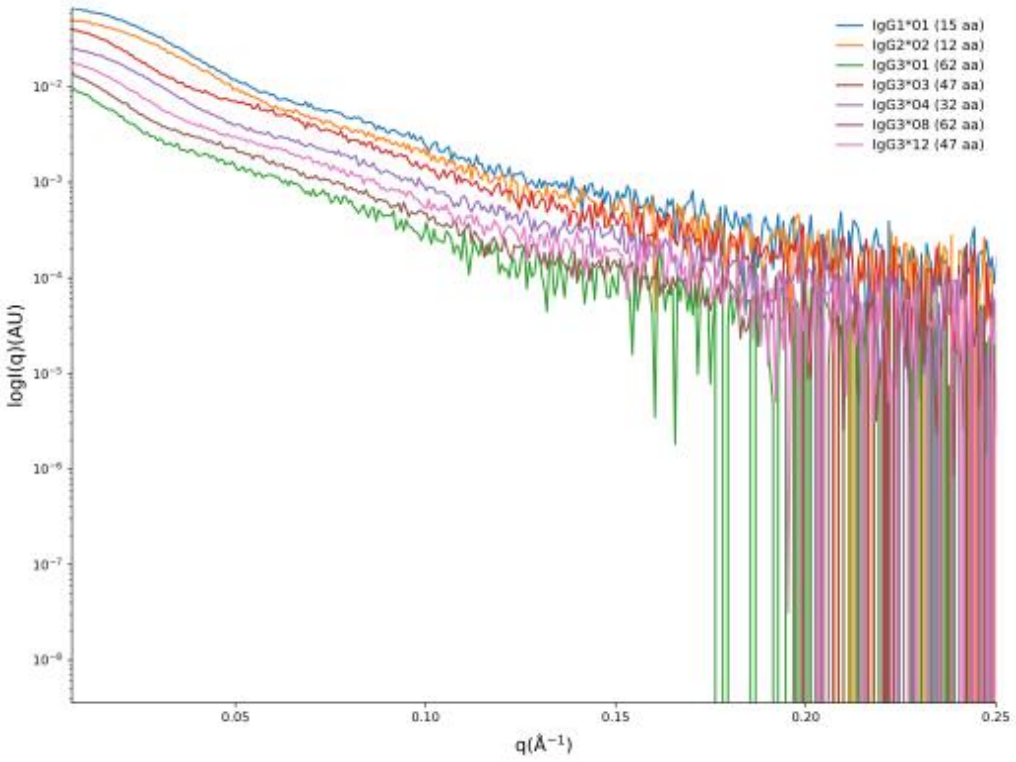

Figure 4.8. Scattering curves (log(I) vs *q*) of the anti-CD20 allelic variants. Intensity is arbitrary and the scattering curves are offset for convenience of viewing. Next to the sample name, there is the hinge length of the antibodies in number of amino acid residues.

Appendix G: ADCC and ADCP assays

G1: Four-parameter logistic model in RStudio

Algorithm 4.1. R script for four-parameter logistic models of the ADCC and ADCP assay results.

```
library(readr)
library(tidyr)
library(ggplot2)
library(dplyr)
library(drc)

setwd("/Users/username/Downloads")

df <- read_csv("File name.csv",
            col_types = cols(
              Sample = col_character(),
              `Log Concentration (pg/mL)` = col_double(),
              `Fold induction` = col_double(),
              SD = col_double()  # Assume standard deviation column is named 'SD'
            ))

model_list <- df %>%
  group_by(Sample) %>%
  do(model = drm(`Fold induction` ~ `Log Concentration (pg/mL)`,
              data = .,
              fct = LL.4()))

fitted_df <- data.frame()

# Loop through each sample and add the fitted values and standard deviation to the data frame
for (i in seq_along(model_list$model)) {
  x_values <- seq(min(df$`Log Concentration (pg/mL)`), max(df$`Log Concentration (pg/mL)`), length.out
= 100)
  # Predict y values using the fitted model
  y_values <- predict(model_list$model[[i]], newdata = data.frame(`Log Concentration (pg/mL)` =
x_values))
  sample_df <- data.frame(x = x_values, y = y_values, Sample = unique(df$Sample)[i])
  fitted_df <- bind_rows(fitted_df, sample_df)
}

ggplot(df, aes(x = `Log Concentration (pg/mL)`, y = `Fold induction`, color = Sample)) +
  geom_point() +
  geom_errorbar(aes(ymin = `Fold induction` - SD, ymax = `Fold induction` + SD), width = 0.1) +
  geom_line(data = fitted_df, aes(x = x, y = y, color = Sample), linetype = "dashed") +
  labs(title = "",
       x = "Log [antibody] (pg/mL)",
       y = "Fold induction") +
  scale_y_continuous(limits = c(0, 15), breaks = seq(0, 15, 5)) +
  theme_bw() +
  theme(panel.grid.major = element_blank(),  # Remove major gridlines
        panel.grid.minor = element_blank(),  # Remove minor gridlines
        panel.border = element_blank(),
        axis.line = element_line(colour = "black"))

EC50_values <- model_list %>%
  summarise(EC50 = ED(model, 50))

EC50_Results <- data.frame(Sample = unique(df$Sample), EC50 = EC50_values$EC50)
```

$$y = d + \frac{(a-d)}{1 + \left(\frac{x}{c}\right)^{b}}$$

Equation 4.1. Four-parameter logistic regression equation, where *a* and *d* are the minimum and maximum values, respectively, that can be obtained, *c* is the point of inflection (i.e., the EC50 value), and *b* is Hill's slope of the curve.

G2: Individual ADCC results – per plate

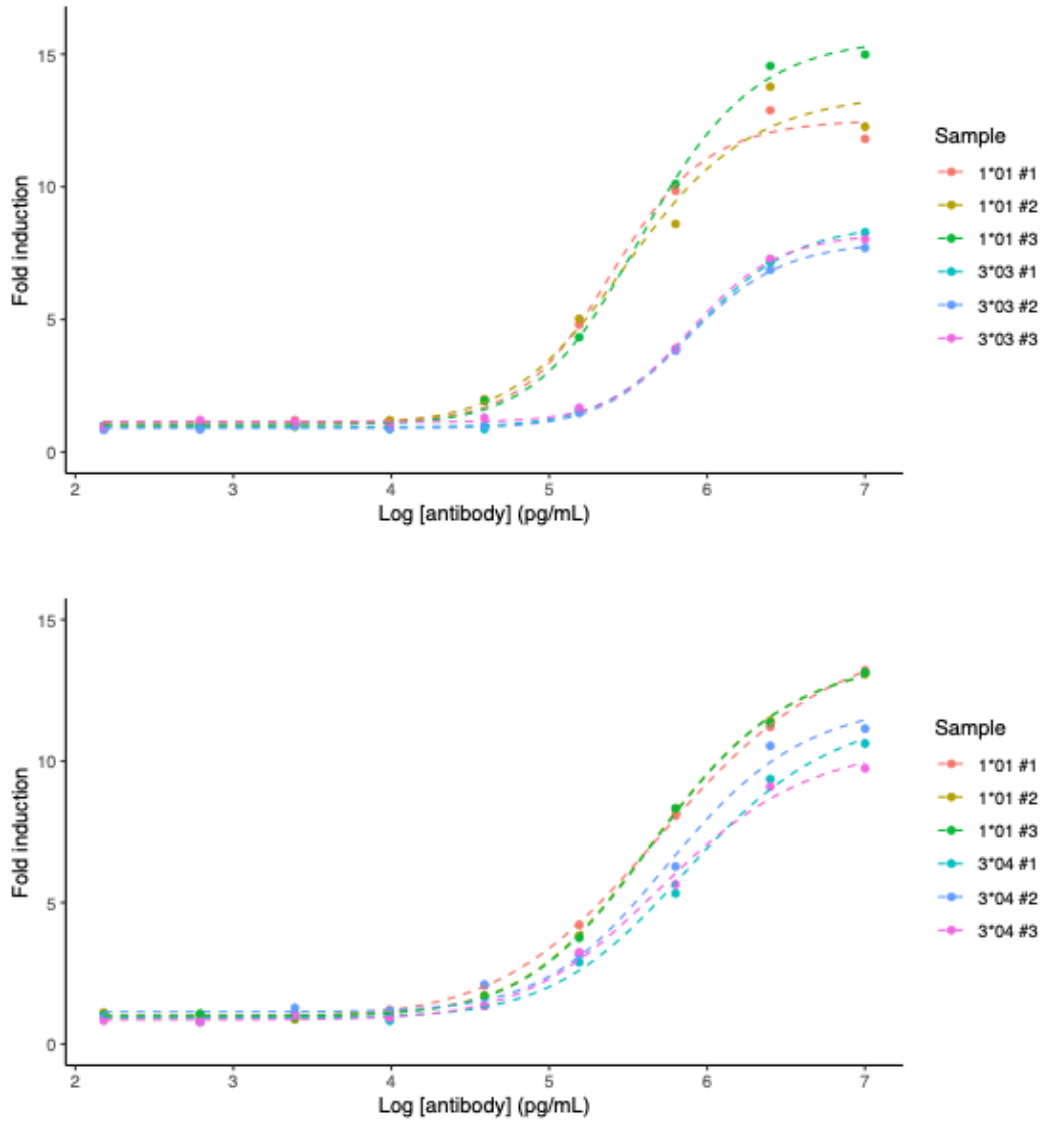

Figure 4.9. Four-parameter logistic model of fold induction values from individual ADCC assay plates for IgG3*03 and IgG3*04. Each sample was in triplicates.

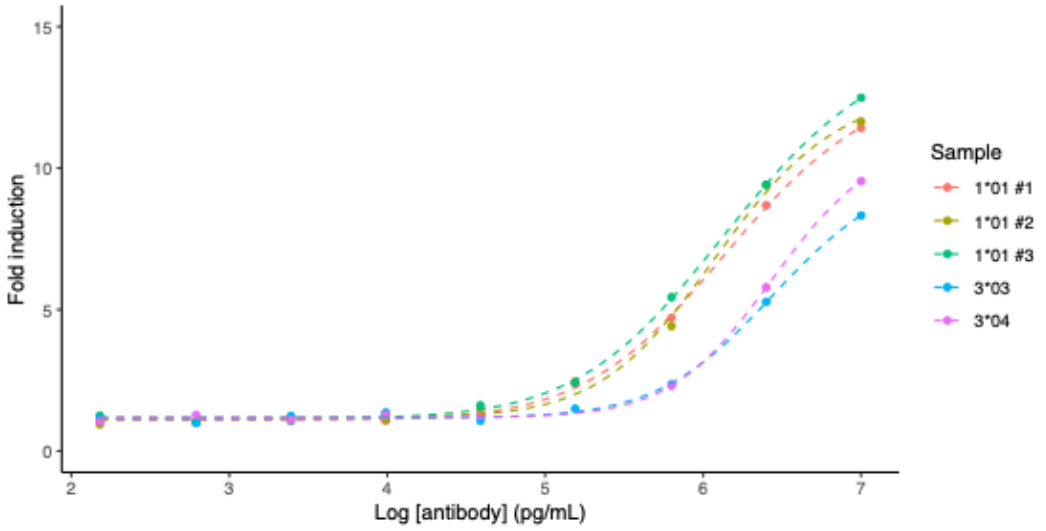

Figure 4.10. Four-parameter logistic model of fold induction values from an ADCC assay in which only IgG1*01 was in triplicates.

G3: Individual ADCP results – per plate

1st assays using WIL2-S

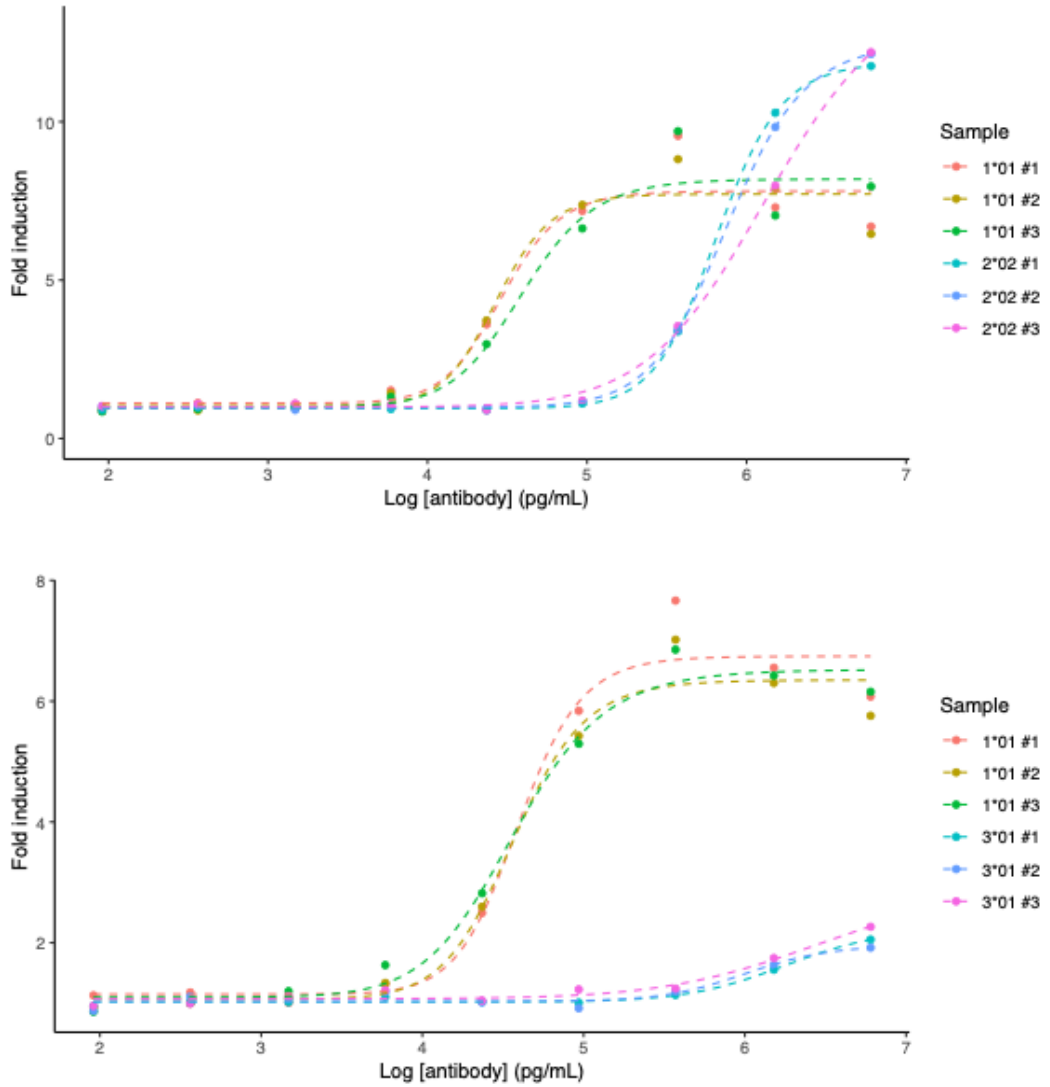

Figure 4.11. Four-parameter logistic model of fold induction values from individual ADCP assay plates from the first assay of IgG2*02 and IgG3*01 CD20 using WIL2-S as target cells. Each sample was in triplicates.

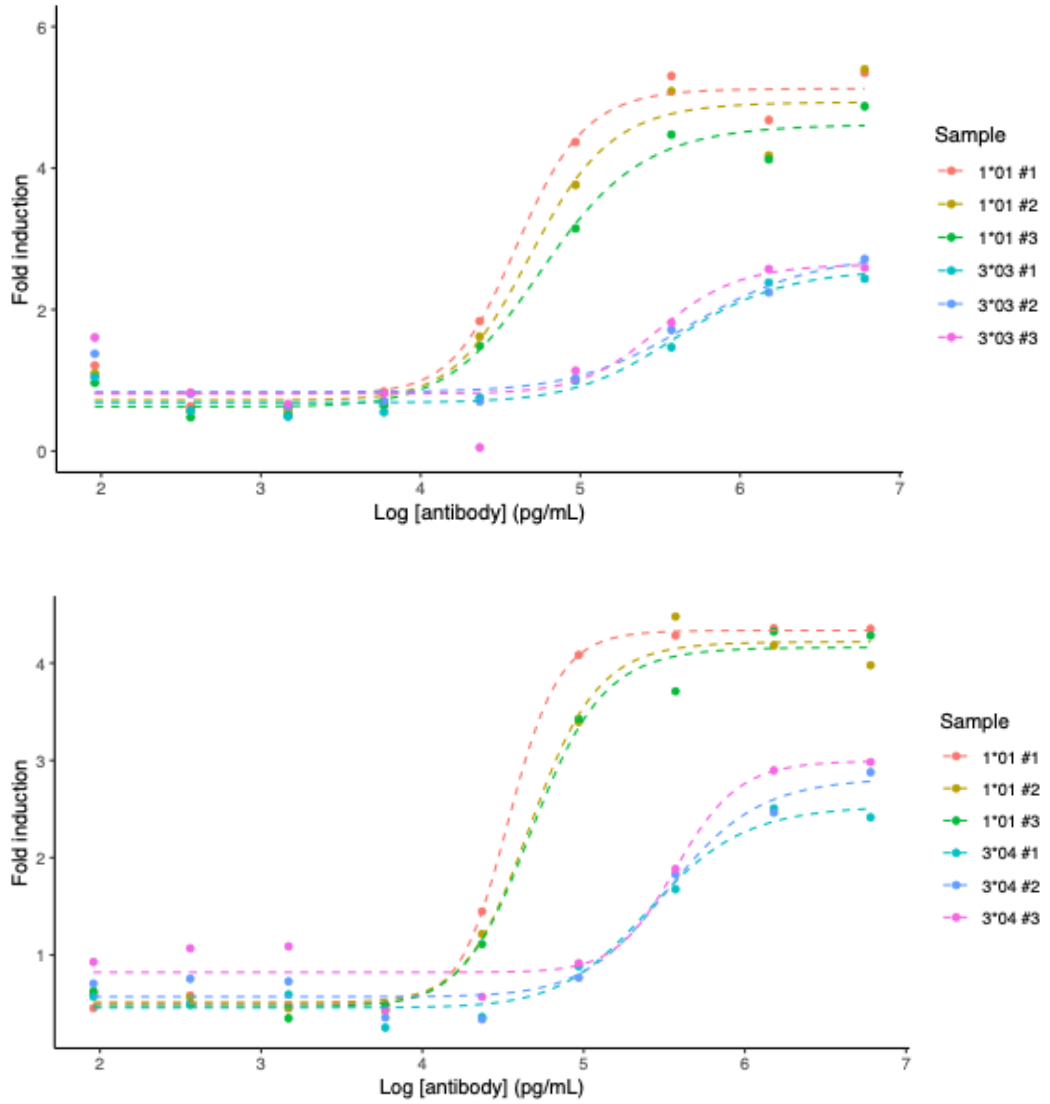

Figure 4.12. Four-parameter logistic model of fold induction values from individual ADCP assay plates from the first assay of IgG3*03 and IgG3*04 CD20 using WIL2-S as target cells. Each sample was in triplicates.

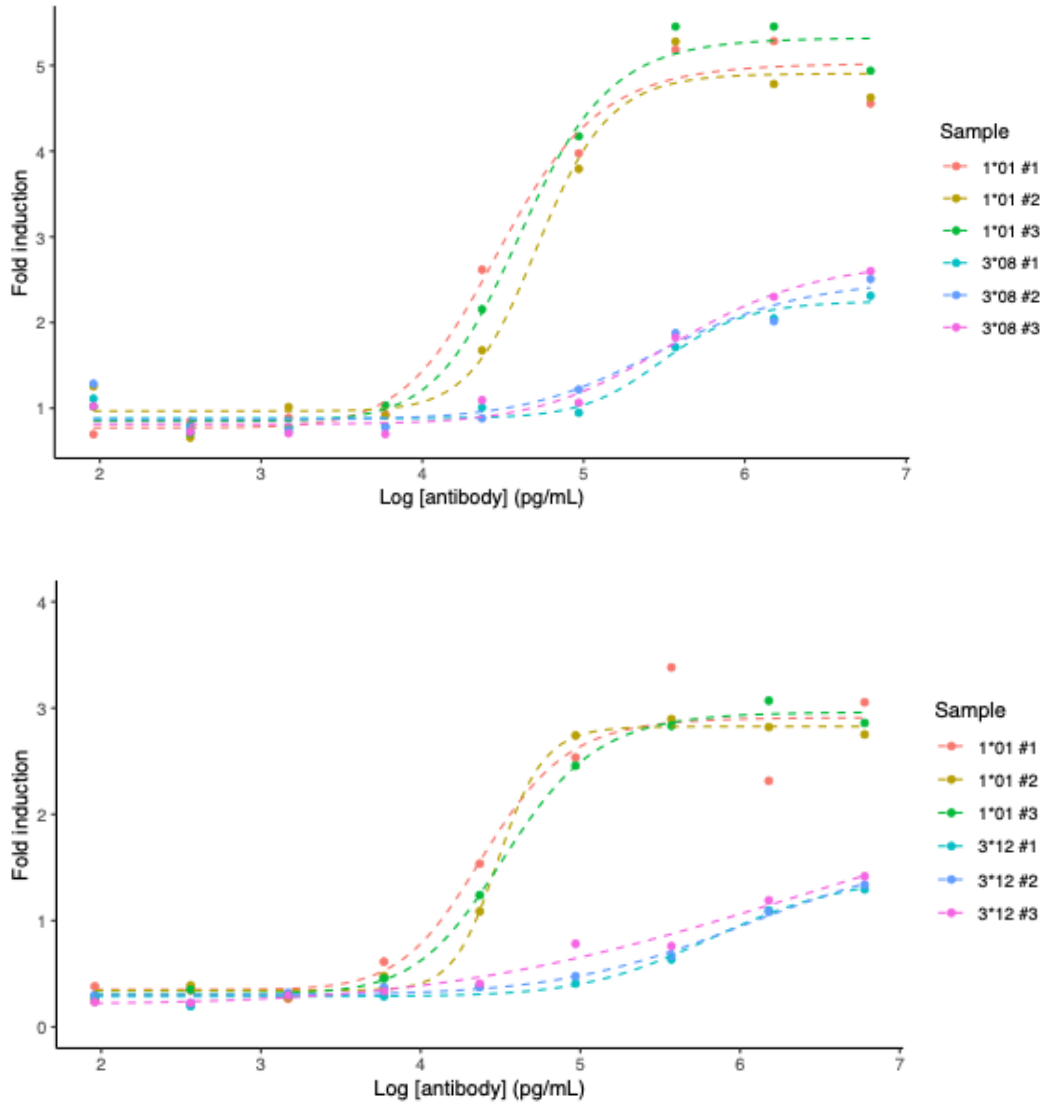

Figure 4.13. Four-parameter logistic model of fold induction values from individual ADCP assay plates from the first assay of IgG3*08 and IgG3*12 CD20 using WIL2-S as target cells. Each sample was in triplicates.

2nd assays using WIL2-S (new antibody expression batch)

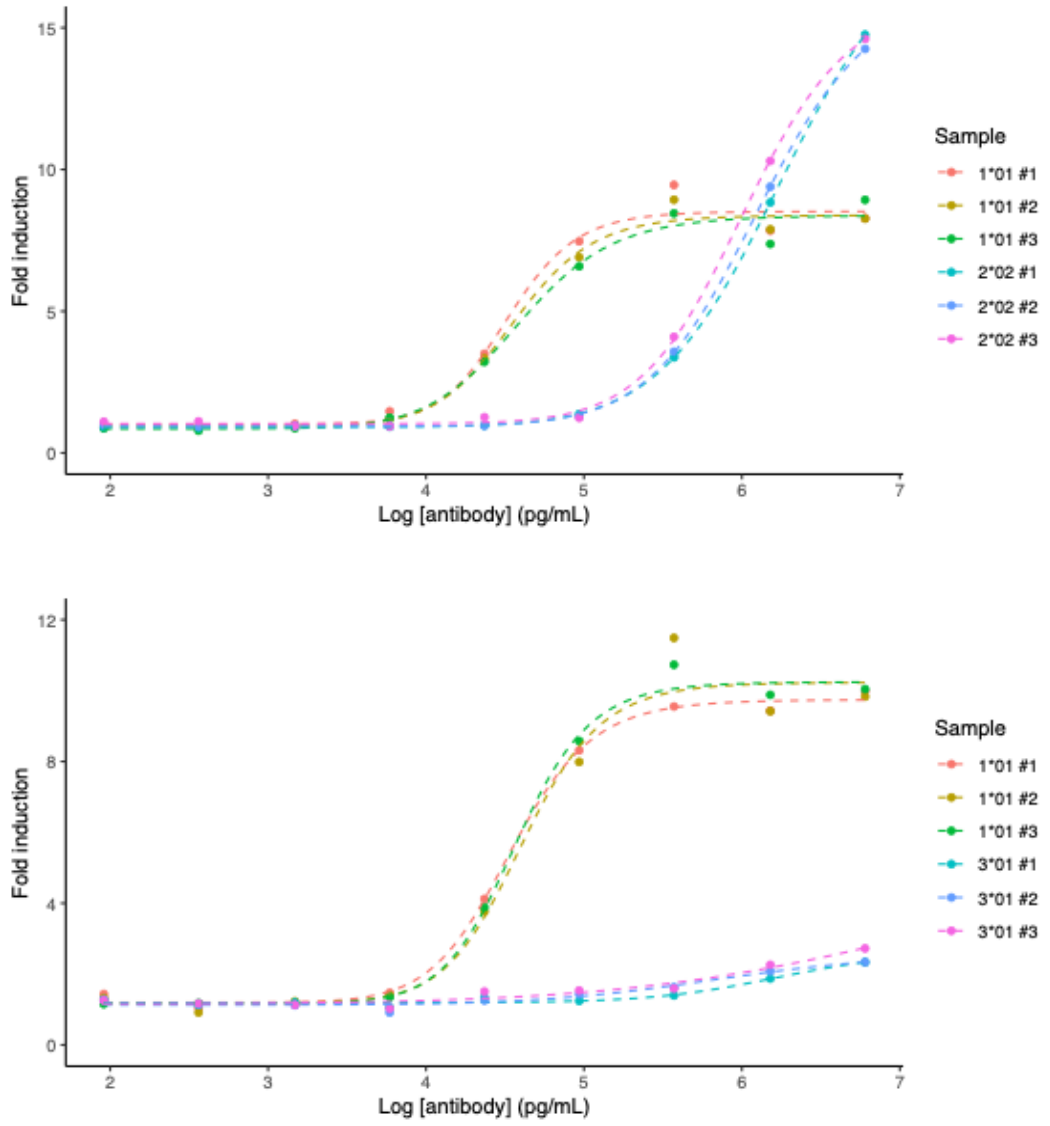

Figure 4.14. Four-parameter logistic model of fold induction values from individual ADCP assay plates from the second assay of IgG2*02 and IgG3*01 CD20 using WIL2-S as target cells. Each sample was in triplicates.

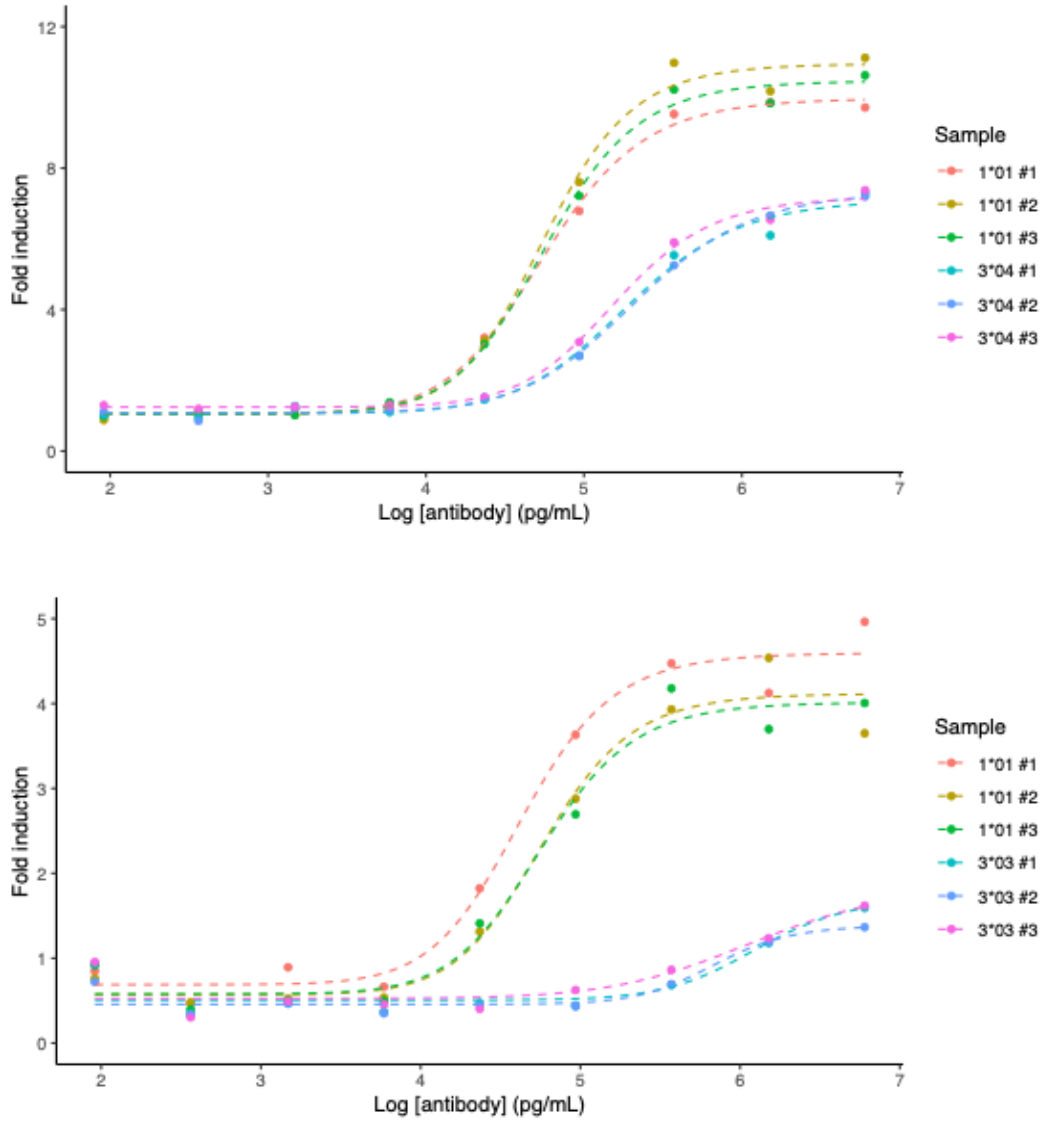

Figure 4.15. Four-parameter logistic model of fold induction values from individual ADCP assay plates from the second assay of IgG3*03 and IgG3*04 CD20 using WIL2-S as target cells. Each sample was in triplicates.

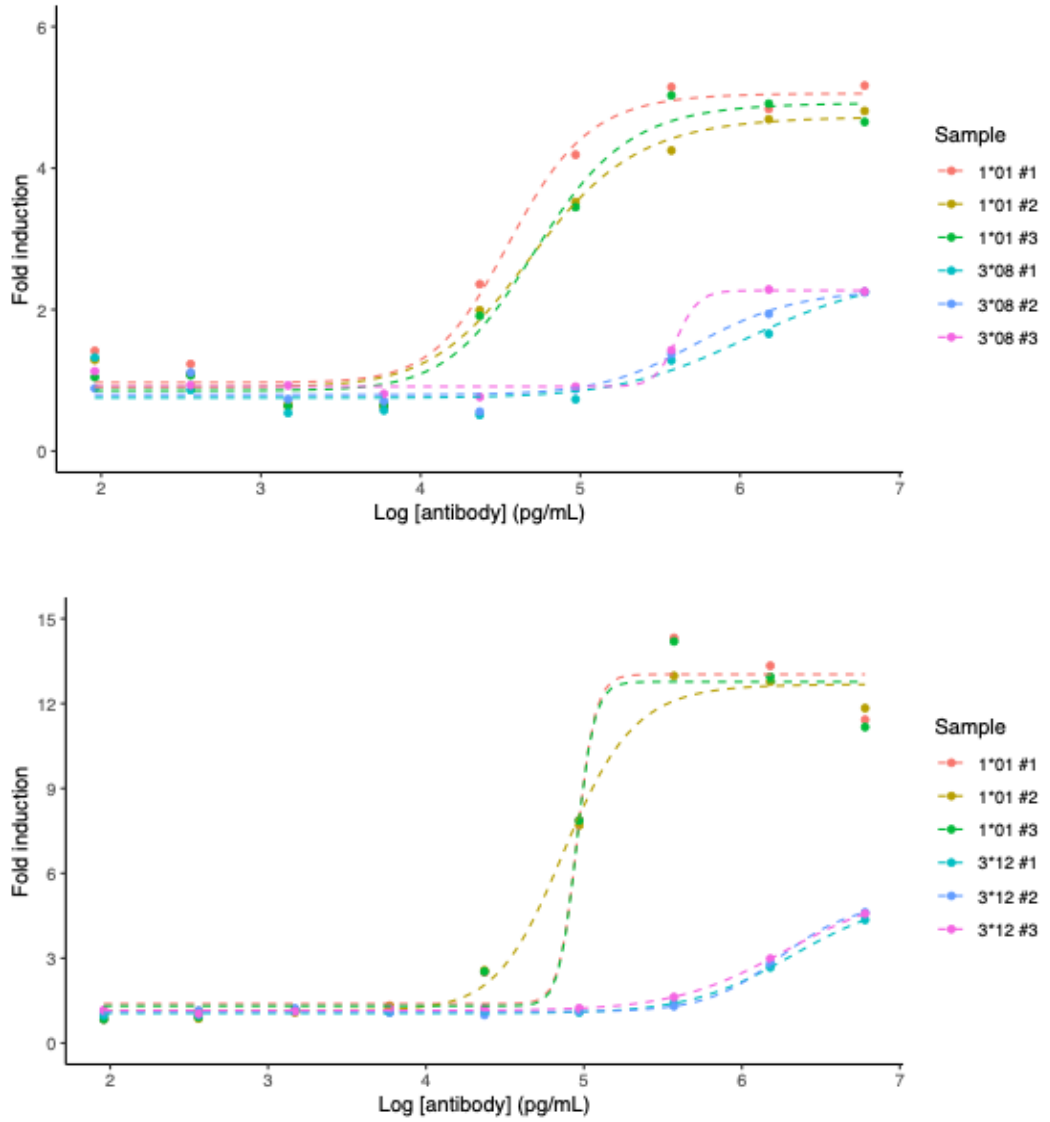

Figure 4.16. Four-parameter logistic model of fold induction values from individual ADCP assay plates from the second assay of IgG3*08 and IgG3*12 CD20 using WIL2-S as target cells. Each sample was in triplicates.

Assays using Raji cells

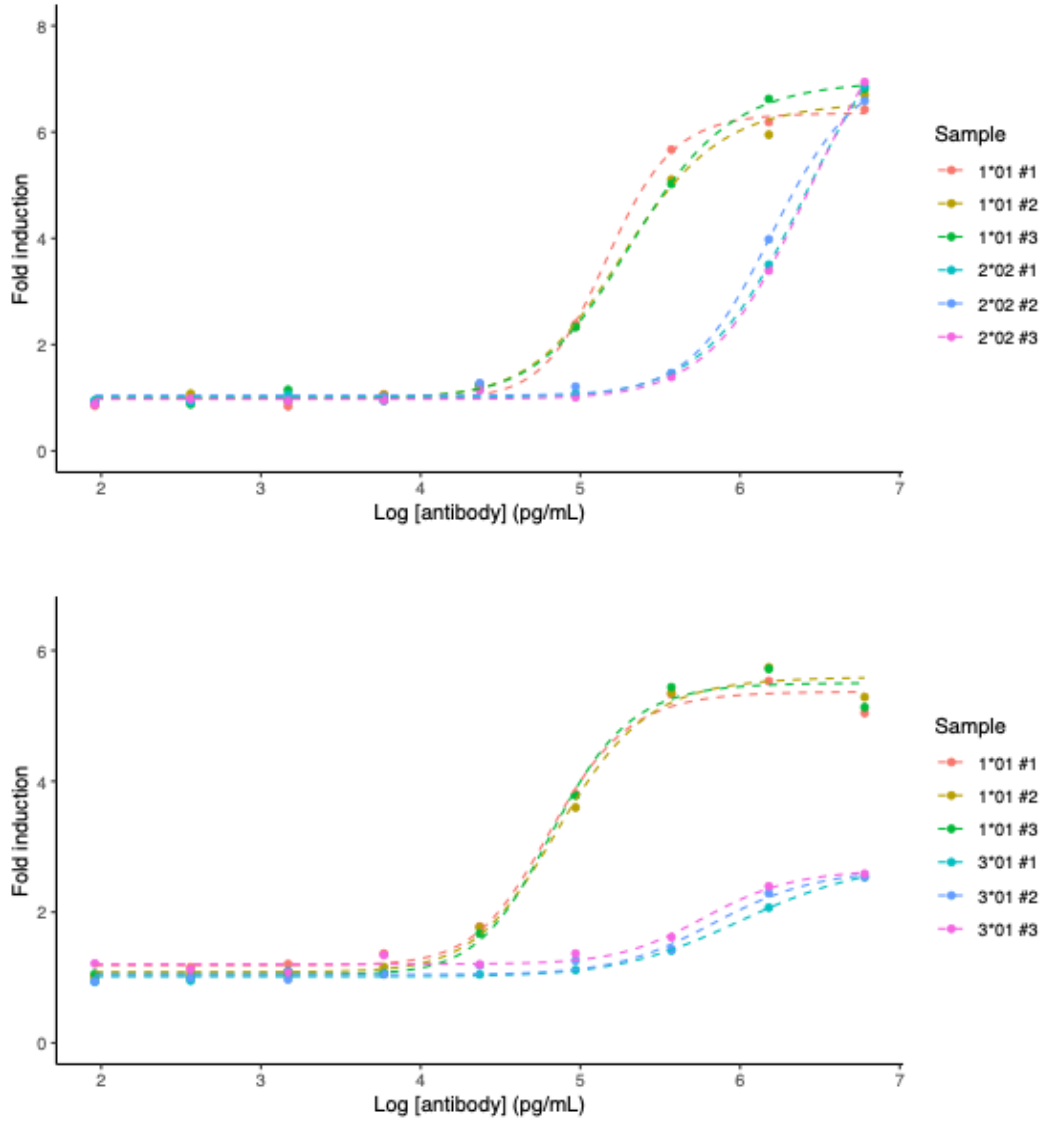

Figure 4.17. Four-parameter logistic model of fold induction values from individual ADCP assay plates of IgG2*02 and IgG3*01 CD20 using Raji as target cells. IgG1*01 was used as a reference in all plates. Each sample was in triplicates.

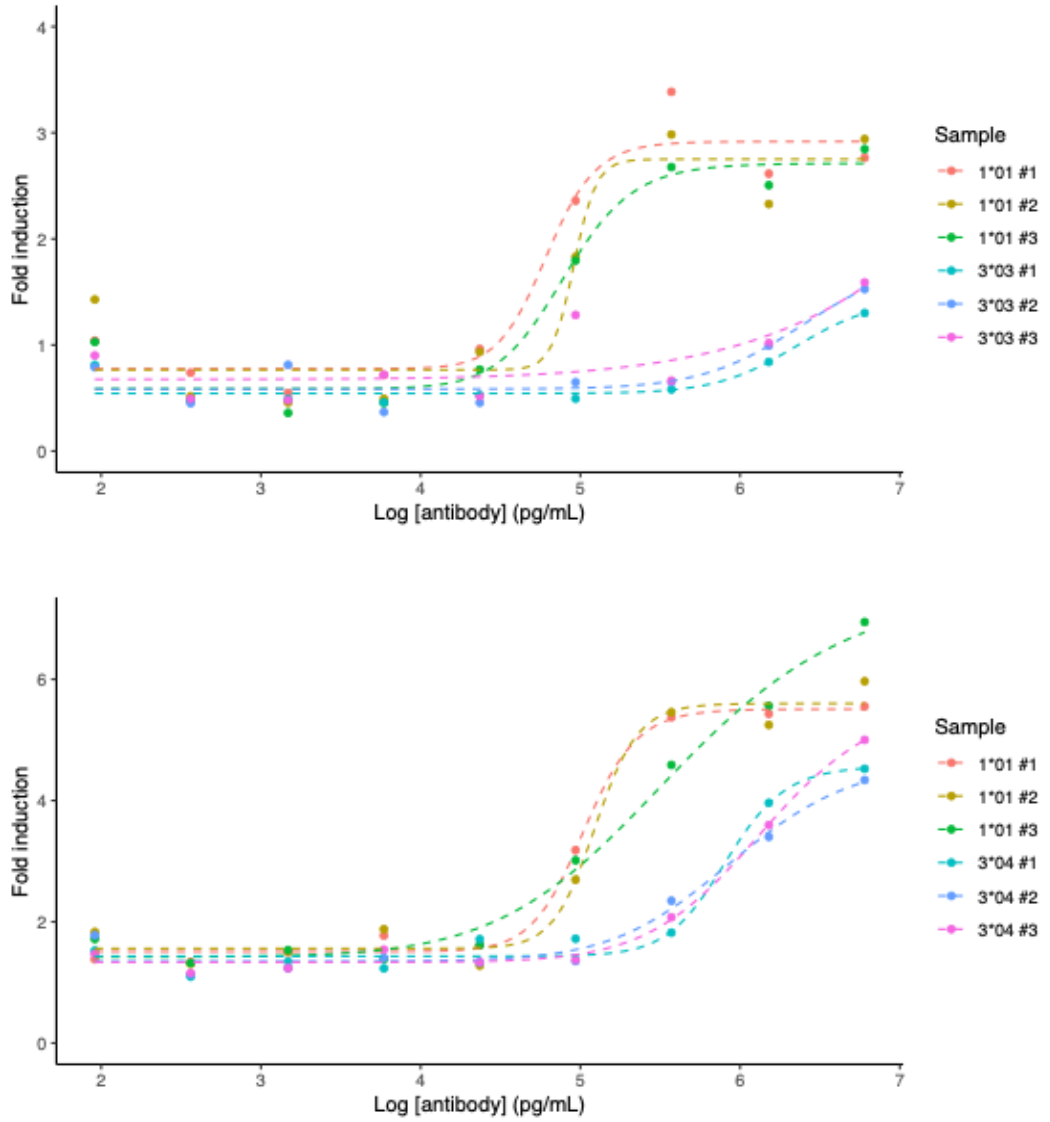

Figure 4.18. Four-parameter logistic model of fold induction values from individual ADCP assay plates of IgG3*03 and IgG3*04 CD20 using Raji as target cells. IgG1*01 was used as a reference in all plates. Each sample was in triplicates.

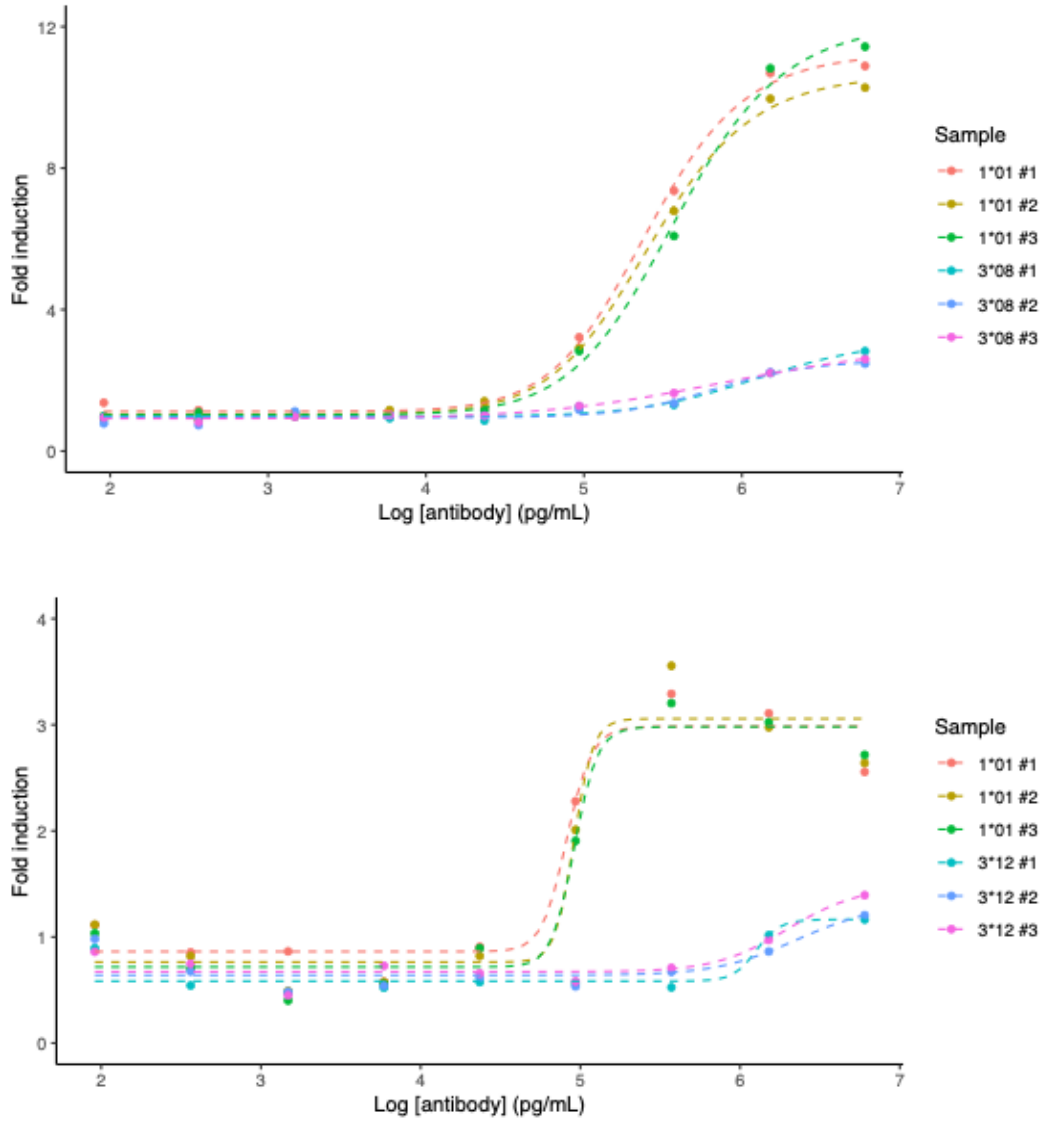

Figure 4.19. Four-parameter logistic model of fold induction values from individual ADCP assay plates of IgG3*08 and IgG3*12 using Raji as target cells. IgG1*01 was used as a reference in all plates. Each sample was in triplicates.

G4: Correlation plot in RStudio

Algorithm 4.2. R script for correlation plot and calculation of p-value in RStudio.

```
library(ggplot2)

data <- read.csv("Correlation plot IgG3.csv")

colnames(data) <- gsub(" ", "_", colnames(data))

model <- lm(EC50 ~ Hinge_Length, data = data)

p_value <- summary(model)$coefficients[2, 4]

ggplot(data, aes(x = Hinge_Length, y = EC50)) +
  geom_point() +
  geom_smooth(method = "lm", se = TRUE) +
  labs(title = "",
       x = "Hinge length (amino acids)",
       y = "EC50 Value (pg/mL)") +
  scale_x_continuous(breaks = c(12, 15, 32, 47, 62)) +
  theme_minimal() +
  theme(
    panel.grid.major = element_blank(),
    panel.grid.minor = element_blank(),
    axis.line = element_line(color = "black"),
    axis.ticks = element_line(color = "black")
  ) +
  ggtitle("") +
  # Annotate the plot with the p-value
  annotate("text", x = Inf, y = Inf, label = paste("p-value =", round(p_value, 4)),
           hjust = 1.1, vjust = 1.5, size = 5, color = "blue")
```